Wave Attenuation by Vegetation

A.C.S Mol

March, 2003

Preface

This report is a result of a study on the attenuation of waves by vegetation. The study has been carried out within the framework of a three months internship that is part of the study Civil Engineering & Management (CT&M) at the University of Twente (UT). This work has been carried out at the WL Delft Hydraulics institute in Delft.

The author wishes to thank in the first place Mindert de Vries and Déborah Idier, respectively the supervisors at WL Delft and the UT for the great support throughout this study. Furthermore great thanks go out to Dano Roelvink, Ilca Tánczos and Arjen Luijendijk, all from WL Delft, for their advices and their helpfulness. At last, thanks go out to Tjeerd Bouma from the Netherlands Institute of Ecology (NIOO) for providing valuable data and also advices, and to Nico Booij for sharing his expertise in wave modelling.

Working at WL Delft was a pleasant experience; the informal working atmosphere and the availability of a large amount of knowledge and expertise within this institute creates good learning conditions for trainees and good opportunities for a decent research.

Arjan Mol
Delft, March 13, 2003

Summary

Measurements have been carried out at the Paulinaschor, a salt marsh in the Westerschelde, to obtain information of the effect of vegetation on wave attenuation. The data have been analyzed. It appears that wave height is strongly reduced by the vegetation, especially for low water depths. Further analysis of the data has been done, to achieve wave energy dissipation. An attempt has been made to formulate a theoretical approach, which is suitable for calculating wave energy dissipation due to vegetation on the basis of certain vegetation characteristics such as stem diameter, plant height and plant density. This theory has been tested by a comparison between the theoretical dissipations and the – so called – observed dissipations. This resulted in quite satisfying correlations; correlation coefficients of about 0.6 – 0.8 were calculated. By means of this analysis is a friction coefficient determined, describing the friction exerted by the vegetation. This coefficient depends on the various vegetation characteristics as mentioned before, but also at a second friction factor, that is more plant specific.

Subsequently, the wave model SWAN has been suited for modelling waves over vegetation areas. The Collins friction factor is used for calibration. Values for this factor turned out to be 2 orders of magnitude bigger than the default value, for bare bottoms. A further study on this Collins coefficient showed that this coefficient is, except for a constant factor, the same as the friction coefficient that was calculated on the basis of the various characteristics. Using these calculated friction coefficients, converted to Collins coefficients, the SWAN model has been validated. The model results showed a good agreement with reality. Only the wave attenuation at the edge of the salt marsh did not correspond very well with the observed attenuation. A possible explanation could be that vegetation is modelled in SWAN through an enlarged bottom friction, in stead of 3D obstacles. Also due to the fact that the development of the orbital velocity in the vegetation is not known exactly, deviances between model outcome and observed attenuation may occur.

Contents

List of Figures

List of Tables

List of Important Symbols

List of Figures

List of Tables

List of Important Symbols

P	Pressure	(mbar)
H	Wave height	(m)
h	Water depth	(m)
ρ	Density of (sea)water	(kgm^{-3})
g	Acceleration of gravity	(ms^{-2})
c	Propagation velocity of a single wave	(ms^{-1})
c_g	Wave group velocity	(ms^{-1})
E	Wave energy density	(Jm^{-2})
ω , σ	Angular frequency	(Hz)
k	Wave number	(m^{-1})
T	Wave period	(s)
L	Wave length	(m)
F	Wave energy flux	$(Jm^{-1}s^{-1})$
D	Wave energy dissipation	$(Js^{-1}m^{-2})$
U_{orb}	Amplitude of horizontal orbital velocity	(ms^{-1})
τ_b	Bed shear stress	$(kgm^{-1}s^{-2})$
f_w, c_w	Friction coefficients	(-)
d	Stem diameter of vegetation	(m)
n	Vegetation density	(m^{-2})
h_{veg}	Vegetation height	(m)

1 Introduction

1.1   Background

Salt marshes are transitional areas between land and water, occurring along the inertial shore of estuaries and sounds where salinity ranges from near ocean strength to near fresh in upriver marshes. The goods and services that these wetlands provide have often been greatly undervalued. Besides the recreational and ecological value of these areas, wetlands play a great role in storm buffering and water storage and thus an important tool in coastal protection. More recently, also the economic value of wetlands has been recognized. Wetlands provide many goods of significant economic value, like clean water and fisheries. Because of the underestimation of these wetlands values in the past, a great part of the wetlands has disappeared during the last century.

In particular estuarine wetland environments are under pressure from land reclamation especially in the Netherlands, where salt marshes have been extensively diked and drained in order to create additional agricultural land. Nowadays, fortunately, it is clear that estuarine wetlands are particularly important in shoreline stabilization and storm buffering. In this field, more and more research has been done lately, especially on the influence of the salt marsh vegetation on water movement and morphology.

This study will focus on the interaction between salt marsh vegetation and wave attenuation. This relation will be used for the calibration of a wave model. The study is part of a much more extensive investigation to the effect of biology on water movement and morphology, also referred as *eco-morphology* (figure 1.1).
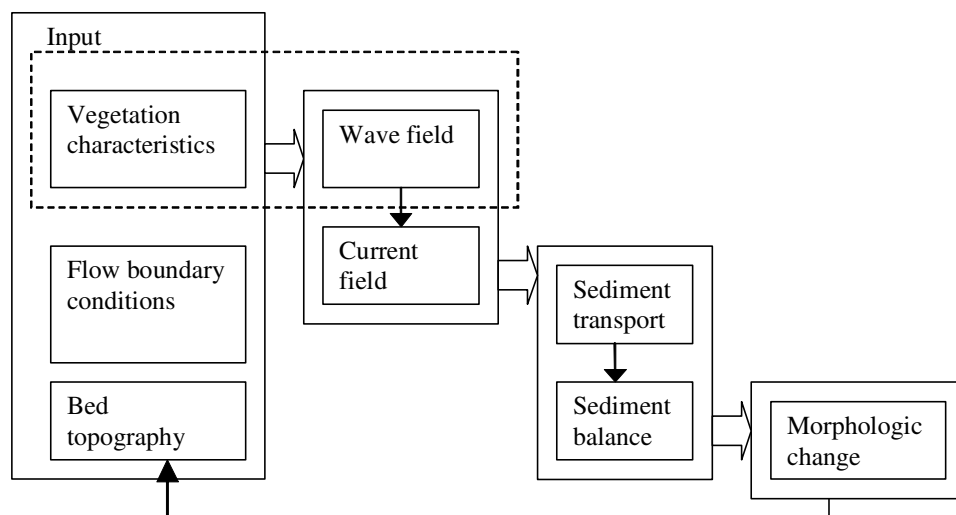
Figure 1.1: Position of this study (dashed box) in the eco-morphology.

1.2   Estproc

This study is carried out within the framework of the ESTPROC (Estuary Process Research Project) project. Aim of this project is the investigation to deliver research on hydrodynamic and sediment processes in estuaries and the interactions between biology and sediments. This fundamental new research will inform the further development of the management tools for estuary morphology, water quality and ecology assessed in Phase 1 (Appendix B) of the Estuaries Research Programme. The main objectives of EstProc are:
- Improved understanding of Hydrodynamic Processes in estuaries,
- Undertaking investigation into Sedimentary Processes in estuaries,
- Investigating interactions between Biological and Sedimentary Processes in estuaries.

The Estproc project team comprises:
- HR Wallingford,
- Proudman Oceanographic Laboratory,
- Professor Keith Dyer / University of Plymouth,
- St Andrews University, Gatty Marine Laboratory (Sediment Ecology Research Group),
- ABP Marine Environmental Research,
- WL | Delft Hydraulics,
- Plymouth Marine Laboratory,
- University of Cambridge, Cambridge Coastal Research Unit,
- University of Southampton, School of Ocean and Earth Sciences,
- Digital Hydraulics Holland B.V.,
- Centre for Environment, Fisheries and Aquaculture Science.

More information of the ESTPROC project can be found in appendix B.

1.3   Research Objective

The objective of this study reads:

An analysis of field data from the Paulinaschor will be made to establish the relationship between vegetation characteristics and wave attenuation for the proposal and testing of a parameterization of vegetation influence to wave attenuation for use in the SWAN model.

The outcome of this study is a wave model that is suited in predicting wave characteristics over submerged vegetation fields. Measurements at the *Paulinaschor* (figure 1.2), a salt marsh in the Westerschelde, are the basis of the research. An analysis of these data is needed to find out how the salt marsh vegetation influences the waves. This relation will then be quantified through a parameterization of the vegetation influence that can be used in the SWAN model. The model will be validated by comparison of the measurements and the model outcome.
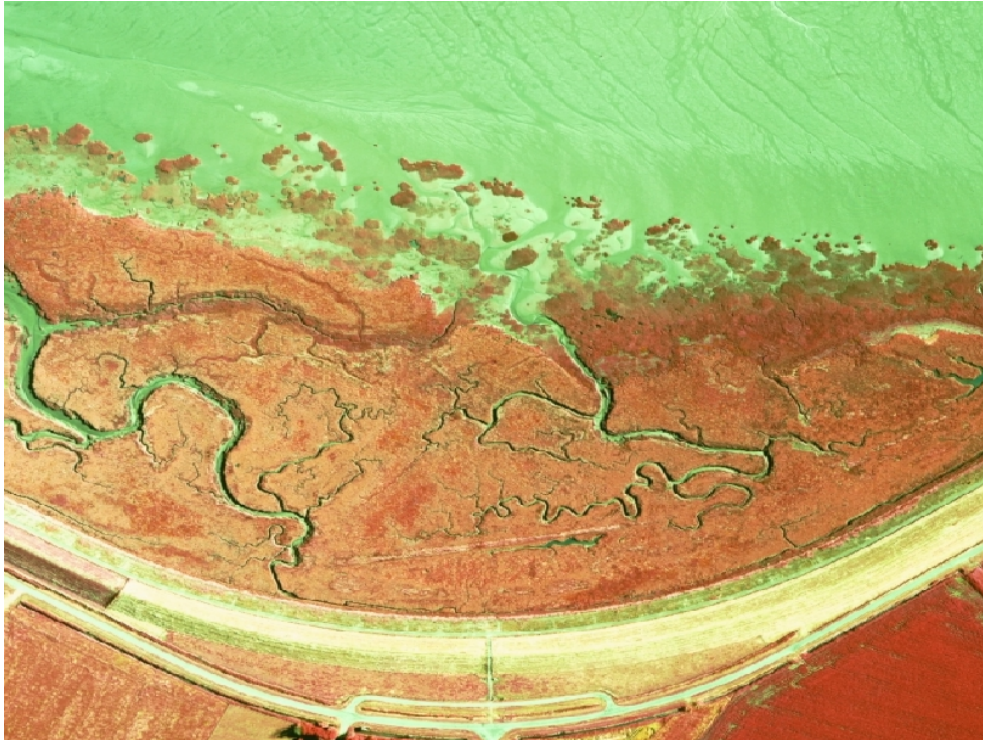
Figure 1.2: Satellite image of Paulinaschor (orange = salt marsh, green = water).

1.4   Research Questions

In this section a set of research questions has been formulated. Answer to these questions is essential in realizing the objective. A distinction between main and sub questions has been made.

Main questions
1. What is the influence of salt marsh vegetation on the characteristics of the present waves?
2. Which parameter(s) of the SWAN model is/are suited for describing the influence of salt marsh vegetation on waves?
3. Is SWAN capable of describing wave attenuation due to vegetation correctly?

Sub questions

1.1 Which measurements are available?
1.2 What are the characteristics of the project area?
1.3 Which vegetation characteristics will be used?
1.4 Which wave characteristics will be investigated?
1.5 What is the quantification of the wave and vegetation characteristics?
1.6 Which other factors, besides vegetation, have significant influence on wave characteristics?
1.7 Is it necessary to perform a correction for these influences?
1.8 In which way should the relationship between vegetation and waves be described?

2.2   Which parameters of SWAN are available?
2.3   Can one of these parameters be used for vegetation influence in SWAN?
2.4   If so, how can these parameters be linked to the interaction between vegetation and waves?

3.1   How can SWAN be tested for this feature?
3.2   Which input data are required for the test runs?
3.3   Are all data available?
3.4   Which schematization of the area will be used?
3.5   Can the model be used in other situations?

1.5   Report Structure

First a description of the field site is done in chapter 2. The Paulinaschor will be described and also information is given about salt marshes in general. Salt marsh vegetation and how waves are affected by the vegetation will be subject of the discussion in the last part of this chapter.

In chapter 3 the measurements that have been carried out at the Paulinaschor will be clarified. Which data are measured, at which location is measured and how the data are collected, are the main questions in this chapter. In the following chapter, the analysis of the measurements is described. The wave attenuation at the salt marsh is presented here.

Subsequently, chapter 5 discusses some theoretical formulations to describe wave attenuation by vegetation. The results of this analysis will be compared to the results of the analysis of the measured data.

After that, in chapter 6, the wave model SWAN is introduced. Basic equations of this model are given and there will be a selection of a suitable parameter, if available, to describe the vegetation influence towards wave attenuation. In the following chapter, the SWAN model will be tested, by a calibration and some sort of validation, for this feature. Finally some conclusions of this study are presented, along with some discussion points, in chapter 8.

Because of the large amount of graphs that is needed for showing all results, these graphs have been put together in Appendix A.

2 The Field Site

This chapter provides an introduction to the Paulinaschor. Before focusing only at this salt marsh, a general discussion about salt marshes is given in the first paragraph, followed by some statements about the values of salt marshes, in the second paragraph. The importance of these wetlands, not only from an ecological point of view, but also in the light of economic and coastal security reasons, will be cleared out. Next, some facts about the Paulinaschor and the Westerschelde will be given in order to get a better understanding of the project area. Subsequently the vegetation at the Paulinaschor will be described. In the last paragraph the importance of a study to vegetation-wave interaction is demonstrated.

2.1   Salt marshes

Salt marshes prosper in relatively sheltered coastal area, with enough sediment available to stimulate accretion. Macrophytes begin to appear at the highest bottom levels, with inundation times lower than approximately 10%. The presence of vegetation generally results in an enhanced sediment trapping and enhanced accretion rates. A top view of the salt marsh reveals the characteristic branched pattern of channels (figure 1.2). Up to three or four orders of channels can be distinguished depending on the size of the salt marsh. The main channels have a width of the order of meters while the smallest channels, or gullies, are only 10 to 30 centimetres wide. Because of their drainage function the channels are an essential part of the salt marsh.
Salt marshes are part of the intertidal flat. The marshes are situated at the *upper zone* of the intertidal flat, as can be seen in figure 2.1. The marshes are bordered by mudflats at the gully side and are backed mostly by dikes or dunes.
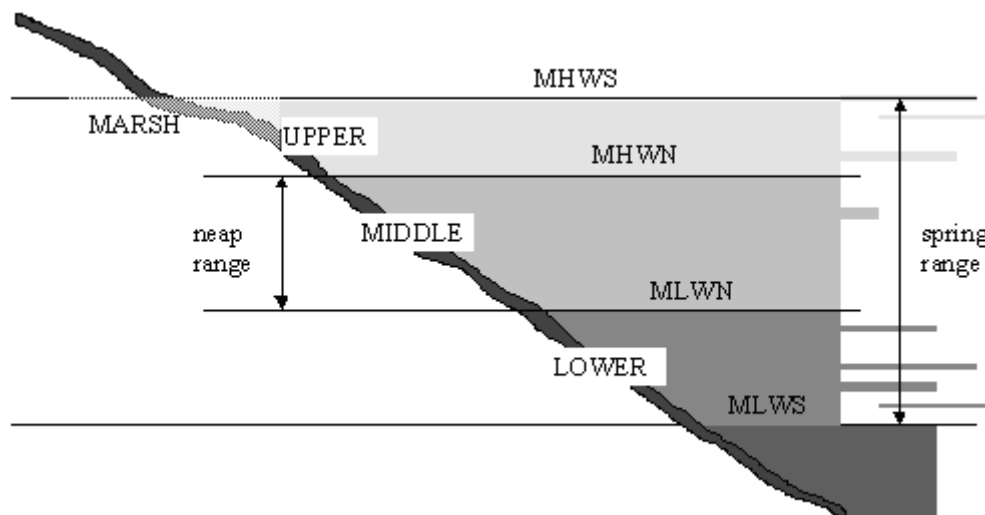
Figure 2.1: The different zones of an intertidal flat.

In the Netherlands, salt marshes can be found only in the Waddenzee and in the province of Zeeland (figure 2.2). The Dutch salt marshes make up 7% of the world's total salt marsh cover. Historically large tracts of these estuarine marshes were diked and drained to provide additional cultural land. However, more recently there has been increased recognition of the goods and services that these wetlands may provide. These goods and services are described in the next section.
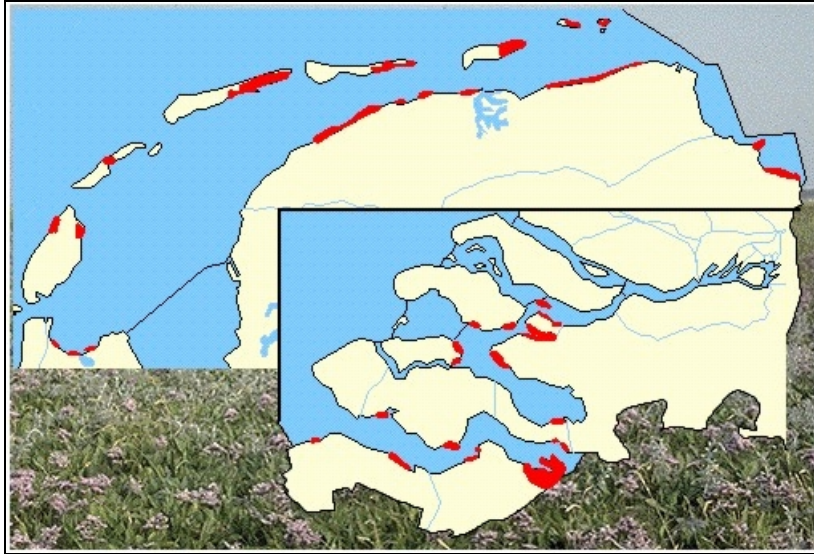
Figure 2.2: Location of salt marshes in The Netherlands.

2.2   The value of salt marshes

Wetlands, and in particular salt marshes, provide valuable goods and services. The great values of salt marshes will be shortly described in this paragraph.

Salt marshes are ecological systems with high biological productivity; nutrients stored and recycled within them provide the foundation of the estuarine food chain. The dead leaves and stems of marsh plants enter the water, are broken down by bacteria, and become food for fiddler crabs, worms, snails, finfish, and shellfish. The marshes provide nesting, feeding, and refuge areas for shorebirds and other wildlife, and they store floodwater, stabilize the shoreline, and act as buffers against wave energy. The marshes function as living filters where pollutants are contained, diluted, or stabilized as tidewater and storm water flow through marsh grass and over mud flats. The vegetation in wetlands helps filter out excess nutrients, which contribute to water quality problems in many coastal areas. Ensuring the long term survival of large, healthy, and productive salt marshes is of critical local, regional, and international importance. The significance of salt marshes to nearby communities cannot be underestimated. In many coastal communities, salt marshes are at the centre of local cultural and community life. Salt marshes are necessary to sustain the commercial viability of the coastal fisheries upon which many coastal communities rely. For example, in the U.S.A 70% of the total value of U.S. commercial fishing is salt marsh reliant. The total take of U.S. commercial fisheries in 1999 was more than 4.2 metric tons, or more than $3.5 billion worth of fish, so salt marshes contributed approximately $ 2.45 billion dollars to the U.S. GDP in fish alone in 1999 (Fisheries of the United States).

Salt marshes play a great role in coastal protection. Salt marshes have much potential for coastal protection by absorbing wave energy that consistently contributes to the wear and tear of sea dikes. Another example from the USA from the Boston Harbour shows that the natural salt marsh defences save $17 million a year in flood protection.

Salt marshes may help to prolong the life of the dikes, but they cannot protect the land from exceptionally high water levels. Besides that, most violent storms are also likely to occur during winter times when salt marsh vegetation has died back and there is minimal obstruction to water motion. Nevertheless, the use of salt marshes as protection tools, with so many positive side-effects, will become more and more accepted nowadays.

2.3   The Paulinaschor and the Westerschelde

The Paulinaschor is a marsh in the Westerschelde (figure 2.3). This estuary has been subject of many researches the past few years. The many functions this estuary has are hardly to combine.
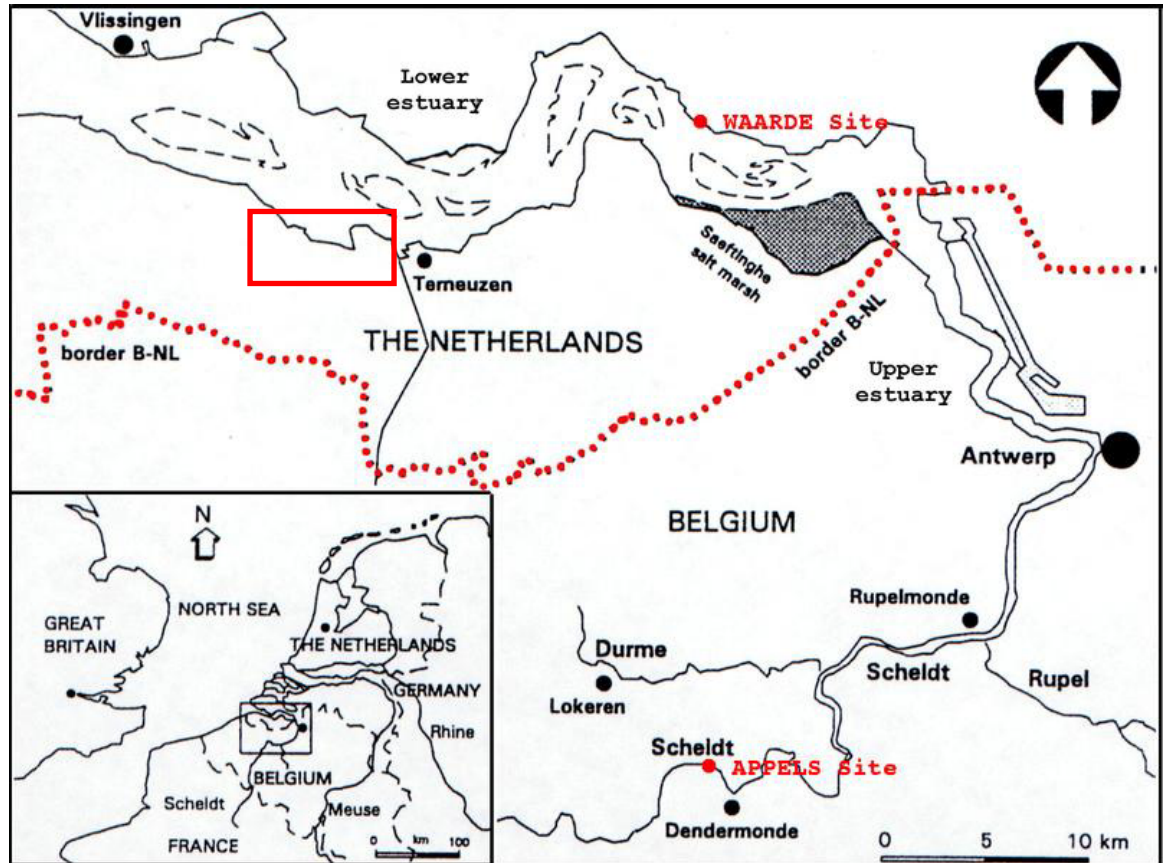
Figure 2.3: Location of the Westerschelde in the Netherlands. The red box denotes the Paulinaschor.

The Westerschelde is the main entrance to the harbour of Antwerp (Belgium). In 1995, the Netherlands and The Flemish District signed an agreement in which was decided that the Westerschelde should be deepened to ensure full access to the harbour of Antwerp. Another item of the Dutch-Flemish agreement is the implementation of an ecological recovery plan to compensate for the destructive effects on nature. The safety function of the estuary is also affected by negative developments during the last century. In particular estuarine wetland environments are under pressure from land reclamation. Salt marshes have been diked extensively and drained in order to create additional agricultural land. That is why the Westerschelde lost a lot of valuable space for the storage and transport of water. Bank protection is also an important issue with regard to safety.

Fortunately, nowadays, more and more cooperation takes place between Holland and Belgium, and even France, concerning the Schelde. The reports 'Lange termijnvisie Schelde-estuarium' and 'Ontwikkelingsschets 2010 Schelde-estuarium' are good examples of this cooperation. These reports outline a long-term vision of the Schelde estuary, in which the three main functions 'safety', 'accessibility' and 'naturalness' are well balanced. Also the 'International Committee for the protection of the Schelde', in which France is involved too, is an association that deals with the Schelde.

The Paulinaschor is located on the south bank of the Westerschelde, west of Terneuzen in the province of Zeeland. The salt marshes of the Paulinapolder are the remainders of what was a sizeable area of salt marshes in the mouth of the Braakman, a former arm of the sea.

The marsh is a relative small marsh in comparison to the other salt marshes of the Westerschelde. The tidal range in this area, strengthened by shoaling effects from water flowing out of the Schelde, is very large. Figure 2.4 shows the water levels for the 9th of September 2002 in Terneuzen. The maximum tidal range for this day was over 5 meters.
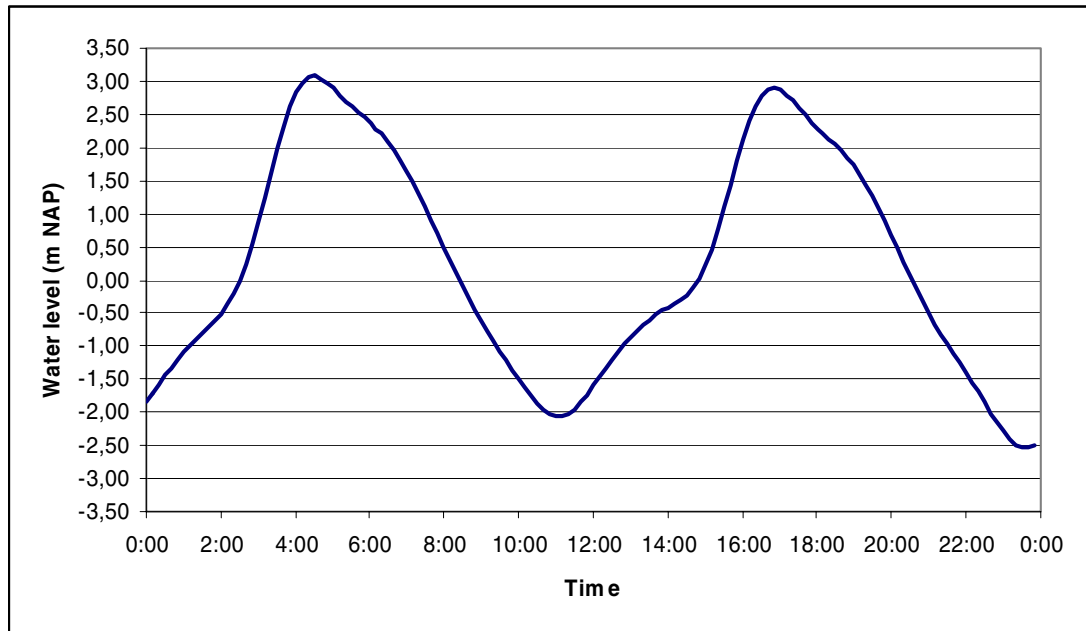
Figure 2.4: Water levels in Terneuzen during 9 September 2002.

2.4   Salt Marsh Vegetation

Salt marshes are vegetated areas, typically formed by salt-resistant plants in a characteristic zoning, strongly dependent on inundation frequency. The vegetation distribution is patchy at the edges of the salt marsh to get denser and uniform closer to land. However, open spaces covered with a thin layer of water are found there as well. The sediment is deposited along the channels forming a somewhat elevated edge. In the summer a thick mud layer is building up on the unvegetated parts of the salt marsh. This sediment is transported on to the rest of the marsh when the water levels rise after summer. Along the channels cliffs may be observed. Salt marsh vegetation is clearly zoned. This zoning is determined by salinity levels and by the dryness and oxygenation of the roots and thus by inundation frequency and duration. The vegetation in the lower salt marsh (pioneer zone) can have a patchy distribution; here one can find circle-shaped clusters of Spartina, separated by bare flat. If the density inside the clusters is high, the water flows around and over the clusters rather than through them. The density of the clusters (distance between them) affects the local hydrodynamics.

Typical species found in the pioneer zone of Dutch salt marshes are Salicornia and Spartina Anglica. A little higher appears the sea meadow grass (Puccinellia/kweldergras). Still higher species such as Limonium, Aster and Artemisia become typical. The highest zone is the home of the least salt resistant species such as Elymus and reed species.

Typically, density and length of the plants increase with the soil elevation. For instance Salicornia is distributed sparsely and will not exceed a length of 30 centimetres. Aster can grow to above 1 meter of height and produces a stiff stem with many branches and leafs. Middle and upper zones can be densely vegetated with thousands of stems per square meter. The vegetation of the marsh will change during the year. This means that height and density

will increase during the spring and summer. During the winter season most of the vegetation will die and will be washed away.

The vegetation that is of importance for this study is Spartina Anglica (figure 2.5). This vegetation type can be found on the part of the salt marsh where the measurements have been carried out.

Figure 2.5: Spartina vegetation on the Westerschelde.

The Spartina plants are rather stiff plants of about 40 cm high. The leaves grow out of the stem under an angle of approximately 45°. Typical stem diameter is 3 – 4 mm and the densities that can be found on the Paulinaschor are ranging from 1000 to 2000 stems per square meter.

2.5   Wave attenuation by vegetation

Waves are created by wind and are an important factor in vertical mixing within estuaries. In the Netherlands waves also cause significant damage to coastal dikes at great financial cost to coastal protection bodies. Over the next 15 years €700 million will be invested in dike renewal in the Netherlands. In the UK more cost-effective 'soft' coastal engineering approaches are being considered as sustainable options for coastal management. Möller describe 'soft' coastal engineering as the realignment of current 'hard' engineering defence lines, such as sea walls, further landward reintroducing formerly reclaimed land back into the tidal zone. These coastal setback areas result in an increase in the area available for salt marsh formation, which is assumed to reduce sea wave energy, allowing the new defence line to be constructed to a lower standard. In The Netherlands, where land area is an expensive commodity it will be less likely that agricultural land will be sacrificed to such coastal set back areas. Nevertheless salt marsh vegetation bordering the 'hard' engineering sea defences, characteristic of the Dutch coastline, may offer some protection from sea wave energy.

A study carried out by Yang (1998) on wave attenuation by *Scirpus Mariqueter* vegetation revealed that wave energy could be entirely dissipated when a wave moved shoreward approximately 50 m through the marsh vegetation. Wave heights found over the marsh were on average 43% less than those on the adjacent tidal flat. This is in accordance with results

obtained by Möller, Spencer. French, Leggert & Dixon (1999) who state that wave attenuation does not vary linearly with distance across the salt marsh and that most wave energy is dissipated or reflected over the first 10 to 50 meters of salt marsh surface.

3 Data Collection

This chapter describes the gathering of the data; which data are collected and how was the measuring campaign organized. The first paragraph starts with a description of the measurements that have been carried out. In the second paragraph an overview is given on the field site from which data is collected especially for this study. Next, some notes are made concerning the raw data which is the basis of this study. After that, in paragraph 4, a selection has been made of suitable data sets that will be analyzed in the next chapters.

3.1   Measurements

The data that will be used in this study are the results of a measurements campaign in 2002 at the Paulinaschor. The measurements took place during two periods. The first period was the 7th of August till the 15th of August 2002. Second period was from the 5th of September till the 12th of September. This operation was executed not only by WL Delft Hydraulics, but also by the NIOO (Netherlands Institute of Ecology). Besides this study, which involves the Paulinaschor, other projects within the ESTPROC frame are carried out. Especially the study on wave attenuation at different salt marshes in the UK (R.Turner) and laboratory flume experiments at both WL Delft and the NIOO are close connected to this study. Some close cooperation took place with the executors of these projects during this study, especially in the modelling part. Results of these studies are not yet available, but some discussion points about other field sites will be mentioned sometimes in this report.

Two types of measurements were done. Both types of measurements concerned velocity and pressure measurements. The first type of measurements was carried out by means of frames (figure 3.1). These frames were placed on the salt marsh, in the gully of the salt marsh and out on the mudflat. With this data, large-scaled research can be done to the working of the whole intertidal system. These measurements are used for example by E. Low (2002) and by L. Kusters (2003). The measurements that will be used in this study are the transect measurements. The field area is much smaller than the area of the measuring frames. Therefore much more detailed information is gathered which is far more useful in studying the complex physical processes taking place at salt marshes. In this research mainly the pressure measurements will be used.

Figure 3.1: Example of measuring frame in the salt marsh creek

3.2   Transect line-up

At the Paulinaschor, ten locations with measuring devices formed a measuring transect. Eight of the ten instruments formed a line (i.e. a transect) perpendicular to the salt marsh edge. In that way, the wave attenuation over the salt marsh can be studied the best. Figure 3.2 shows a schematic plan view of the transect. The ten measuring locations are indicated by the codes P0 t/m P9. Also the distances between the devices are given.
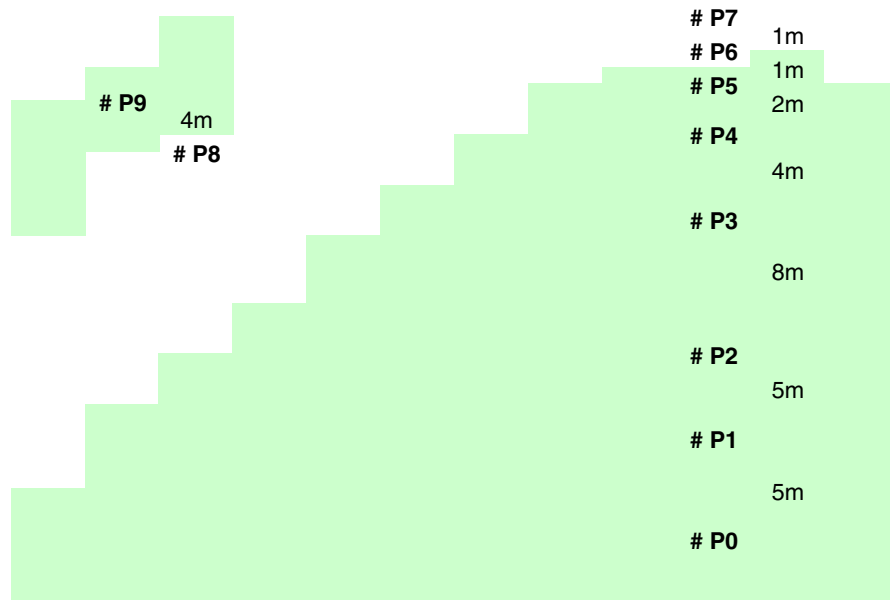
Figure 3.2: location of the sensors at the salt marsh. P0 is the landward side.

As figure 3.2 indicates, two locations were just outside the marsh at the mudflat. All measuring devices were equipped with a pressure gauge. The gauges were fixed at 200 mm above the bottom. Since the pressure gauges were in open connection with the air, only water pressure was measured. The two locations P8 and P9 were not in the line of the 8 other gauges.

These gauges are more suited for investigation to wave attenuation in the creeks of a salt marsh, which is not the objective of this investigation. Therefore, the measurements that are taken from this location will not be used in this study. Besides the pressure gauges, ten velocity gauges were present in the field. These devices were not all fixed at different locations. By placing a couple of speed gauges on top of each other at one certain place, a good view of the vertical velocity profile can be obtained. Although the main concern of this study is not the development of velocity profiles in vegetation fields, this information can be well used in other researches to vegetation influence on flow dynamics. Figure 3.3 gives a good view of a single measuring device in the vegetation.

Figure 3.3: Measuring location in vegetation.

All the measuring devices were connected to two loggers, which stored all the data. Figure 3.4 shows some gauges and the connection to the logger 'tower'.

Figure 3.4: A 'logger tower' and some gauges near the edge of the salt marsh.

The loggers were equipped with a master and a slave unit. The master unit was able to store six variables at each time. In this case the master unit of each logger stored two pressure values and 4 velocity (horizontal and vertical velocity at two locations) values. The slave unit could store nine values each time; one extra pressure value and two velocity values (horizontal and vertical). Figure 3.5 gives a schematic overview of the organization structure of the data storage for the pressure measurements only. This organization (for pressure only) was the same during both measuring periods. The pressure gauges P0 through P9 correspond to the location codes in figure 3.2. In appendix C the structure is shown for all measurements in both periods.
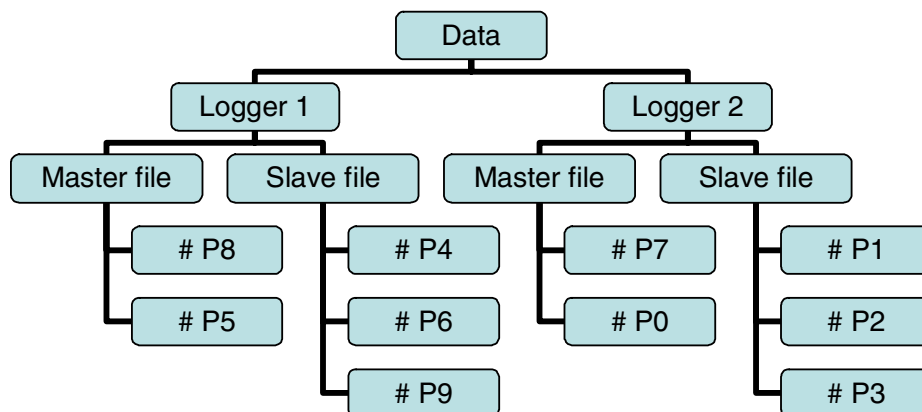
Figure 3.5: Organization structure for the data storage

3.3   Raw data

The available dataset consisted of nine files. This is one file more than what would be expected on the basis of the description of data storage in the previous paragraph:
(2 loggers) x (slave + master) x (two measuring periods) = 8 files.
Because of some problems during the measurements one file was not completed. The rest of the measurements were stored in an extra file.
The measurements were done only 8.53 minutes of each quarter of an hour. This was because of the limited data storage capacity. By taking measurements only a part of a quarter, the measurement period increases to almost twice as long. It is much more interesting to gather information of a bigger period than gather the double amount of information of a smaller period, in which smaller changes in circumstances occur. The measuring frequency was 4 Hz, so 2048 measurements per 15 minutes were taken. After each quarter of an hour, an average value of the measured data was calculated and stored in the data files. In the data files, the lines with the raw measurements start with the number 100 or 101, while the lines with the average values of the past quarter (in fact 8.53 minutes) start with 200 or 201. The 200/201-lines also contained information about the date and time of that moment. The date was given by a number. This number indicates the day of the year 2002. So day number 1 represents the first of January 2002. The time format was hh:mm:ss.00, so seconds were given in two decimals. On the basis of the given time in the average lines, the moment of recording of all other measurements could be extracted.
Thus the first column indicated whether a line contained raw or average data. The columns next to this one were allocated for velocity measurements. The pressure data could be found in the last two or three columns, depending on the sort file, master or slave.
These data, which are still in millivolts, have to be converted to pressure units. Since the pressure gauges had an output of 500 millivolts in dry conditions and 2500 millivolts under a pressure of 350 mbar, the conversion formula reads:

$$P(mbar) = 0.175(P(mvolts) - 500) \qquad\qquad (3.1)$$

More information of the file formats of the data files for all measurements (including the frame measurements) can be found in appendix D.

3.4   Data selection

Not all available data will be used for the analysis. An analysis of all the data would take too much time because of the large amount of measurements: two weeks of measurements, with a frequency of 4 Hz are quite a lot of data. Besides that, since the salt marsh is inundated only with high water, a part of the data, the output of the pressure gauges during dry conditions on the salt marsh, is not useful for research. So only periods of high tide can be used for investigating wave attenuation. The question now is which high waters will be used. A quick look at the data shows that wave heights generally are very low, most of the time far below 10 cm. The weather was very calm during the measuring periods in August and September, and so were the wind conditions. A decision was made to take for each measuring period, two periods of high tide for which relative large waves showed up. This selection has been made by plotting the pressures in excel for each high tide, followed by a global determination of the pressure variation. Obviously, the biggest pressure variations correspond to the biggest wave heights. This rough method lead to a selection of the following four periods:

- Period 1: 10th of August, 16:30 – 19:00 hour
- Period 2: 12th of August, 17:45 – 20:45 hour
- Period 3: 10th of September, 17:15 – 20:00 hour
- Period 4: 11th of September, 18:15 – 21:00 hour

The periods are chosen in such a way that the start of each period corresponds to the top of the tidal flood wave, involving large water depth at the marsh, until the moment that the water level is just as high as the vegetation height or even less. In this way, wave attenuation by vegetation can be analyzed for a large range of water depths at the marsh. The advantage of using measurements of two different periods (August and September) is that vegetation characteristics, such as vegetation density, stalk thickness and vegetation height, may differ. The more variation in such parameters, the better insight can be obtained in the influence of vegetation on the attenuation of waves.

The measurements corresponding to the selected periods are now copied from the original data files and pasted in manageable excel files. Each excel file contains 8.53 minutes of measurements of the total period, thus 2048 values. The reason of choosing rather short periods is that for the analysis of wave attenuation, the water depth is required also. With the fast changing water levels caused by the large tidal range, water depths would change too much with the choice of bigger periods. Carry out the calculations with an average water depth cannot be justified in that case.

The data are now ready for further analysis, which will be described in chapter 4.

4 Data Analysis

In this chapter is the analysis of the measurements outlined. The input of this analysis are the pressure data, already converted to mbar units. The first paragraph describes the steps that will be taken to extract real wave heights out of the input data. In the following paragraphs, the wave attenuation at the salt marsh is described in various ways.

4.1   Determination of the wave heights

Now that the unit of the pressures is converted to mbar, it is easily to calculate the height of the water column, corresponding to this pressure. For convenience, 1 mbar of seawater pressure will be equated with 1 cm seawater height. Since the pressure gauges were located just above the bottom (200 mm), water depths are measured, but not the wave heights. The average water depth has to be subtracted from the measurements, in order to obtain actual wave heights. But the problem is that tidal fluctuations are present also. One average water depth can therefore not be calculated. Figure 4.1 shows an example of how the water depth changes in time under influence of the tide.
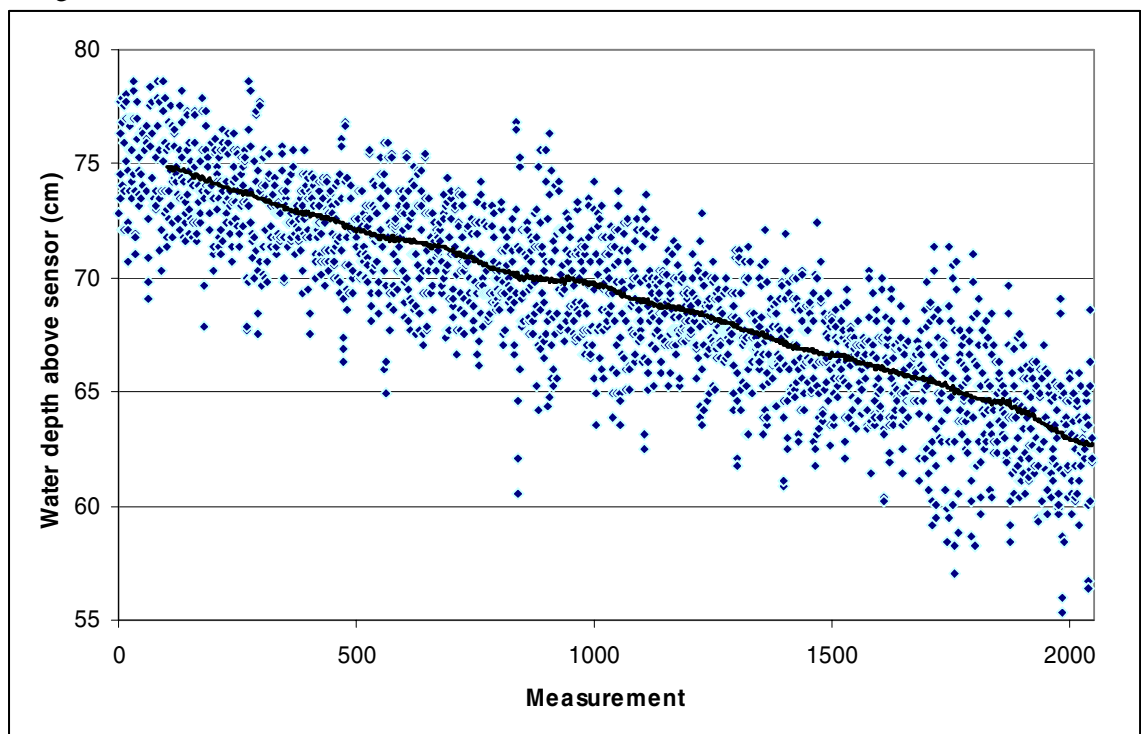
Figure 4.1: tidal influence on water depth, 10-8-200, 2048 measurements (= 512 seconds).

Thus, the first step is to filter out the tidal fluctuation. In this study, a simple filtering method is chosen: a moving average is subtracted from the water depth data. That method will be explained now.
For each single measurement a so-called moving average is calculated. This average is calculated on the basis of a certain amount of measurements that are 'around' the measurement for which the average is calculated. For example, when you have 100 measurements and the moving average is determined on the basis of 11 values, the moving average of the 50th measurement is the average value of measurement 45 t/m 55.

Subsequently, the moving average of the 51st measurement is determined on the basis of the measurements 46 t/m 56, etc. So, this average is called 'moving' because it is moving along the measurements. In figure 4.2 the procedure of calculating the moving average is illustrated, for measurement 50 and 62. The period of this moving average is 11 in this example, because each average is based on 11 values.

45 46 47 48 49 50 51 52 53 54 55 56 57 58 59 60 61 62 63 64 65 66 67

Moving average belonging to 50

Moving average belonging to 62
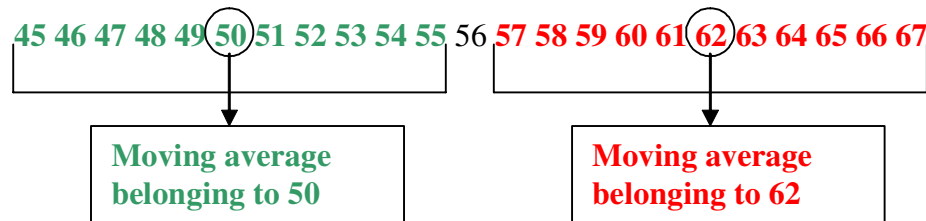
Figure 4.2: Calculating the moving average.

Back to the real case, the problem is: what is the best period is for calculating the moving average. By using a moving average with a relative small period, short wave information maybe lost, because the moving average contains high frequency (short wave) information itself then. When subtracting the average values from the water depth data, using a period that is too high, low frequent water depth variations, which are not caused by short surface waves, will not be filtered out. An example of such a low frequent fluctuation can be seen in figure 4.1. A fluctuation with a period of about 1000 measurements (250 seconds) can be observed. So the selection of the period for the moving average is on the basis of two conditions. The first is that the period must be much greater than the short wave period, which is about 2.5 s. Secondly; the moving average period must be much smaller than the period of low frequent fluctuation, which is about 250 seconds. When selecting a moving average of 25 seconds, the two conditions, in mathematical form become:

$$T_{ma} = 10T_{sw} \gg T_{sw}$$

$$T_{ma} = 0.1T_{lw} \ll T_{lw}$$

(4.1)

where *ma* denotes 'moving average', *sw* stands for 'short wave' and *lw* for 'long wave'.

A period of 25.25 seconds (= 101 measurements, must be an odd number) seems to be a suited value for the moving average value. A negative consequence of this method is that the first and last 50 measurements of each dataset cannot be used anymore, because a moving average for these values cannot be calculated; there are no 50 measurements before the first measurement.

The moving average is shown also in figure 4.1, besides the data points, represented by the black line. The wave height data can be obtained by subtracting the moving average from the water depth data (figure 4.3).
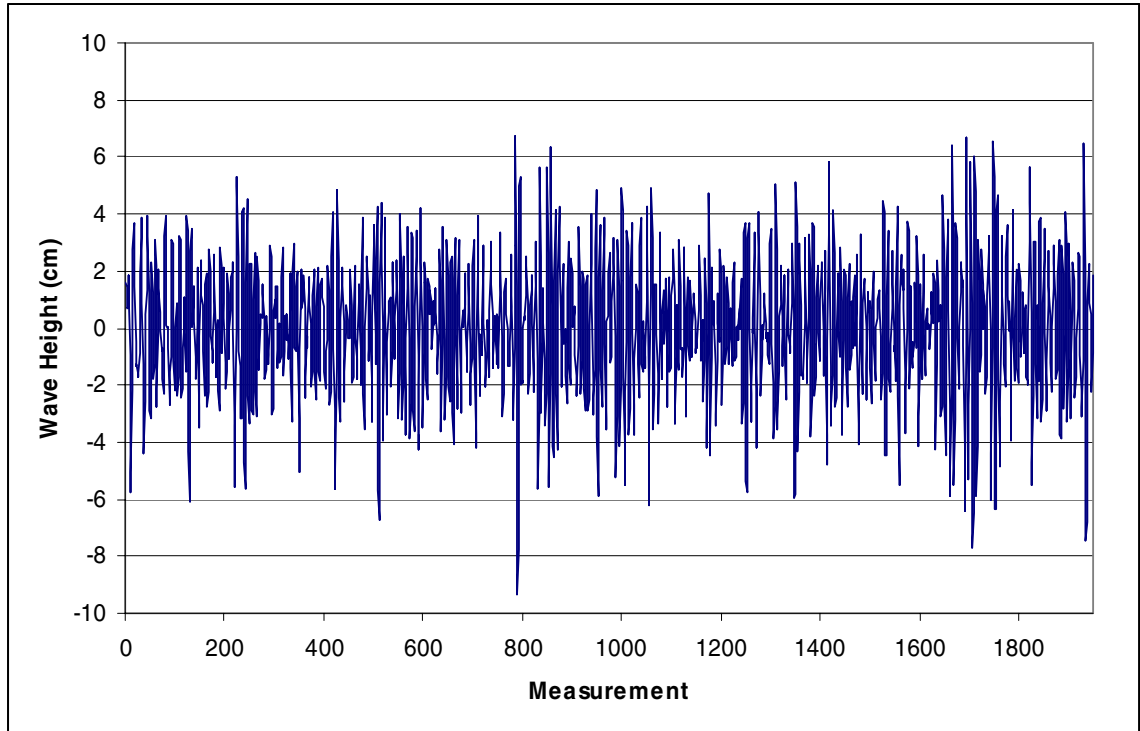
Figure 4.3: Obtained wave heights from figure 4.1 with moving average method.

But still no representative values of the actual wave heights are available, only data files with time series of the waves. For the analysis and calculations, information like significant wave height (Hs) or the root mean square wave height (H_{rms}) is required. Besides, also period information and spectral wave data may be needed.

This kind of information can be obtained using the program *Delft-Auke PC*. This program is developed by WL Delft. Auke is a set of programs for data acquisition and control of wave boards in experimental facilities for hydraulic research as well as processing of signals from instruments. Three Auke programs are used here:

1. **Conasc**: converts an ASCII data file to a DELFT-AUKE series file. The input of this program are ASCII files (like text files, -.txt) with one column of wave data. The output is used for the other two Auke programs that will be used.
2. **Waves**: determines the development of series values between two positive zero crossings.
3. **Spectrum**: computes the spectral densities of series are. Together with the densities a set of parameters is computed and sent to the chosen output device.

More information on *Delft-Auke* can be found in Appendix E. The basic assumptions and formulations of this program are described as well as information about the three Auke programs that are described above. Also the output that *Waves* and *Spectrum* deliver is shown.

4.2   Wave attenuation over the salt marsh

Now that all kind of information is available for various types of wave heights at all measuring locations at different times, corresponding with different water levels, a first analysis of the attenuation of the waves can be made. In graph 4.1 to 4.4 the significant wave heights, extracted from the Auke output, are plotted against the distance at the salt marsh for the four periods. The values at the x-axis show the distance to the salt marsh edge, so x = 0 corresponds to the salt marsh edge itself. In each graph, the various lines represent different water levels. The water levels are shown in the legend in meters above NAP. Each graph clearly shows that for some water levels, wave height is decreasing along the salt marsh, especially when water levels are low. With water levels above 2 m NAP the damping is almost negligible. For a better understanding of these water level values, bottom heights of the transect are showed in figure 4.4.
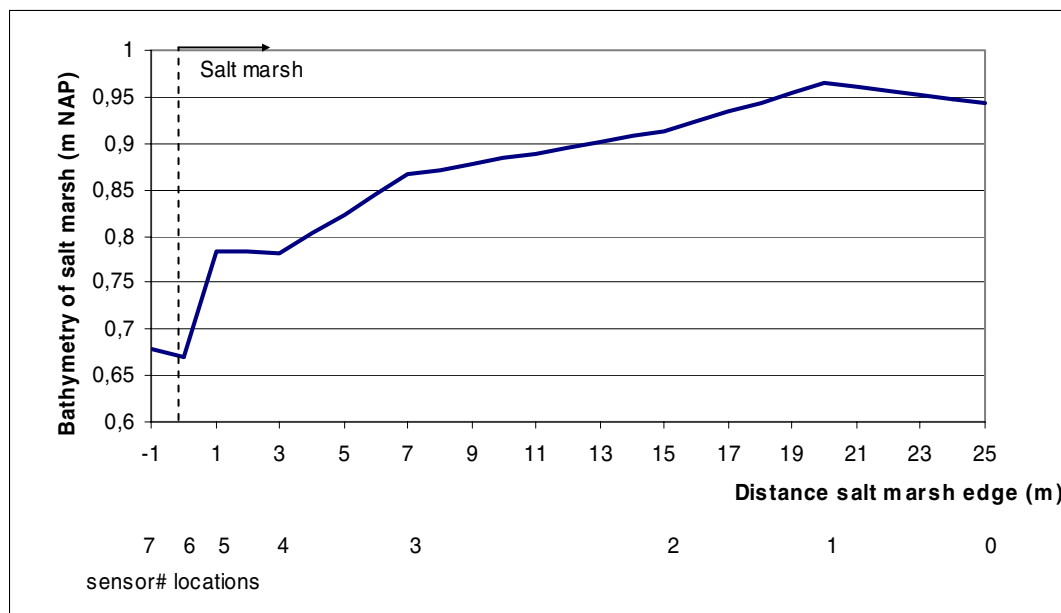
Figure 4.4: Bathymetry of the salt marsh.

The average bottom height of the marsh is about 0.9 meters NAP. Then a water level of 2 m NAP corresponds to a water depth of 1.1 meter at the salt marsh. In table 4.1 the wave damping is given for all different water levels in the four periods. The damping is defined as:

$$Damping = \frac{H_0}{H_7} \times 100\% \tag{4.2}$$

The subscript number denotes the sensor location from which the wave height is determined, so #7 corresponds to the boundary location, just at the mudflat. (The time notations in the first column correspond to the staring time of each 8.53 minutes during measuring period.)

Also from this table, it becomes clear that most damping take place during low water levels. The reason for this is that the vegetation height relative to water depth is just much bigger than for high water levels. The vegetation height is approximately 40 cm.

Time period	Water level [m NAP]	Water depth at boundary (P7) [m]	Damping [%]
10_Augustus			
16:30	2,5664	1,8874	**84,7**
17:15	2,1865125	1,5075125	**85,1**
18:00	1,8077875	1,1287875	**88,1**
18:30	1,473325	0,794325	**60,0**
18:45	1,2795	0,6005	**33,9**
12_Augustus			
17:45	2,78825	2,10925	**107,6**
18:30	2,469	1,79	**101,9**
19:15	2,047375	1,368375	**86,1**
19:45	1,748875	1,069875	**71,2**
20:15	1,36625	0,68725	**49,4**
20:30	1,124625	0,445625	**19,5**
10_September			
17:15	2,7470625	2,0680625	**108,5**
18:00	2,463175	1,784175	**104,5**
18:45	2,0374375	1,3584375	**85,4**
19:15	1,7689875	1,0899875	**77,2**
19:30	1,608175	0,929175	**83,9**
19:45	1,4091125	0,7301125	**56,8**
11_September			
18:15	2,578425	1,899425	**97,2**
19:00	2,20985	1,53085	**102,1**
19:45	1,785525	1,106525	**78,2**
20:15	1,4607625	0,7817625	**62,3**
20:30	1,2607375	0,5817375	**44,6**
20:45	1,0349625	0,3559625	**12,8**

Table 4.1: Wave damping.

Looking at graph 4.1 to 4.4 not only wave damping shows up. Especially with low water levels, an increase of wave height can be noticed at x=0, the edge of the salt marsh. There must be some kind of shoaling effects responsible for this feature. Shoaling appears when waves enter shallow water. There is a small cliff at the transition between the mudflat and the marsh of about 10 cm. But also the vegetation, that starts right at the salt marsh, can act as a wall, which the waves may feel as some higher level bottom that increases the shoaling effect and also may cause reflection.

In the next paragraph the focus will be on wave energy and energy fluxes. Analyzing energy fluxes should count out the shoaling effect, because energy fluxes are not influenced by shoaling.

4.3 Wave energy

Waves contain a certain amount of potential and kinetic energy. The total energy density for a surface wave is the sum of the potential and the kinetic energy density and is calculated by:

$$E = \frac{1}{8}\rho g H^2 \qquad\qquad (4.3)$$

During their propagation waves transport energy in the horizontal direction of propagation. The propagation velocity of this energy is equal to the group velocity of the waves, which is determined by:

$$c_g = n \cdot c \qquad\qquad (4.4)$$

with c the velocity of a single wave:

$$c = \frac{\omega}{k} \qquad\qquad (4.5)$$

and n is described as:

$$n = \frac{1}{2}\left(1 + \frac{2kh}{\sinh 2kh}\right) \qquad\qquad (4.6)$$

Now the energy flux *F* can be determined:

$$F = c_g \cdot E \qquad\qquad (4.7)$$

The only problem left is to determine the wave number *k*. This value equals:

$$k = \frac{2\pi}{L} \qquad\qquad (4.8)$$

The wave length L cannot be calculated very easily. The cause for this problem is the so-called dispersion relation, in which the wave length is a function of itself:

$$L = L_0 \tanh\frac{2\pi h}{L}, \text{ with } L_0 = \frac{gT^2}{2\pi} \qquad\qquad (4.9)$$

The determination of the wave length is an iterative process. Fortunately, some other methods are available to estimate this value more accurately. The method used here is bases on some equations formulated in a matlab script (appendix F), obtained form D. Roelvink (WL Delft).

For each measuring location and for each moment energy fluxes are calculated on the basis of the equations mentioned above. The required input for the calculations are the root mean square wave heights (H_{rms}), the mean periods (T_{01}) and water depths (*h*). The first two values are obtained from Auke PC. The reason for using this specific values is that these values give a good representation of the whole wave field and not only, like the significant wave height, of the biggest part of the waves. The last one can be calculated on the basis of pressure data.

As it has been done for the wave heights, graph 4.5 to 4.8 show the energy fluxes for the different periods with varying water levels. From a theoretical point of view, assuming constant wind conditions, the energy flux cannot increase in propagation direction. But even in the graphs of the fluxes, there is in an increase in energy flux around the edge of the salt marsh. This may be caused by:
1. Besides the shoaling effect, there can be some reflection caused by the cliff and the vegetation. Because of that some wave energy is reflected and the wave energy density just before the salt marsh increases and so does the energy flux with the same group velocity. This is a calculation error. Reflection has not been taken into account and so energy is transported only in the main propagation direction, according to the calculations. Another result of this process may be the steep gradient in wave height and energy flux after the wave enters the salt marsh.
2. Although the energy flux remains constant during shoaling processes, the calculations above may not have count the total shoaling process out completely. As mentioned in the previous paragraph, the shoaling effect is caused not only by the

change in bathymetry, but also by the vegetation, acting as a wall. This effect is not taken into account in the calculations.

Because of the problems around the salt marsh edge, in the further analysis the locations 6 and 7 will be mostly left out of consideration to avoid more problems.

4.4   Energy dissipation

In a steady situation the incoming and outgoing wave energy of an element Δx (x-direction is normal to the shore) should be the same, which leads to the following energy flux balance:

$$\frac{\partial F}{\partial x} = \frac{\partial}{\partial x}\left[E \cdot c_g\right] = 0 \tag{4.10}$$

In general, due to friction and wave breaking energy losses will take place especially in shallow water. Therefore, the energy flux balance is provided with a negative source term, representing the dissipation of wave energy:

$$\frac{\partial}{\partial x}\left[E \cdot c_g\right] = -D \tag{4.11}$$

In case of the Paulinaschor, wave breaking will be neglected, since *H/h<<0.5*. Dissipation due to bottom friction will also be neglected, because vegetation has a much greater influence at energy dissipation. The energy flux balance now reads as follows:

$$\frac{\partial}{\partial x}\left[E \cdot c_g\right] = -D_{vegetation} \tag{4.12}$$

Using two energy fluxes at two successive locations, the wave energy dissipation between those points can be calculated using the following formula, which is deduced from equation 4.12:

$$D = \frac{\Delta F}{\Delta x} = \frac{F_x - F_{x+a}}{a} \tag{4.13}$$

Now that the dissipation is known for all points, the question is how dissipation is related to vegetation characteristics. Therefore it is necessary to do some theoretical analysis of wave energy dissipation. Once a fundamental theoretical basis has been formulated, in which dissipation can be calculated on the basis of vegetation characteristics like height and density, the observed dissipations can be related to certain vegetation characteristics and the theory can be checked.

5 The Influence of Vegetation on Dissipation

This chapter describes a theoretical approach to wave energy dissipation due to vegetation. In the first paragraph an attempt has been made to formulate theoretical formulas that describe the relation between vegetation characteristics and wave energy dissipation. In the following two paragraphs two methods are used to apply the theoretical formulations from the first paragraph on the real case. A comparison between theory and reality is made in paragraph 5.4. In the final paragraph an attempt has been made in describing a friction factor that is representative for the vegetation.

5.1   Theoretical background of wave energy dissipation

Before trying to put up some theoretical formulation for dissipation due to vegetation, the theoretical relation of bottom dissipation will be described, following the formulations of van Rijn:
The dissipation is equal to the time-averaged work done by the friction force at the bottom, giving:

$$D_{bottomfriction} = \frac{1}{T}\int_0^T \tau_b U_\delta dt \tag{5.1}$$

Substitution of

$$U_\delta = \hat{U}_\delta \sin(\omega t) \tag{5.2}$$

and

$$\tau_b = \frac{1}{2}\rho f_w \hat{U}_\delta^2 \sin^2(\omega t) \tag{5.3}$$

yields:

$$D_{bottomfriction} = \frac{\rho f_w \hat{U}_\delta^3}{2T}\int_0^T \sin^3(\omega t)dt = \frac{4}{3\pi}\rho f_w \hat{U}_\delta^3 \tag{5.4}$$

This formulation suggest that dissipation due to bottom friction is related to some sort of friction coefficient f_w and the third power of the amplitude of the horizontal orbital velocity at the bottom, $\hat{U}_\delta$ (from now on referred to as U_{orb}). This equation is the basis of the following approach to describe wave energy dissipation as function of some vegetation characteristics:

The dissipation due to a piece of vegetation stem with height dz is:

$$\frac{4}{3\pi}\rho \cdot U_{orb}^3 \cdot f_w \cdot d \cdot dz \tag{5.5}$$

Herein is d the diameter of the stem.
The dissipation over one square meter per dz of vegetation height is now:

$$\frac{4}{3\pi}\rho \cdot U_{orb}^3 \cdot f_w \cdot d \cdot n \cdot dz \tag{5.6}$$

in which n is the vegetation density per square meter.
Calculating the dissipation over the total vegetation height requires integration over the vegetation height of the orbital velocity amplitude and vegetation density when these two are considered to vary over water depth z:

$$D_{vegetation} = \frac{4}{3\pi} \rho \cdot f_w \cdot d \cdot \int\limits_{z=-h}^{-h+hveg} n \cdot U_{orb}^3 \, dz \qquad (5.7)$$

In this approach three vegetation characteristics are included. Vegetation density, stem diameter and vegetation height (in the integral). Also the friction factor f_w is a vegetation characteristic. But this factor is vegetation type specific. The factor carries plant information like the vegetation stiffness and the roughness of the plant surface. This factor cannot be compared to the friction factor for bottom roughness in equation 5.4, because this value does not represent all characteristics of the vegetation that causes the dissipation. A comparable factor to the bottom friction of equation 5.4 should also contain the other vegetation characteristics like density, height and diameter.

It is clear that for the determination of the dissipation due to vegetation detailed information of the vegetation is required. For the Paulinaschor case, that information is available (NIOO). Vegetation samples have been taken from each transect location. Over an area of 0.25 m^2 all the plants are cut off. The total number of plants for each sample is calculated. From these samples sub-samples are taken of 31 plants (for one sub-sample this number was higher). These sub-samples have been analyzed. Not only stem height and diameter is measured, also information of the number of leaves per stem, the height of the leave implant (i.e. where the leave grows out of the stem) and the length of the leafs is gathered. With this information vertical plant structure density profiles can be calculated.

Although the vegetation characteristics are recorded in September, based on expert judgement the same characteristics will be assumed for August.

Roughly two methods will be used to apply above theory on the real case. The difference in the two approaches is the way in treating the plant density. In one approach plant density is assumed to be constant over depth for simplification, this assumption has not been made in the second approach. Besides the distinction between treating the density, for each approach a sub-distinction has been made for treating the horizontal orbital velocity amplitude. One way to calculate this value is just using the linear wave theory:

$$U_{orb}(z) = \omega \cdot a \frac{\cosh k(h+z)}{\sinh kh} \qquad (5.8)$$

The other way is using the shallow water approximation, which implies that

$$k \cdot h < 0.1\pi \qquad (5.9)$$

When this is true $\sinh kh$ approaches kh and $\cosh kh$ approaches 1.
The orbital velocity now reads:

$$U_{orb} = \frac{\omega \cdot a}{k \cdot h} = \frac{1}{2} H \sqrt{\frac{g}{h}} \qquad (5.10)$$

Equation 5.10 shows that this way of treating the velocity neglects the dependency of the water depth z. Using shallow water conditions can be doubted in this case. Equation 5.10 is not valid in most cases of this study. However, it is also unknown if the orbital velocity profile in vegetation fields is as linear wave theory describes it. Some former flume experiments shows that flow velocity in vegetation fields decreases rapidly just in the top of the vegetation. Further down in the vegetation the velocity remains almost constant. If this profile is also applicable for orbital velocities is unclear right now. Therefore, the approaches will be used simultaneously.

5.2   Plant density constant in z-direction

In this approach is only the stem density used as total vegetation density. The density is assumed to remain constant in vertical direction. Furthermore the calculations are made using an averaged plant height. Although density doesn't vary in z-direction, it does vary

along the transect and so does the vegetation height and stem diameter. These values are available for each measuring location. Table 5.1 summarizes these data.

Location	Plant height (cm)	Stem diameter (mm)	Stem density (m^{-2})
P0	41,75	4,3	872
P1	29,75	3,53	796
P2	38,28	3,9	620
P3	33,57	2,89	1476
P4	36,29	3,85	1308
P5	30,68	3,75	1704

Table 5.1: Vegetation characteristics.

The dissipation can now be calculated with the following equation:

$$D_{vegetation} = \frac{4}{3\pi} \rho \cdot f_w \cdot d \cdot n \cdot \int_{z=-h}^{-h+hveg} U_{orb}^3 dz \tag{5.11}$$

This equation is distracted from equation 5.7, but now the density can be left out of the integral since it is not z-dependable anymore.

5.2.1 Linear wave theory

For the linear wave theory approach of the orbital velocity, it follows that:

$$D_{vegetation} = \frac{4}{3\pi} \rho \cdot f_w \cdot d \cdot n \cdot \int_{z=-h}^{-h+hveg} \left(\frac{\cosh k(h+z)}{\sinh kh} \omega a \right)^3 dz \tag{5.12}$$

With $\omega = 2\pi / T$ and $a = H / 2$ this can be written as:

$$D_{vegetation} = \frac{4H^3 \pi^2 \rho \cdot f_w \cdot d \cdot n}{3T^3 \sinh^3 kh} \int_{z=-h}^{-h+hveg} \cosh^3 k(h+z) dz \tag{5.13}$$

After integration it follows that:

$$D_{vegetation} = \frac{4H^3 \pi^2 \rho \cdot f_w \cdot d \cdot n}{3T^3 \sinh^3 kh} \left[\frac{3\sinh k(h+z)}{4k} + \frac{\sinh 3k(h+z)}{12k} \right]_{-h}^{-h+hveg} \tag{5.14}$$

Followed by:

$$D_{vegetation} = \frac{H^3 \pi^2 \rho \cdot f_w \cdot d \cdot n}{3kT^3 \sinh^3 kh} \left(3\sinh kh_{veg} + \frac{\sinh 3kh_{veg}}{3} \right) \tag{5.15}$$

5.2.2 Shallow water approximation

When using the shallow water approximation, the orbital velocity comes out of the integral, since it is not z-dependent anymore. Using equation 5.11 it follows that:

$$D_{vegetation} = \frac{4}{3\pi} \rho \cdot f_w \cdot d \cdot n \cdot U_{orb}^3 \int_{z=-h}^{-h+hveg} dz = \frac{4}{3\pi} \rho \cdot f_w \cdot d \cdot n \cdot U_{orb}^3 \cdot h_{veg} \tag{5.16}$$

Using equation 5.10, it follows:

$$D_{vegetation} = \frac{1}{6\pi} \rho \cdot f_w \cdot d \cdot n \cdot h_{veg} \cdot H^3 \cdot \left(\frac{g}{h} \right)^{3/2}$$ (5.17)

5.3 Variable plant density in z-direction

Based on the detailed vegetation data from the NIOO, the vegetation density does not seem to be constant over the depth. Another comment on the previous method is that plant density is determined only by the number of plant stems, while most space is taken by the leafs. Using this approach, plant density will be interpreted as plant structure density. Plant structure includes besides the stem, also the leaves of the plant. Plant structure is assumed to vary over depth z in this method, which means that equation 5.7 must be used and not the simplified formulation using a constant density in z-direction.

Some assumptions using this method are:
The horizontal thickness of the leafs is equal to the stem diameter to avoid complex formulations. The term 'horizontal thickness' is introduced here because the leafs make an angle of approximately 45° with the plant stem. The leaf length is corrected for this angle. So when a leaf's stem implant is at a height of 10 cm and the leaf length is 10 cm, the top of the leaf is not situated at a height of 20 cm but at:
10+10cos(45) cm<20 cm
The leafs seems to be shorter that way, hence will the horizontal thickness used, to keep the total leave surface constant (figure 5.1).
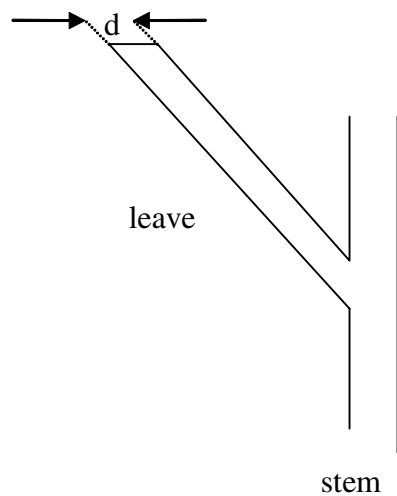
Figure 5.1: horizontal leaf thickness is denoted by d.

With the available vegetation data, such as leaf length, implant height and stem height, the structure density as function of depth has to be determined. This is realized by counting the number of structures per cm of height per plant. In figure 5.2 this method is represented in a schematic way. Note that in this figure plant density is not determined per cm height but, because of the simplicity of this case, determined exactly. Next, these numbers have to be summed up for all plants of the sub-samples (as described in paragraph 5.1).
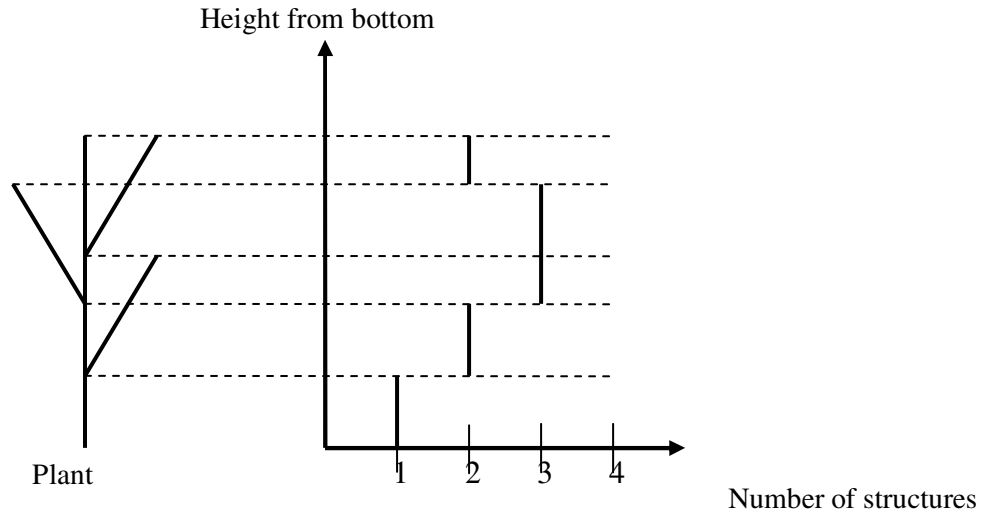
Figure 5.2: determination of structure density as function of z.

The total plant structure density as a function z is known now for each sub-sample, denoted as *n'(z)*. Since the density per m^2 is required, this *n'(z)* has to be converted using the next formula:

$$n(z) = 4 \frac{\text{(number of plants per 0,25 m}^2)}{\text{sample size}} n'(z) \qquad (5.18)$$

The results of this analysis for all transect locations can be found in graph 5.1 to 5.6.
The graphs clearly show that highest densities can be found at half maximum plant height.

Now that plant density is known the dissipation can be calculated using the two methods for the determination of the orbital velocity.

5.3.1   Shallow water approximation

First, the shallow water approximation will be used. In this case, the orbital velocity comes out of the integral again and dissipation can be calculated as follows, using equation 5.18:

$$D_{vegetation} = \frac{16}{3\pi} \rho \cdot f_w \cdot d \cdot U_{orb}^3 \frac{\text{(number of plants per 0,25 m}^2)}{\text{sample size}} \int\limits_{z=-h}^{-h+hveg} n'(z)dz \quad (5.19)$$

Together with 5.10 it follows that:

$$D_{vegetation} = \frac{2}{3\pi} \rho \cdot f_w \cdot d \cdot H^3 \left(\frac{g}{h} \right)^{3/2} \frac{\text{(number of plants per 0,25 m}^2)}{\text{sample size}} \int\limits_{z=-h}^{-h+hveg} n'(z)dz \,(5.20)$$

The only z-dependable factor is *n'(z)*. The problem is that no exact formula is known for this density. Because of the capricious shape of the density graphs, it is not easy to determine an accurate trend line of which the equation can be calculated. Therefore a numerical approach of the integral will be used. This is very simple, especially when for *dz* the value of 1 cm is chosen, because structure density was determined for each *d z* = 1cm. Adding all these values for *z = -h to h$_{veg}$* and division by 100 (for compensating the usage of cm) gives $\int\limits_{z=-h}^{-h+hveg} n'(z)dz$ with *dz* = 1 cm.

Now the dissipation can be calculated. Table 5.2 gives an overview of the required vegetation input.

Location	Sample size	# plants per 0.25 m^2	factor	Integral 1	Integral 2
P0	31	218	7,03	28,66	201,54
P1	31	199	6,42	23,64	151,75
P2	31	155	5,00	24,3	121,50
P3	31	369	11,90	22,32	265,68
P4	37	321	8,68	27,99	242,83
P5	31	426	13,74	21,72	298,47

Table 5.2: Vegetation related input data with 'factor' the multiplying factor for calculating density per 0.25m^2 (# of plants/0.25m^2/sample size),'integral 1' the integral of n'(z) over vegetation height for each sub-sample and 'integral 2' the first integral corrected for 0.25m^2.

5.3.2 Linear wave theory

When the assumption of shallow water conditions is considered as not valid, equation 5.7 will be used in calculating the horizontal orbital velocity amplitude. However, this equation must be used now for the dissipation, without any simplifications. The problem that arises now is that there is no formulation for the density as function of depth. In previous paragraph the integral over the density could be calculated by using a numerical approach and in paragraph 5.2.1 the integral over the orbital velocity was determined, but these methods cannot be used simultaneously here, since:

$$\int_{z=-h}^{-h+hveg} n \cdot U_{orb}^3 dz \neq \int_{z=-h}^{-h+hveg} n\, dz \cdot \int_{z=-h}^{-h+hveg} U_{orb}^3 dz \qquad (5.21)$$

To avoid this problem, an attempt is made to calculate the whole integral with a numerical approach. This means that the horizontal orbital velocity amplitude has to be calculated for each dz (= 1 cm), for each time and location. After applying a 3rd power to these orbital velocities, the values are multiplied by the density $n'(z)$ for each dz. The results of this calculations are summed up for all $z = -h$ to $-h+h_{veg}$ and divided by 100 because of the cm-units. Thus the following approach is used:

$$\int_{z=-h}^{-h+hveg} n \cdot U_{orb}^3 dz \approx \sum_{z=1}^{h_{veg}/\Delta z} n(z)\, U(z)_{orb}^3 \cdot \Delta z, \text{ with } \Delta z = 1 \text{ cm} \qquad (5.22)$$

The actual formula for calculating the dissipation is now:

$$D_{vegetation} = \frac{4}{3\pi}\rho \cdot f_w \cdot d \cdot \sum_{z=1}^{h_{veg}/\Delta z} n(z)\, U(z)_{orb}^3 \cdot \Delta z$$

$$D_{vegetation} = \frac{4}{75\pi}\rho \cdot f_w \cdot d \cdot \frac{(\text{number of plants per 0,25 m}^2)}{\text{sample size}} \sum_{z=1}^{h_{veg}/\Delta z} n'(z)\, U(z)_{orb}^3 \cdot \Delta z \quad (5.23)$$

No input data for this method will be showed here, because the last part of above formula has to be calculated for each location and each time, which means too many data for convenient tables.

5.4 A comparison between theory and observed dissipation

In chapter 4 the method to calculate the observed wave energy dissipation is discussed. This chapter deals with a theoretical approach, to calculate the dissipation on the basis of orbital velocity and some vegetation characteristics. For each time and location the dissipation can

be calculated in both ways. In this manner a comparison can be made between theory and reality. The only unknown factor in the theoretical approach is the friction factor f_w. When leaving this factor out of the calculations and plotting of the observed dissipations against the theoretical ones, this friction factor f_w can be determined on the basis of the slope of the line in the graph. The accuracy of the theoretical formulations can also be revealed on the basis of the correlation between the points. When all points are on a straight line, the correlation coefficient becomes 1, which means that theory is able to predict the exact dissipation. This will not be the case, since assumptions have been made, measuring errors and calculation errors are unavoidable, etc. The correlation can demonstrate which method in calculating theoretical dissipation is the most accurate one and also if the assumptions that are made are correct.

In graph 5.7 this graph is shown for the constant density method with the orbital velocity calculated according to linear wave theory. In graph 5.8 this method is illustrated using shallow water conditions in determining the orbital velocity. graphs 5.9 to 5.10 show the same plots, but for the varying density method. All graphs show the linear trend line that is the best fit through the points and is forced to cross (0,0) because this is a logical certainty. The value R^2 and the equation of the trend lines can also be found in the graphs.

In table 5.3 the results of the comparison are summarized by means of the friction factor f_w (i.e. the slope of the trend line through the points) and the coefficients R^2 and R, the real correlation coefficient.

Method	Friction coefficient f_w	R^2	R
$n(z)$=constant, U linear wave theory	0,46	0,46	0,68
$n(z)$=constant, U shallow water conditions	0,48	0,66	0,81
$n(z)$=variable, U linear wave theory	1,29	0,51	0,71
$n(z)$=variable, U shallow water conditions	1,06	0,65	0,80

Table 5.3: Results of comparison between theory and reality.

The results of above analysis are satisfying. For the shallow water approximation, the correlation coefficients are around the 0,8 with both ($n(z)$constant or variable) methods. For correlation, it does not make much difference whether the detailed approach of a variable structure density is used or not. The friction coefficient on the other hand is fairly different for both methods. In the next paragraph, more discussion can be found concerning the friction.

5.5   Friction due to vegetation

From the previous paragraphs is has become clear that the factor f_w is not a good measure for the total friction that is caused by the vegetation. The fact that this factor differs so much using different approaches for vegetation density supports this point of view. It is obvious that, in comparison with the dissipation due to bottom friction of Van Rijn (equation 5.4), some variables are added to this equation, for making it suitable in describing dissipation due to vegetation, that also influences the total amount of friction. These variables are vegetation density n, vegetation height h_{veg} and stem thickness or diameter d. Together with the factor f_w these variables determine the total friction factor. This total friction factor will

be called c_w. For the different approaches in treating density and orbital velocity, different formulations are needed to calculate this total friction. The equations can be extracted from the formulations that calculate the dissipation for each method.

Constant density over depth, shallow water conditions
This is the simplest case. From equation 5.17 it follows that:

$$c_w = f_w \cdot d \cdot n \cdot h_{veg} \qquad (5.24)$$

Constant density over depth, linear wave theory
Using this method, c_w can not be calculated exactly. The vegetation height is tied up in the integral over the orbital velocity, which is not a part of the total friction. But as a good approach equation 5.24 can be used here as well, with h_{veg} the average vegetation height, and not as in equation 5.7 the maximum value of it.

Variable density over depth, shallow water conditions

$$c_w = 4 f_w \cdot d \cdot \frac{(\text{number of plants per } 0,25 \text{ m}^2)}{\text{sample size}} \int_{z=-h}^{-h+hveg} n'(z) dz \qquad (5.25)$$

Variable density over depth, linear wave theory
For the same reasons as with the previous approach (constant density), equation 5.25 will be used here.
The total vegetation frictions c_w can now be calculated for the different measuring locations and with the different approaches. The results are given in table 5.4.

	$n(z)$ constant		$n(z)$ variable	
fw:	*1,06*	*1,29*	*0,48*	*0,46*
	U **shallow**	*U* **lin wt**	*U* **shallow**	*U* **lin wt**
Location	*cw*	*cw*	*cw*	*cw*
P0	1,66	2,02	1,68	1,61
P1	0,88	1,08	1,04	0,99
P2	0,98	1,19	0,92	0,88
P3	1,52	1,85	1,49	1,42
P4	1,93	2,36	1,81	1,73
P5	2,07	2,53	2,17	2,07

Table 5.4: Total friction c_w for the different methods.

Now the difference in friction factor f_w that showed up in the previous paragraph can be explained. The method in which plant density is considered to be constant over depth, treats plant density as only the number of stems per m². Consequence of this is that information about the friction caused by the leafs is all stored in the friction factor f_w. The other method treats the density as structure density in which leafs are included. Now, the friction that the leafs cause is placed out of the friction factor, which reduces this value pretty much.
It is useful to realize what else this friction factor f_w describes. It strongly depends on the plant stiffness and it may also depend upon the roughness of the plant's surface and the shape of the plant. It is clear that this factor is close connected to the vegetation type. The fact that the other vegetation characteristics like density, height and diameter are left out of this factor is quite useful. These characteristics may vary for the same vegetation type at different places and times, while the characteristics inside this f_w factor are more or less constant in all cases. In doing this analysis for more vegetation types, the matching friction

coefficients can be calculated. In that way, wave energy dissipation can be calculated using above theory, at any location with any vegetation type for varying vegetation characteristics, like density, height and diameter.

6 The SWAN Model

SWAN is a numerical wave model to obtain realistic estimates of wave parameters in coastal areas, lakes and estuaries from given wind, bottom, and current conditions. The model is based on the wave action balance equation (or energy balance in the absence of currents) with sources and sinks.

The Swan model will be used to model the influence of vegetation on wave attenuation. Therefore the model has to be calibrated and validated. This will be described in the next chapter. This chapter deals with the theoretical background of the model. The first paragraph will give an overview of the basic equations of the model. The subject of the second paragraph is the way dissipation is modelled in SWAN. In the last paragraph, some research will be done on the possibility of putting in the vegetation influence into SWAN. The outcome of this investigation must be a certain parameter which is able to describe the different vegetation characteristics.

6.1   The basic equations of SWAN

In SWAN the waves are described with the two-dimensional wave action density spectrum, even when non-linear phenomena dominate (e.g., in the surf zone). The rational for using the spectrum in such highly non-linear conditions is that, even in such conditions it seems possible to predict with reasonable accuracy this spectral distribution of the second order moment of the waves (although it may not be sufficient to fully describe the waves statistically). The spectrum that is considered in SWAN is the action density spectrum $N(\sigma,\theta)$ rather than the energy density spectrum $E(\sigma,\theta)$ since in the presence of currents, action density is conserved whereas energy density is not (e.g., Whitham, 1974). The independent variables are the relative frequency σ (as observed in a frame of reference moving with the action propagation velocity) and the wave direction θ (the direction normal to the wave crest of each spectral component). The action density is equal to the energy density divided by the relative frequency:

Error! Objects cannot be created from editing field codes. In SWAN this spectrum may vary in time and space.

6.1.1   Action balance equation

In SWAN the evolution of the wave spectrum is described by the spectral action balance equation which for Cartesian coordinates is (e.g., Hasselmann et al., 1973):

$$\frac{\partial}{\partial t}N + \frac{\partial}{\partial x}c_x N + \frac{\partial}{\partial y}c_y N + \frac{\partial}{\partial \sigma}c_\sigma N + \frac{\partial}{\partial \theta}c_\theta N = \frac{S}{\sigma} \qquad (6.1)$$

The first term in the left-hand side of this equation represents the local rate of change of action density in time, the second and third term represent propagation of action in geographical space (with propagation velocities c_x and c_y in x- and y-space, respectively). The fourth term represents shifting of the relative frequency due to variations in depths and currents (with propagation velocity c_σ in σ-space). The fifth term represents depth-induced and current-induced refraction (with propagation velocity c_θ in θ-space). The expressions for these propagation speeds are taken from linear wave theory. The term

S $(=S(\sigma,\theta))$ at the right hand side of the action balance equation is the source term in terms of energy density representing the effects of generation, dissipation and nonlinear wave-wave interactions.

6.1.2   Wind input

Transfer of wind energy to the waves is described with a resonance mechanism and a feedback mechanism. The corresponding source term for these mechanisms is commonly described as the sum of linear and exponential growth:

$$S_{in}(\sigma,\theta)=A+B\,E(\sigma,\theta) \tag{6.2}$$

in which A and B depend on wave frequency and direction, and wind speed and direction.

6.1.3   Dissipation

The dissipation term of wave energy is represented by the summation of three different contributions: white capping $S_{ds,w}(\sigma,\theta)$, bottom friction $S_{ds,b}(\sigma,\theta)$ and depth-induced breaking $S_{ds,br}(\sigma,\theta)$.

1. Whitecapping is primarily controlled by the steepness of the waves. In presently operating third-generation wave models (including SWAN) the white capping formulations are based on a pulse-based model (Hasselmann, 1974), as adapted by the WAMDI group (1988):

$$S_{ds,w}(\sigma,\theta)=-\Gamma\,\tilde{\sigma}\frac{k}{\tilde{k}}E(\sigma,\theta) \tag{6.3}$$

where Γ is a steepness dependent coefficient, k is wave number and $\tilde{\sigma}$ and $\tilde{k}$ denote a mean frequency and a mean wave number, respectively (cf. the WAMDI group, 1988).

2. Depth-induced dissipation may be caused by bottom friction which can generally be represented as:

$$S_{ds,b}(\sigma,\theta)=-C_{bottom}\frac{\sigma^2}{g^2\sinh^2(kh)}E(\sigma,\theta) \tag{6.4}$$

in which C_{bottom} is a bottom friction coefficient. JONSWAP suggested to use an empirically obtained constant. It seems to perform well in many different conditions as long as a suitable value is chosen (typically different for swell and wind sea).

3. The process of depth-induced wave-breaking is still poorly understood and little is known about its spectral modelling. In contrast to this, the total dissipation (i.e., integrated over the spectrum) due to this type of wave breaking can be well modelled with the dissipation of a bore applied to the breaking waves in a random field. the expression that is used in SWAN is:

$$S_{ds,br}(\sigma,\theta)=\frac{D_{tot}}{E_{tot}}E(\sigma,\theta) \tag{6.5}$$

in which E_{tot} is the total wave energy and D_{tot} (which is negative) is the rate of dissipation of the total energy due to wave breaking SWAN results. Chen and Guza (1997) inferred from observations and simulations with a Boussinesq model that the high-frequency levels are insensitive to such frequency dependency because an increased dissipation

The remaining equations of the model are not of great importance to this subject and are left out of this paragraph. The whole theory of SWAN can be found in appendix A6.

6.2   The modelling of dissipation

In the last paragraph three types of dissipation are described that are modelled in SWAN. For this study the focus is on the formulation of dissipation due to bottom friction. The bottom friction models that have been selected for SWAN are the empirical model of JONSWAP, the drag law model of Collins and the eddy viscosity model of Madsen et al. The formulations for these bottom friction models can all be expressed in the following form (equation 6.4):

$$S_{ds,b}(\sigma,\theta) = -C_{bottom}\frac{\sigma^2}{g^2\sinh^2(kh)}E(\sigma,\theta) \qquad (6.4)$$

in which C_{bottom} is a bottom friction coefficient that generally depends on the bottom orbital motion represented by U_{orb}:

$$U_{orb}^2 = \int_0^{2\pi}\int_0^{\infty}\frac{\sigma^2}{\sinh^2(kh)}E(\sigma,\theta)d\sigma d\theta \qquad (6.6)$$

Hasselmann et al. (1973) found from the results of the JONSWAP experiment $C_{bottom} = C_{JON} = 0.038$ m^{2}s^{-3} for swell conditions. Bouws and Komen (1983) selected a bottom friction coefficient of $C_{JON} = 0.067$ m^{2}s^{-3} for fully developed wave conditions in shallow water. Both values are available in SWAN.

The expression of Collins (1972) is based on a conventional formulation for periodic waves with the appropriate parameters adapted to suit a random wave field. The dissipation rate is calculated with the conventional bottom friction formulation of equation 6.4 in which the bottom friction coefficient is

$$C_{bottom} = c_f \cdot g \cdot U_{orb} \qquad (6.7)$$

with c_f the Collins friction factor (default value is 0.015).

Madsen et al. (1988) derived a formulation similar to that of Hasselmann and Collins but in their model the bottom friction factor is a function of the bottom roughness height and the actual wave conditions. Their bottom friction coefficient is given by:

$$C_{bottom} = f_w\frac{g}{\sqrt{2}}U_{orb} \qquad (6.8)$$

in which f_w is a non-dimensional friction factor estimated by using the formulation of Jonsson:

$$\frac{1}{4\sqrt{f_w}} + \log_{10}\left[\frac{1}{4\sqrt{f_w}}\right] = m_f + \log_{10}\left[\frac{a_b}{K_N}\right] \qquad (6.9)$$

in which m_f =-0.08 (Jonsson and Carlsen, 1976) and a_b is a representative near-bottom excursion amplitude:

$$a_b^2 = 2\int_0^{2\pi}\int_0^{\infty}\frac{1}{\sinh^2(kh)}E(\sigma,\theta)d\sigma d\theta \qquad (6.10)$$

and K_N is the bottom roughness length scale. For values of a_b / K_N smaller than 1.57 the friction factor fw is 0.30 (Jonsson, 1980).

The question that arises now is which of the approaches is the most adequate in trying to model the influence of vegetation. During a SWAN workshop organized within the framework of the ESTPROC project, N. Booij, one of the developers of SWAN, declared that the best approach in this case is using the either the Madsen or the Collins expressions. Reasons for this are the fact that the friction coefficients in these two methods represent some sort of friction height, which can be quite applicable for describing vegetation influence. Due to some sort of bug within the Madsen formulation in the SWAN version that will be used (see next chapter), the Collins friction factor will be used.

In the next paragraph some further analysis will be done towards the Collins expressions.

6.3   The Collins versus the c_w friction factor

In the last paragraph of chapter 5 a way of describing the vegetation influence through a friction factor c_w is described. This factor was determined by vegetation characteristics like density, vegetation height, stem diameter and a vegetation type specific factor f_w. In the SWAN model, the Collins friction factor seems to be a good parameter to put vegetation influence into the wave model. It would be convenient to find out the relationship between these two factors, the c_w and the Collins factor. For that purpose, SWAN wave dissipation due to bottom friction (equation 6.4) will be rewritten to a form comparable to the way wave dissipation is described according to Van Rijn (equation 5.4).

Equation 6.4 reads:

$$S_{ds,b}(\sigma,\theta) = -C_{bottom}\frac{\sigma^2}{g^2\sinh^2(kh)}E(\sigma,\theta)\tag{6.4}$$

From equation 6.4 and 6.7 it follows that:

$$S_{ds,b}(\sigma,\theta) = -c_f U_{orb}\frac{\sigma^2}{g\sinh^2(kh)}E\tag{6.11}$$

With $\sigma = \omega$ $(= 2\pi/T)$ and E according to equation 4.3 this becomes:

$$S_{ds,b}(\sigma,\theta) = -c_f U_{orb}\cdot\rho\cdot H^2\frac{\omega^2}{8\sinh^2(kh)}\tag{6.12}$$

Furthermore, from linear wave theory it is known that:

$$U_{orb}(z) = \omega\cdot H\frac{\cosh k(h+z)}{2\sinh kh}\tag{6.13}$$

Approaching the bottom, thus $z = -h$, the horizontal velocity amplitude becomes constant:

$$U_{orb}(z) = \frac{\omega\cdot H}{2\sinh kh}\tag{6.14}$$

With this formulation, equation 6.11 can be written as follows:

$$S_{ds,b}(\sigma,\theta) = -c_f U_{orb}\cdot\rho\cdot\frac{1}{2}\cdot U_{orb}^2 = -\frac{1}{2}\cdot c_f\cdot\rho\cdot U_{orb}^3\tag{6.15}$$

This last equation shows a great similarity with the way dissipation was described by Van Rijn (equation 5.4). The slight differences are:
-    the minus sign in the SWAN expression. This is just a result of how dissipation is defined. In SWAN a negative dissipation causes a decrease in wave energy density, while in the approach of the previous chapters positive dissipation has been interpreted as the cause of energy loss.
-    the second difference is the factor ½. In van Rijns formulation this factor is slightly different, namely $4/(3\pi)\approx 0,42$.

The great similarity in the two formulations of wave energy dissipation gives a good opportunity to make SWAN suitable for vegetation influence. It seems possible to use the friction factors from paragraph 5.5 (see table 5.4) for a validation of the SWAN model. First, a rough calibration of the model is required to find out if the Collins values are of same order of magnitude as the c_w friction factor. These calibration and validation processes will be carried out in the next chapter.

7 SWAN Calibration and Validation

This chapter describes the calibration and validation of the SWAN model for vegetation influence on surface waves. Both processes are carried out on the basis of field data from the Paulinaschor, described earlier in this report. Usually calibration and validation are two connected processes; calibration gives an estimation of a certain value (calibration parameter) and this value is used to validate the model. Validation is normally done with other data than the data by which the calibration process is executed. But for this study the calibration process is used to get some sort of estimation of the calibration parameter, in this case the Collins friction factor c_f. When this factor is of the same order of magnitude as the friction factors c_w that are calculated in chapter 5, validation will be done with these friction values. If model results are close to reality, the Collins friction factor is a good parameter for representing the vegetation influence on waves. Besides that, the Collins factor can than be calculated easily for other situations, because of it's similarity with the c_w factor.

First, in paragraph 1, the definition of the different cases and input data that SWAN requires will be discussed. The second paragraph describes the calibration process, followed by the validation of the model in the third paragraph. Finally some sensitivity analysis will be carried out in the last paragraph.

7.1 Definition of the cases

All Swan runs described in this chapter will be executed within the Delft3D version of SWAN, that is Delft3D Waves. Delft3D is powerful software package that is capable of handling three-dimensional flow, waves, water quality, ecology, sediment transport and bottom morphology and is capable of handling the interactions between those processes. For the Delft3D Waves application, two wave models can be used: HISWA and SWAN. The advantage of working within the Delft3D environment is the user-friendly interface and consequently, an easy and quick case setup. This paragraph will give an overview of the input data that are required for the different cases. First of all a general discussion about the input data will be brought up, followed by an overview of these specific data for each case that will be modelled in SWAN. Obviously, to achieve useful reference material, the cases that will be modelled are the same cases as the ones that are analyzed in previous chapters.

7.1.1 1D modelling

SWAN is capable of modelling waves over 2D areas. However, in the Paulinaschor situation, wave height is measured only along a transect, that is pretty much 1D. 1D Schematizations are possible in SWAN. The problem with 1D schematizations is that wave energy flows out via the long sides of the model. This is because SWAN does not 'feel' borders along the sides of the model. So a very small wave will propagate, but at the same time, the wave will spread out very quickly, causing a strong decrease in wave height. Figure 7.1 illustrates this problem. The figure shows a wave at the boundary (left side of schematization) with wave height H_0 and wave width W_0. After some travelling of the wave in propagation direction, the wave width has increased to W_1 because of the spreading of the wave under an angle θ. The result of this is an decrease in wave height to H_1. The solution to this problem is to choose a very large schematization width, so that $W >> L$, in which L is the schematization length. By doing so, the waves in middle part (middle of the width) are not yet affected by the energy loss to the sides at the end of the schematization. This is showed in figure 7.2.
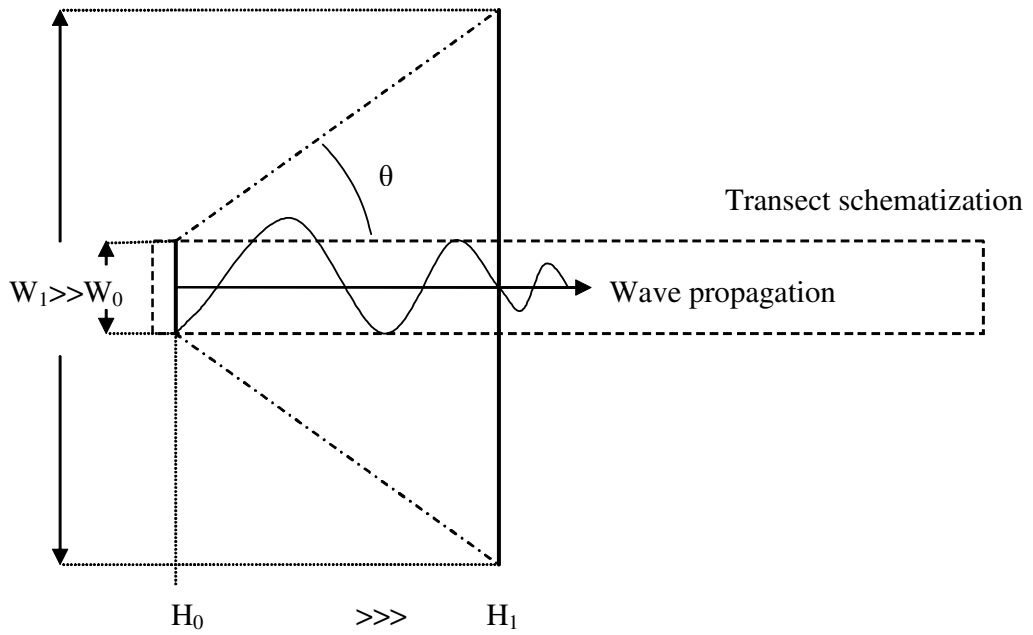
Figure 7.1: Problem of 1D schematization in SWAN.

Figure 7.2 is not at scale, in the real case the width will be chosen larger than the length. The figure shows the area where waves are affected by energy losses through the along sides and the area that is not yet affected by this energy loss. So, the analysis of the results of SWAN should be done using the wave height at the middle line of this schematization.
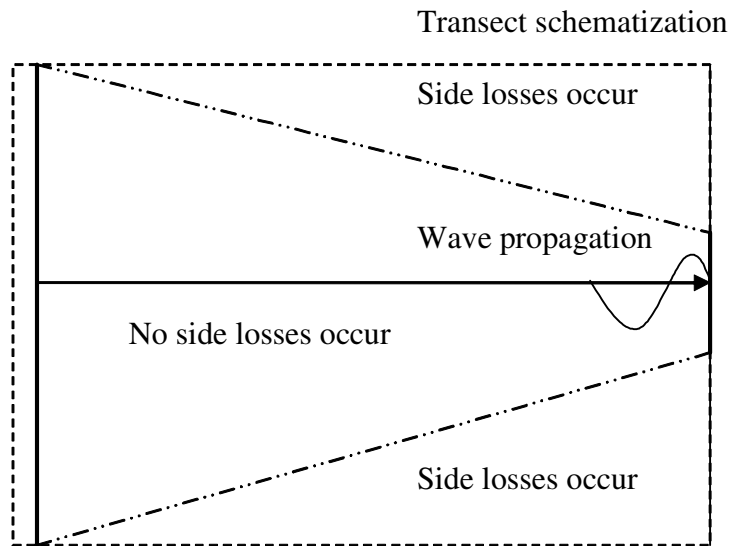
Figure 7.2: Correct schematization of 1D transect (not at scale).

7.1.2   Grids

Now the computational grids can be defined. A computational grid is a grid on which SWAN solves the wave action balance equation. The grid length, in SWAN referred to as the x length, is 26 meter, since this is the transect length. The x grid size is chosen to be 1 meter. In this way, calculations are sufficiently detailed. Furthermore, since the measuring locations at the transect where placed at a integer of x meters from the boundary (P7), the wave heights calculated by SWAN can be compared with the measured heights. To avoid the problem that is described above, the y length is chosen equal to 400 m, with a grid size of 100 m. Then the total number of cells is 26 x 4 = 104. The schematization is showed in figure 7.3. Only the results of $y = 200$ will be used for analysis, as told before.
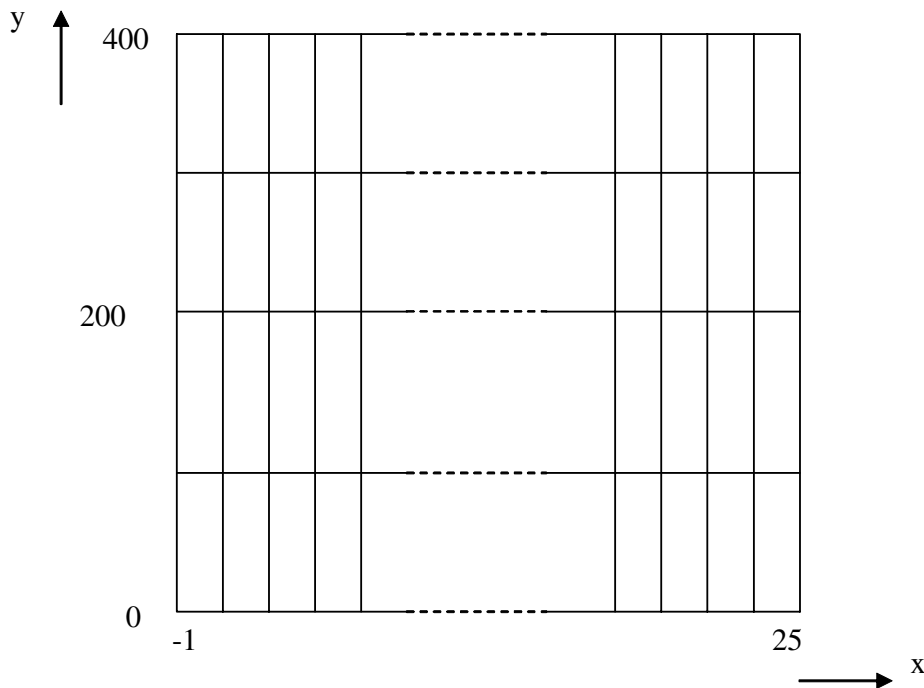
Figure 7.3: transect schematization in SWAN (not at scale).The x origin is chosen at -1, as the figure illustrates, so that the salt marsh's edge is at x = 0.

Now that computational grid is known, the bathymetric grids (bottom grids) can be defined. It is not necessary to put in bottom height in the same grid as the computational grid, but for this case there is no reason to create another grid for the bottom. The bathymetric data (figure 4.4) are interpolated on the computational grid in the x-direction. Since the focus is in fact on a 1D case, the same values will be used for each of the five y coordinates (0, 100, 200, 300 and 400).

7.1.3   Boundary conditions and tidal information

The boundary conditions that are required are:
- significant wave height,
- peak period (i.e. period belonging to the peak frequency of the waves),
- mean wave direction, in degrees clockwise relative to the north,
- width energy distribution; this is the directional standard deviation in degrees, for surface wind waves is the default value 4,
- the boundary orientation; since in the SWAN computations wave boundary conditions may be specified at 4 sides, it is necessary to indicate on which side the

boundary condition is applied by filling in the respective box with the orientations i.e. N (north), NE (Northeast) etc.

For all cases the boundary orientation is chosen at the west side, according to figure 7.3. Since the wave direction is assumed to be perpendicular to the coast (because of the large mud flat in front of the marsh, the waves have already been reflected in this direction), the incoming wave direction has been set to 270°.

The tidal information input concerns the different times and water levels by which the model will be executed for the same boundary condition. Since boundary conditions change for each time according to the measurements, only one time and water level is chosen for each case.

Table 7.1 gives an overview of all the input that is required for each case, aside from the input that is the same for each case and is given above already.

Cases	Boundary		Water level
	H1/3 [cm]	Tp [s]	[m NAP]
August 10			
16:30	6,79	6,40	2,57
17:15	6,53	3,56	2,19
18:00	5,88	2,13	1,81
18:30	7,85	2,29	1,47
18:45	8,56	2,29	1,28
August 12			
17:45	6,28	6,40	2,79
18:30	7,70	2,29	2,47
19:15	7,68	2,29	2,05
19:45	7,90	2,67	1,75
20:15	7,00	.3.56	1,37
20:30	5,81	1,88	1,12
September 10			
17:15	3,52	4,00	2,75
18:00	3,55	3,20	2,46
18:45	6,92	2,46	2,04
19:15	4,99	3,56	1,77
19:30	5,89	2,67	1,61
19:45	6,59	5,33	1,41
September 11			
18:15	5,65	6,40	2,58
19:00	6,06	4,00	2,21
19:45	6,32	3,20	1,79
20:15	6,44	4,00	1,46
20:30	5,40	4,38	1,26
20:45	7,60	2,67	1,03

Table 7.1: Input data for the SWAN runs.

7.2   SWAN calibration

The SWAN calibration is carried out on the basis of the calibration parameter, the Collins friction coefficient. This calibration process will provide information about the order of magnitude of the Collins coefficients in case of wave energy dissipation due to vegetated areas. The default value of the coefficient is 0,015. The model will be calibrated by changing this factor manually just as long as the wave height at the last measuring location P0 is in accordance with the field data. It must been said that for the whole transect one constant friction coefficient is used, while the vegetation data from along the transect show some fairly variation in roughness. Also the much lower friction of the area between P7 and P6, at the mud flat, will be neglected by modelling in this way, but for the purpose of getting some rough estimation about the magnitude of the Collins coefficients, this method will well suited.

For all cases the calibration process is executed. The results are summarized in table 7.2 Along with the Collins coefficients, the water levels and water depths at the boundary are given to provide some insight in the effect of water depth on the Collins coefficient.

Cases	Water level	Water depth	Collins coefficient
		at boundary (P7)	
	[m NAP]	[m]	[-]
August 10			
16:30	2,57	1,89	-
17:15	2,19	1,51	3,95
18:00	1,81	1,13	2,55
18:30	1,47	0,79	2,15
18:45	1,28	0,60	2,24
August 12			
17:45	2,79	2,11	-
18:30	2,47	1,79	-
19:15	2,05	1,37	2,80
19:45	1,75	1,07	2,01
20:15	1,37	0,69	1,22
20:30	1,12	0,45	1,28
September 10			
17:15	2,75	2,07	-
18:00	2,46	1,78	-
18:45	2,04	1,36	2,42
19:15	1,77	1,09	1,99
19:30	1,61	0,93	0,94
19:45	1,41	0,73	1,15
September 11			
18:15	2,58	1,90	-
19:00	2,21	1,53	0,05
19:45	1,79	1,11	1,33
20:15	1,46	0,78	1,02
20:30	1,26	0,58	1,01
20:45	1,03	0,36	0,39

Table 7.2: Results of the calibration

The calibration process could be carried out for all cases. Sometimes, the field data show an increase in wave height along the transect, while the model was not able to predict that

phenomenon, not even with Collins put at zero. This increase in wave height could be caused by changing wind conditions along the transect, while wind conditions in SWAN are set at constant. Also due to the vegetation, more shoaling could be caused than what would be expected on the basis of only the bottom bathymetry.

Nevertheless the calibration results show clearly that the Collins factor is two orders of magnitude bigger than the default value for unvegetated areas. There can be no clear correlation observed between water depth and Collins coefficient. Nevertheless some discussion about the relation between Collins coefficient and water depth will follow now:

- The cases of August 10, 17:15, August 12, 19:15 and September 10, 18:45:
  All these cases are distinguished by a relative large water depth, but still some wave height decrease, as follows from graphs 4.1 to 4.3. Due to that large water depth, a relative large Collins coefficient is needed to achieve the observed decrease in wave height.
- The case of September 11, 19:00:
  The water depth is of the same magnitude as the cases described above, but because wave height is increasing a little, the Collins coefficient can set to a very low value.

This two situations prove that the wave height is rather insensitive to the Collins coefficient under relative deep water conditions. The difference in wave height attenuation is small between the two situations, while the Collins coefficient variation is quite big.

For the remainder of the cases applies the following:

- If water depth decreases, the Collins factor increases. The waves seems to 'feel' the vegetation stronger when water surface approaches the top of the vegetation. Thus a smaller Collins coefficient for low water depth has the same, or even stronger, effect than a larger Collins coefficient by a higher water depth.
- Except for the data of September 11, the Collins coefficient increases again for the situation with lowest water depths. The reason for this is somewhat unclear. It seems that dissipation is reaching a maximum here and that, even though water depth is very low, the Collins coefficient must get bigger to achieve this amount of dissipation. A possible explanation for the fact that this phenomenon is not observed for the lowest water depth of September 11 could be, that in situations like these, with an extreme low water depth - water level is even under the highest vegetation tops - wave energy dissipation is less, because not all vegetation is under the water surface anymore. Because of that, the wave damping is less and so is the calibrated Collins coefficient.

7.3   SWAN validation

Previous parts of this report already stated that the validation of SWAN is not connected to the calibration; the founded values for the calibrated parameter, in this case the Collins coefficient, will not be used for validation. Neither is the validation executed for other cases than the calibration cases.

The validation process will be carried out on the basis of the c_w values that are calculated in chapter 5. It is proved that this c_w friction factor is closely related to the Collins coefficient. From paragraph 6.3 it follows that the difference in the two coefficients is a factor 0,42/0,5=0,84. The calculated c_w values, put together in table 5.4, can now be transformed in Collins coefficients using this factor. This is done in table 7.3.

Location	n(z) constant		n(z) variable	
	U shallow	U lin wt	U shallow	U lin wt
	Collins	Collins	Collins	Collins
P0	1,41	1,71	1,42	1,36
P1	0,75	0,91	0,88	0,84
P2	0,83	1,01	0,78	0,74
P3	1,29	1,57	1,26	1,21
P4	1,64	2,00	1,54	1,47
P5	1,76	2,15	1,84	1,76

Table 7.3: Collins factors for the different field locations.

Since the c_w value was determined using different approaches, the Collins coefficients are also calculated for those four methods.

While during the calibration of SWAN a constant Collins coefficient is used for the whole transect, now the input of variable friction field is desirable. Although this is not a standard option in the Delft3D user interface of SWAN, the stand alone version of the SWAN model can handle this feature. However, the Delft3D version of SWAN will be used; some input files can be adapted in such way that a variable friction field is used during the model run. As for the bottom bathymetry input, the variable friction input must be give up in the same way. So for each cell the value of the Collins coefficient is required. Again, interpolation will provide the friction values between the measuring locations, so that values are available for each meter of x direction. For the different values of the y direction, these values are the same, just like in the bathymetry input. The same friction field will be applied to all cases (paragraph 5.1).

For each case and for each method to determine the friction factor, the SWAN model is validated. Validation is based not only the wave height at the last location, but, thanks to the input of a varying friction field, the wave attenuation over the whole transect can be compared to the model outcome. In this way, a check is possible whether the differences in vegetation characteristics along the transect, through the different Collins coefficients, are translated in a certain characteristic attenuation.

The results of the validation are showed in the following graphs:
Graph 7.1 to 7.5: August 10
Graph 7.6 to 7.11: August 12
Graph 7.12 to 7.17: September 10
Graph 7.18 to 7.23: September 11

The different sub-cases are showed underneath each graph. The four different coloured lines represent the different methods that are used in the determination of the c_w values. For clarity, these four methods are:
-   *n con, shallow water*: vegetation density is assumed to be constant over depth, the orbital velocity amplitude is calculated in accordance with shallow water conditions
-   *n con, lin wt*: vegetation density is assumed to be constant over depth, the orbital velocity amplitude is calculated in accordance with the linear wave theory
-   *n var, shallow water*: vegetation density is assumed to vary with depth, the orbital velocity amplitude is calculated in accordance with shallow water conditions
-   *n var, lin wt:* vegetation density is assumed to vary with depth, the orbital velocity amplitude is calculated in accordance with the linear wave theory

The first conclusions that can be drawn from the graphics are:

- The validation of the SWAN model is quite satisfying. Although differences in wave height at the last location (x = 25, P0) between the model outcome and observed values are present, the attenuation corresponds well to the real wave measurements.

- Validation for the September cases turned out to be better than for August; an explanation for this could be the fact that the vegetation characteristics were measured in September. The vegetation in August is assumed to be equal. It is possible that this was not the case. And if vegetation characteristics were not the same in August as in September, than the Collins coefficients would also be different.

- Looking at the September cases, it is surprising how close SWAN predicts the attenuation, even for the cases with extreme low water depths, in which much wave damping is involved.

- The strong increase in wave height at the edge of the salt marsh, can not be modelled in a good way. This means that, as already mentioned in paragraph 4.2, this increasing wave heights are not the result of a change in bottom height only. It seems more plausible that the vegetation causes some extra shoaling of the waves. Also reflection of the waves by the vegetation could explain this. Although SWAN is able to model the processes of shoaling and reflection, due to the way the vegetation is modelled now, just as an enlarged bottom friction, SWAN does not see the vegetation as an obstacle that causes shoaling and reflection.

- There is little difference in results between the four methods that are used to determine the Collins coefficients. The only thing that stands out somewhat is that the approach *n con, lin wt* is mostly different from the rest. In the September cases this method usually gives the worse prediction, while for the August cases it is just the best one. But this must have something to do with the shift in prediction between August and September, as described above.

- Although the results are good, if more information is gathered about the vertical velocity profile in the vegetation, results may become better. Now two methods are use to calculate the orbital velocity, namely the linear wave theory and the shallow water approximation. But none of these methods will be the exact one for the velocity calculation in the vegetation.

Some more results of the validation are put together in table 7.4. The table shows the amount of damping of the waves between the boundary (x = -1m) and the last field location, P0 (x = 25m). The damping is calculated as follows:

$$Damping = \frac{H_{P0,x=25}}{H_{P7,x=-1}} \times 100\% \qquad\qquad (7.1)$$

Here again the results of SWAN compared to the measurements are in good correspondence with each other. Only for low water depth cases, the damping may show quite some difference, due to the low wave heights at the end of the transect. Small differences are then relatively large.

	Water level	Depth at boundary	Wave damping (%)				
			Observed	n con		n var	
	[m NAP]	[m]		shallow	lin wt	shallow	lin wt
August 10							
16:30	2,57	1,89	**84,7**	95,3	93,7	95,3	95,6
17:15	2,19	1,51	**85,1**	94,1	92,6	94,0	94,3
18:00	1,81	1,13	**88,1**	93,1	91,8	93,1	93,3
18:30	1,47	0,79	**60,0**	73,6	69,8	73,4	74,3
18:45	1,28	0,60	**33,9**	49,8	45,0	49,4	50,5
August 12							
17:45	2,79	2,11	**107,6**	97,6	96,5	97,6	97,8
18:30	2,47	1,79	**101,9**	97,2	96,6	97,2	97,3
19:15	2,05	1,37	**86,1**	92,4	90,9	92,4	92,7
19:45	1,75	1,07	**71,2**	81,5	78,1	81,4	82,1
20:15	1,37	0,69	**49,4**	53,1	47,8	52,8	54,0
20:30	1,12	0,45	**19,5**	22,3	19,2	21,8	22,6
September 10							
17:15	2,75	2,07	**108,5**	99,0	98,4	99,0	99,2
18:00	2,46	1,78	**104,5**	98,1	97,4	98,1	98,2
18:45	2,04	1,36	**85,4**	92,4	90,8	92,4	92,7
19:15	1,77	1,09	**77,2**	87,2	84,2	87,1	87,7
19:30	1,61	0,93	**83,9**	79,3	75,6	79,2	80,0
19:45	1,41	0,73	**56,8**	56,0	50,7	55,8	57,0
September 11							
18:15	2,58	1,90	**97,2**	96,4	95,0	96,4	96,7
19:00	2,21	1,53	**102,1**	93,6	91,8	93,6	93,9
19:45	1,79	1,11	**78,2**	85,9	82,9	85,8	86,4
20:15	1,46	0,78	**62,3**	65,6	60,5	65,4	66,5
20:30	1,26	0,58	**44,6**	46,9	41,6	46,5	47,7
20:45	1,03	0,36	**12,8**	4,9	4,0	4,6	4,9

Table 7.4: Observed wave damping versus model wave damping for the different methods.

7.4   Sensitivity analysis

A sensitivity analysis will be carried out in this paragraph. The purpose of this analysis is to obtain a better understanding of wave attenuation changes according to SWAN, when input data is changed. In this analysis, two situations will be studied. The first one concerns a variation in the friction field. Within the second situation, the boundary wave height will be enlarged. The analysis will be applied to three cases of September 11, namely 19:00, 20:15 and 20:45. In this way the sensitivity is analysed for varying water depths.

7.4.1   Friction sensitivity

Three cases will be discussed:
-   all Collins coefficients are reduced by 50%; according to equations 5.24 and 5.25
    this means that either the average plant height is halved, the plant density is halved,
    the plant diameter is halved, or the friction value f_w is halved, meaning that an other

type of vegetation is present. A combination of above options is also possible, as long as the friction coefficient is reduced by 50%.
-   all Collins coefficients are reduced by 75%; see above reasoning, but now for 75%
-   the Collins coefficients along the whole transect will be set to the default value of 0,015, meaning that no vegetation is present at the marsh

The fact that only cases are studied with lower frictions than the original case is logical, since in the original situation the vegetation density and height were at maximum in these months throughout a year. So by lowering the friction value, wave attenuation can be studies for example in the winter months, when vegetation has died back.

7.4.2   Boundary wave height sensitivity

Since the wave height during the measuring periods were not that high, no good representation is obtained how waves attenuates during conditions of higher waves, for example during storms. In this analysis wave height at the boundary is set to 150% and 200% of its original values. Since storms often occur in autumn or winter, the analysis is also been carried out for the lower friction situation of no vegetation.

7.4.3   Results

The results of above described sensitivity analyses can be found in graph 7.24 to 7.26, for the friction sensitivity, and graph 7.27 to 7.32 (note that the scales are not the same for all graphs) for the boundary wave height sensitivity analysis.
The results are also represented in a numerical way in table 7.5, giving wave damping, according to equation 7.1, for the different cases.

Collins sensitivity

Case	water level [m NAP]	h boundary [m]	Original	Collins -50%	Collins -75%	No vegetation
19:00	2,21	1,53	93,6	98,0	100,3	102,7
20:15	1,46	0,78	65,6	81,4	92,6	106,7
20:45	1,04	0,36	4,9	9,6	18,2	36,9

Hs boundary sensitivity

	water level [m NAP]	h boundary [m]	Original friction		No vegetation	
			Hs 150%	Hs 200%	Hs 150%	Hs 200%
19:00	2,21	1,53	89,6	86,1	102,6	102,6
20:15	1,46	1,11	52,4	45,7	106,8	107,0
20:45	1,04	0,78	3,6	2,7	26,7	19,6

Table 7.5: Wave damping for the different cases of sensitivity analysis.

To start with the friction sensitivity analysis, for the case with the highest water level the Collins variation results only in small differences in wave height. This points out that for relative deep water, wave height is quite insensitive for variations in Collins coefficient. This was also one of the conclusions from the SWAN calibration. When water levels decrease, differences in wave damping becomes bigger; the difference in damping between the original friction situation and the situation with no vegetation is more than 40%. In the

case of the lowest water level (20:45) this difference is decreasing again, because of the fact that the wave are getting so small now, that dissipation is getting less (since dissipation is also determined by wave height, see for example equation 5.17). However, the graph shows clearly that the point where the biggest wave height reduction appears is much further away from the boundary for the situation with no vegetation than for the situation with the original Collins coefficients.

Concerning the boundary wave height sensitivity analysis, it turns out that for the low water conditions the wave heights are reduced strongly to about 3% of its original value. When no vegetation is present, only reduction to 20% is achieved. Even for some higher water levels, vegetation have a significant influence on wave height reduction; reductions to 89,6% and 86,1% for the situation with vegetation versus 102,6% for the situation with no vegetation.

8 Conclusion and Discussion

This chapter summarizes the conclusions that have been drawn throughout this report. Along with each conclusion some discussion points are formulated. These discussion points may give rise to new questions, which can be the basis of new researches. The conclusion are made regarding the research questions (paragraph 1.4).

8.1   Influence of vegetation on waves

- The measurements show that some significant wave damping occurs at the salt marsh, especially with water depths lower than 1 meter. With such water depths, the vegetation height, which is about 40 - 50 cm, covers almost 50% of the water column. The measurements with the lowest water depths show the biggest wave height reduction. For one case, with a water depth at the boundary of 35 cm, wave height reduces to 13% of its value at the boundary.

- At the transition of the mudflat and the salt marsh, some complex processes occur in the wave field. In most cases wave height increases fairly at this point, which can not only be explained by shoaling due to the small cliff of 10 cm that can be found at the marsh's edge. Probably the height of the vegetation also contributes to this shoaling. Wave height are pushed up because the waves experience a decreasing water depth, which is stronger due to the vegetation than for bare bottoms. Besides that, wave energy may be reflected by the vegetation, resulting in an increasing wave height just before the edge. This could also explain the strong decrease in wave height just after the edge.

- The theoretical formulation for calculating dissipation on the basis of certain vegetation characteristics, which is presented in chapter 5, is able to provide accurate results in comparison with the dissipation calculated on the basis of measurement data. Four methods are presented for the calculation of the dissipation in a theoretical way. The methods in which the horizontal orbital velocity amplitude is calculated in accordance with the shallow water approximation show the better correlations between theoretical and observed wave energy dissipation. This implies that the vertical velocity profile within the vegetation is more or less constant. More research on orbital velocity profiles in the vegetation should provide decisive answers to these questions.

- Within the same theoretical formulations, the friction factor f_w, together with the vegetation characteristics plant height, density and stem diameter, can be used to calculate the total amount of friction that is exerted to the flowing water. This friction factor f_w depends on the plant stiffness and flexibility and it may also depend upon roughness of the plant's surface and the shape of the plant. The analysis that is described in this report should be carried out for other field situations and laboratory experiments with other types of vegetation, to obtain information on the magnitude of this friction factor for more types of vegetation.

8.2   SWAN parameter

- The Collins coefficient is a suitable parameter for describing the influence of vegetation on wave attenuation.

- The total amount of friction that is exerted by the vegetation can be derived from this friction factor f_w and the vegetation characteristics. It is been proved that this total friction factor c_w is the same friction factor as the Collins coefficient except for a factor $4/(3\pi)$. Because of that, this factor c_w can be converted into Collins coefficients and subsequently these coefficients can be used for calibration and validation in the wave model SWAN.

8.3   Modelling of wave attenuation by vegetation in SWAN

- Calibration of the SWAN model resulted in Collins coefficients in the order of magnitude of 0,5 to 4. These values are up to 250 times larger than the default value of 0,015, which proves the significant influence of vegetation towards wave damping. Another conclusion drawn from the calibration results was the fact that wave damping was quite insensitive to the Collins coefficient for relative large water depths.
- Validation of the SWAN model has been carried out on the basis of calculated friction factors c_w, that are determined for each location by the different vegetation characteristics. These c_w factors were converted to Collins coefficients and imported in SWAN. It turned out that SWAN is well able to predict wave attenuation over vegetated areas. The results are better for the September cases than for the August cases. This can be explained to the fact that the vegetation measurements were carried out in September. Since the same data were used for the August cases, this may result in an error, if vegetation characteristics were different for the two studied periods. As suggested above, more research is needed to the way vegetation affects the orbital velocities. Subsequently, the calculation of the Collins coefficients will be more accurate and, maybe, also the wave modelling.
- SWAN is not able to model the attenuation at the edge of the salt marsh, as described in point 2 of this discussion. The explanation for this is the fact that the way the vegetation is modelled now, just as an enlarged bottom friction, will not result in enhanced shoaling and reflection by the vegetation. SWAN does not see the vegetation as an obstacle that causes shoaling and reflection. It would be useful to adapt SWAN in future for this. SWAN is already able to model rigid obstacles, maybe it is possible to take into account vegetation in a similar way.
- Another useful research option in the light of vegetation modelling through the Collins coefficient would be to implement an algorithm, which calculates the friction factor for different vegetation types and vegetation characteristics. In fact, such calculations are done during this study, but only for one vegetation type. Therefore, this study is pretty suitable in setting up such an algorithm if the analyses that are described in this report are carried out for other location with different vegetation types which was already suggested in the fourth point of this discussion.

References

Online articles:

Wenner, E. (Marine Resources Research Institute) Dynamics of the salt marsh,
        (http://water.dnr.state.sc.us/marine/pub/seascience/dynamic.html)

Seitz, L. Protecting U.S. Salt Marshes from the Effects of Global Warming,
        (http://www.cns.bu.edu/~aseitz/lorna/MarshPaper2.pdf)

Rocque, A.J (2000) White Sands Beach Salt Marsh
        (http://dep.state.ct.us/wtr/nps/succstor/whtsnd.pdf)

Websites:

Het Zeeuwse Landschap
        http://www.hetzeeuwselandschap.nl/kaart/index.php?kaart=52

The Scheldt Estuary
        http://www.geo.uu.nl/~hyacinth/scheldt_page.htm

Project Zeeweringen
        http://www.zeeweringen.nl/werkinuit.html

Intetnationale Commissie bescherming schelde
        http://www.icbs-cipe.com/NL/a_frameset.htm

National Oceanic and Atmospheric Administration (2000) Fisheries of the United States
        (http://www.st.nmfs.gov/st1/publications.html)

Literature

Holdgate, M. (1997). From Care to Action. Earthscan Publications Ltd., London, U.K.

Technische Schelde Commissie (2001) Lange termijn visie Schelde-estuarium

ProSes (2002) Ontwikkelingsschets 2010 Schelde-estuarium

Möller, I, Spencer, T, French, J.R., Legget, D.J., & Dixon, M. (2001). The Sea-Defence
        Value of Salt Marshes: Field Evidence from North Norfolk. J. CIWEM 15:117

Yang, S.L. (1998) The Role of Scirpus Marsh in Attenuation Hydrodynamics and Retention
        of Fine Sediment in the Yangtze Estuary. Estuarine, Coastal and Shelf Science
        47:227-233

Mann, K. H. (2000) Chp 3 Salt Marshes. In Ecology of Coastal Waters – With Inplications
        for Management. Blackwell Science Inc., Massachusetts, USA.

A. Crosato, I. Tánczos, M. de Vries, Z.B. Wang (2002). Quantification of
        Biogeomorphological Variables for Dutch Tidal Systems

E. Low (2002). Sea Wave Attenuation by Salt Marsh Vegetation

Van Rijn, L.C. (1990) Priciples of fluid flow and surface waves in rivers, estuaries, seas and ocenas.

Holthuijsen, L.H., Booij, N., Ris, R.C., Haagsma, IJ. G., Kieftenburg, A.T.M.M., KrieziSwan, E.E. (2000) User manual, short version

WL Delft Hydraulics (2000) Delft Auke Process description

WL Delft Hydraulics (2002) Delft3d WAVE user manual, version 2.01

Verschuren, P., Doorewaard, H. (2000) Het ontwerpen van een onderzoek

Hulscher, S.J.M.H., Ribberink, J.S., Knaapen, M.A.F (2001) Marine Dynamics II, University of Twente

A   Graphs

A.1   Chapter 4 Graphs

Wave attenuation at the salt marsh
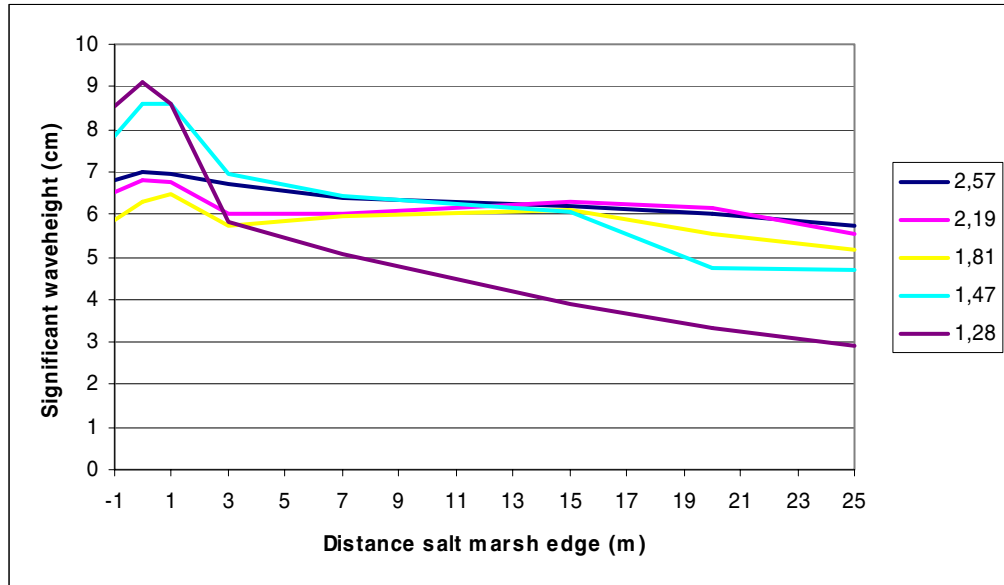
Graph 4.1: Wave attenuation of period 1 (10th of August) for different water levels (m NAP)
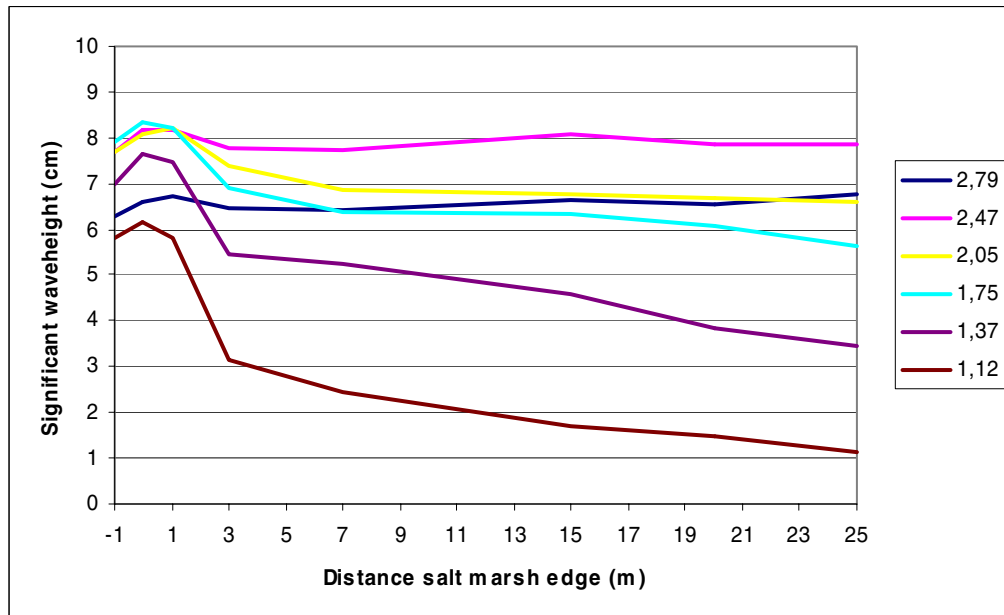
Graph 4.2: Wave attenuation of period 2 (12th of August) for different water levels (m NAP)
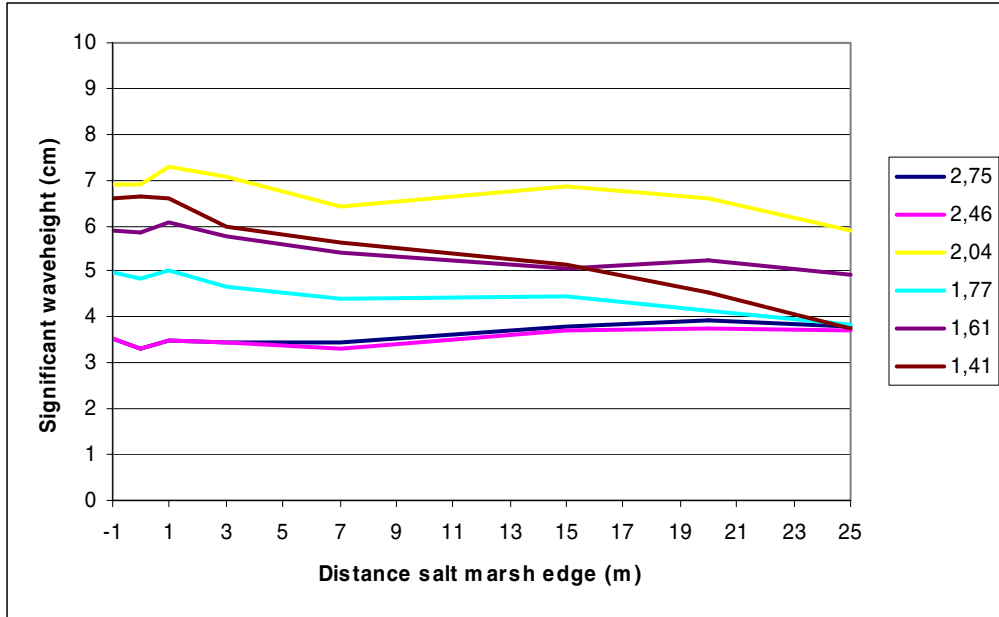
Graph 4.3: Wave attenuation of period 3 (10th of September) for different water levels (m NAP)
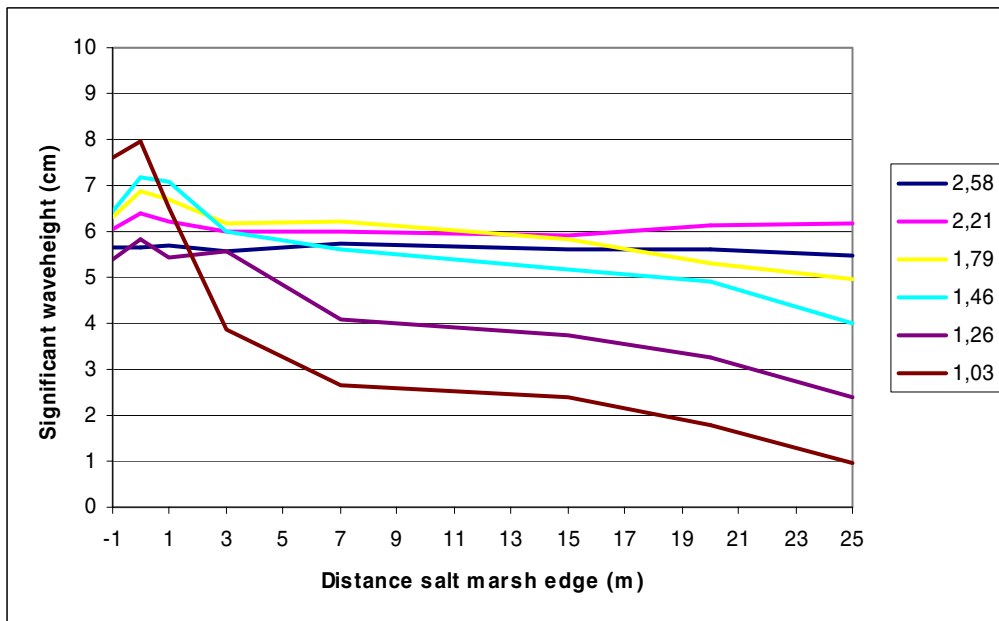
Graph 4.4: Wave attenuation of period 4 (11th of September) for different water levels (m NAP)

Energy flux along the salt marsh
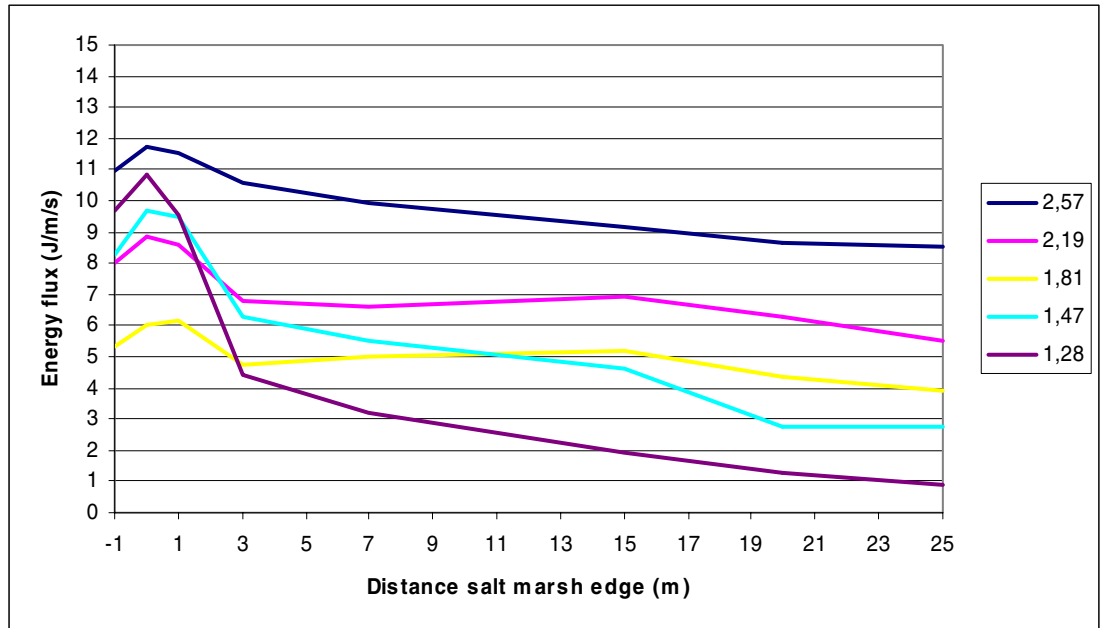
Graph 4.5: Energy flux of period 1 (10th of August) for different water levels (m NAP)
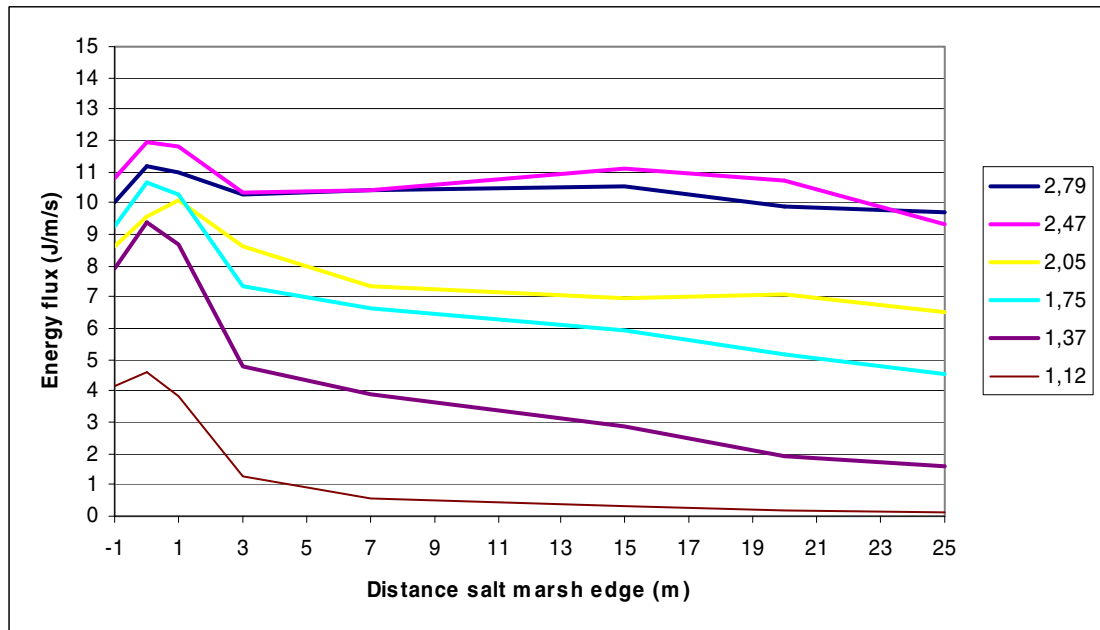
Graph 4.6: Energy flux of period 2 (12th of August) for different water levels (m NAP)
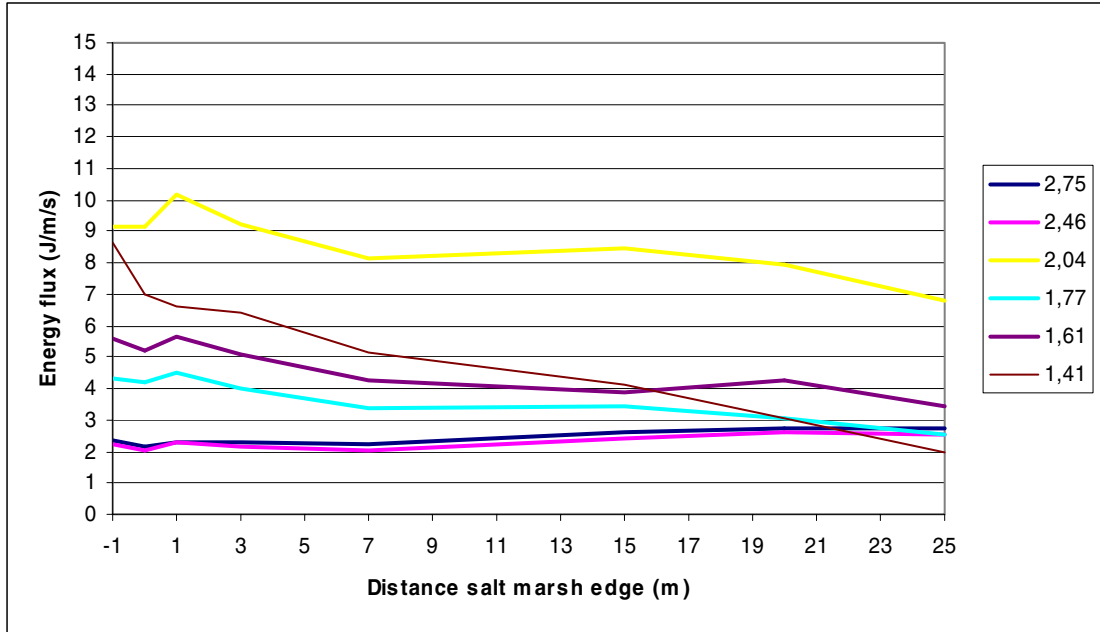
Graph 4.7: Energy flux of period 3 (10th of September) for different water levels (m NAP)
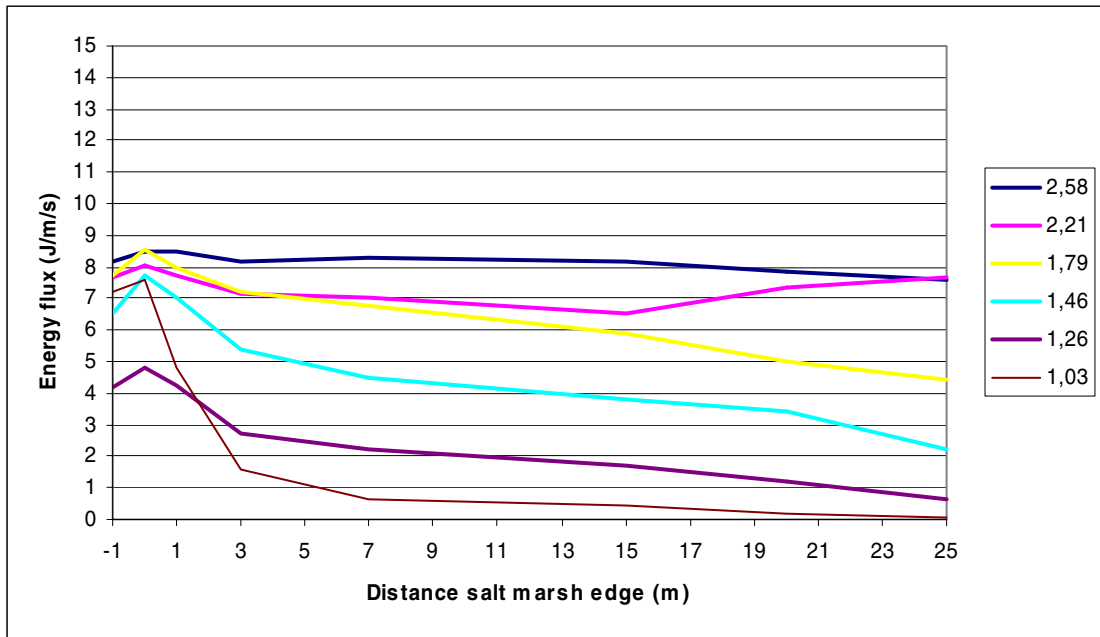
Graph 4.8: Energy flux of period 4 (11th of September) for different water levels (m NAP)

A.2   Chapter 5 Graphs

Plant structure densities
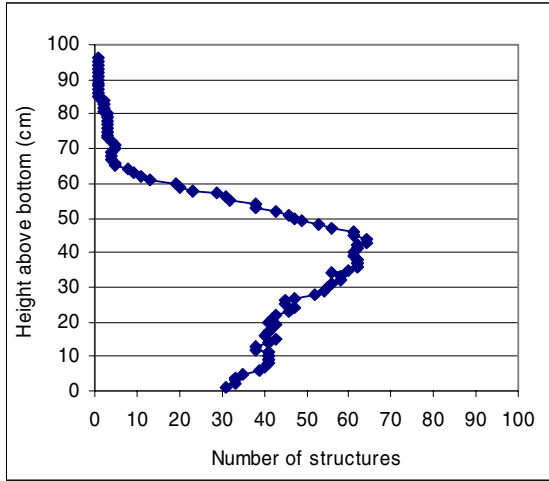
Graph 5.1: plant structure density profile at P0
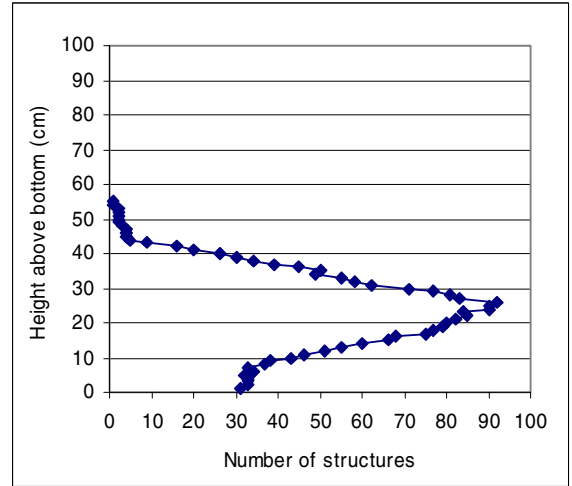
Graph 5.2: plant structure density profile at P1
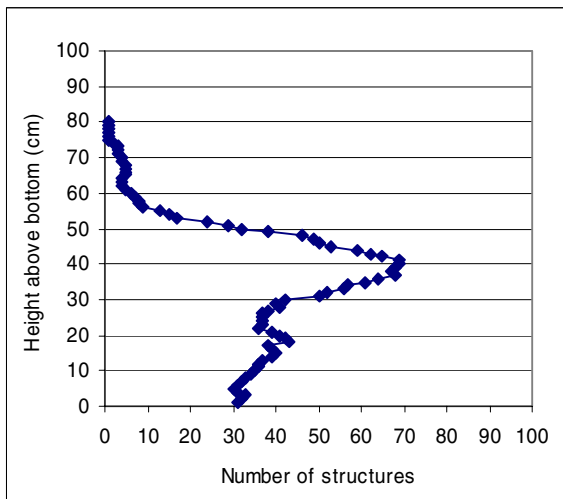
Graph 5.3: plant structure density profile at P2
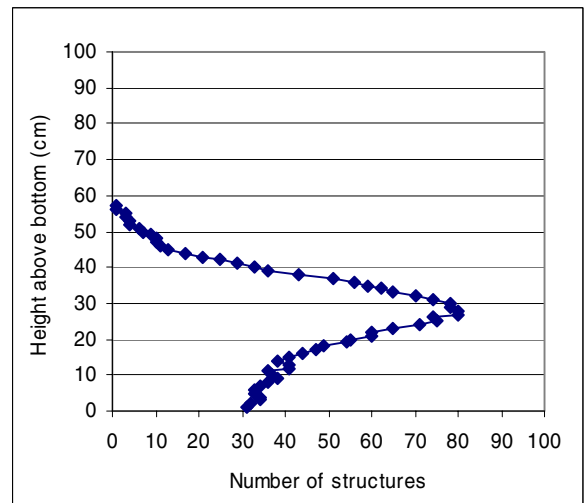
Graph 5.4: plant structure density profile at P3
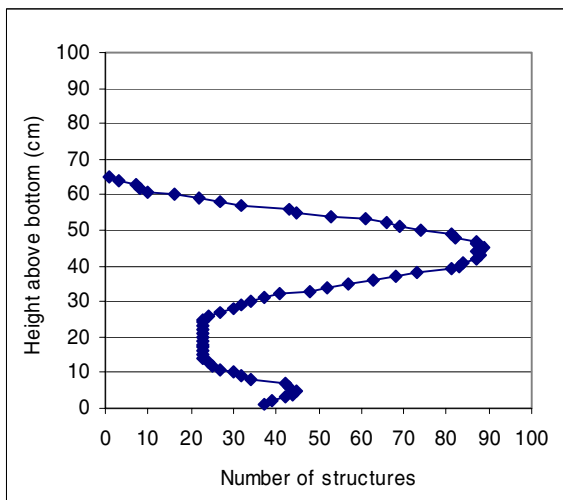
Graph 5.5: plant structure density profile at P4
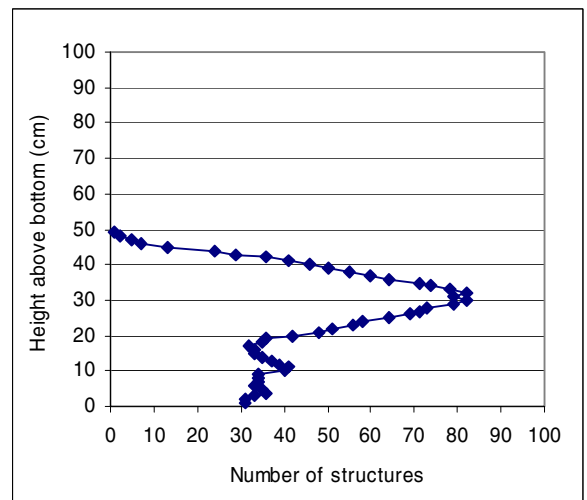
Graph 5.6: plant structure density profile at P5

Comparison between theoretical and observed dissipations
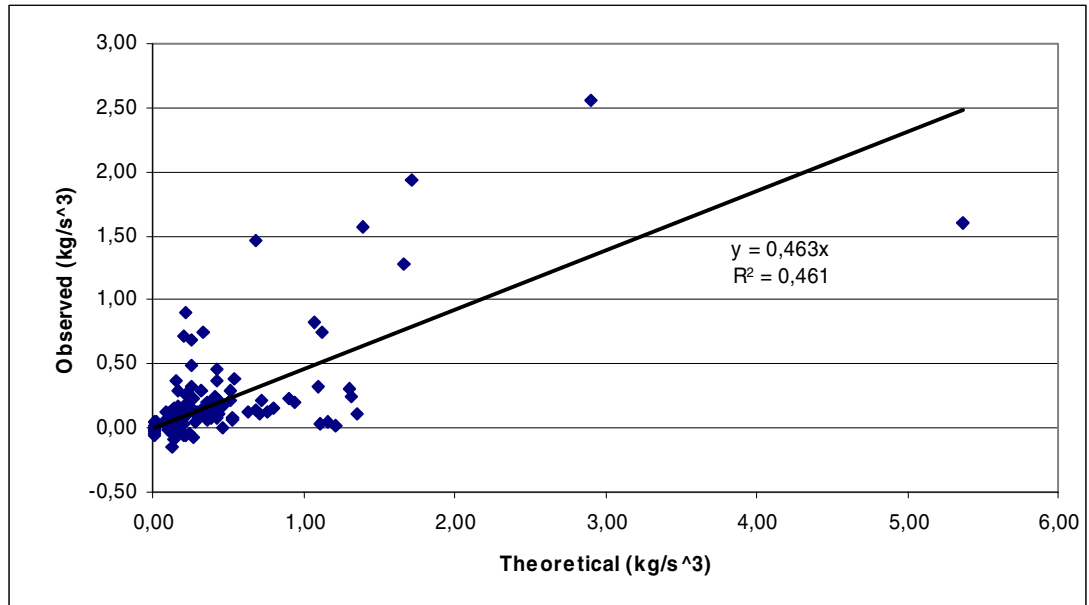
Graph 5.7: Observed vs theoretical dissipation, using *n(z)*=constant and linear wave theory
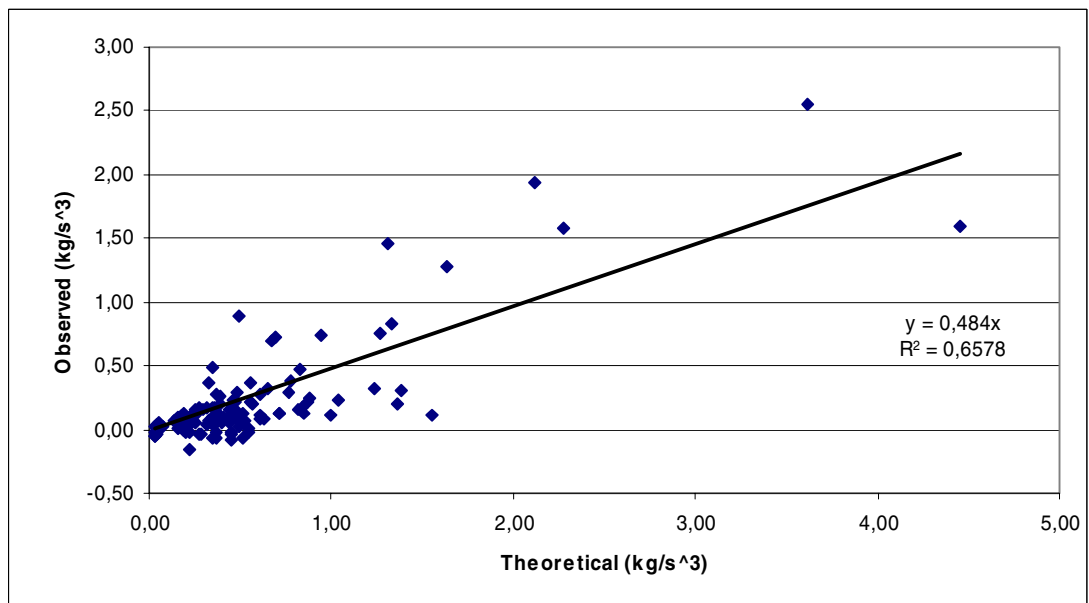
Graph 5.8: Observed vs theoretical dissipation, using *n(z)*=constant and shallow water
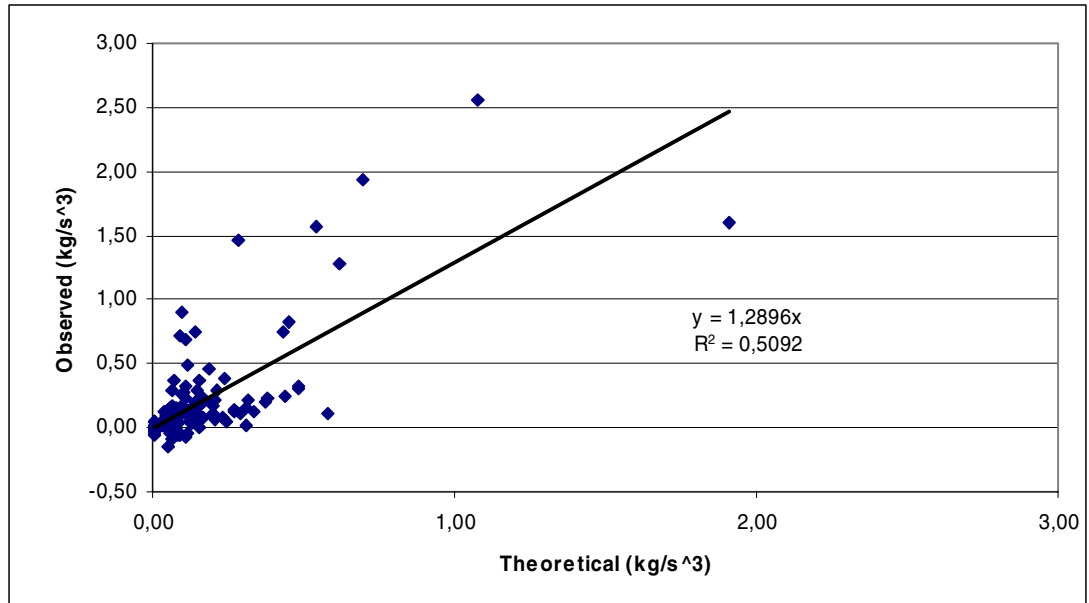
Graph 5.9: Observed vs theoretical dissipation, using *n(z)*=variable and linear wave theory
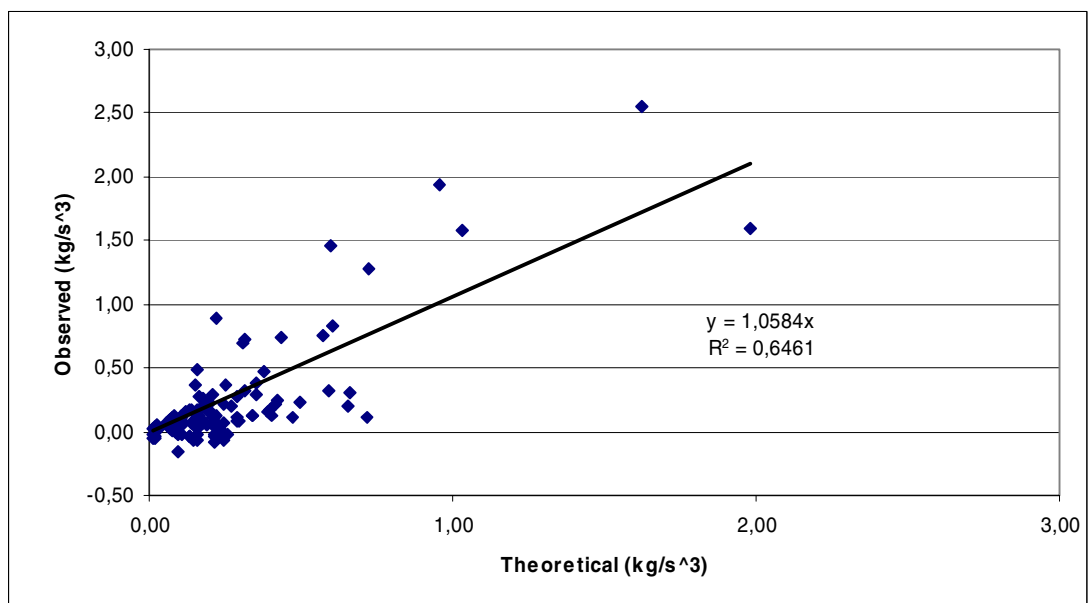
Graph 5.10: Observed vs theoretical dissipation, using *n(z)*=variable and shallow water

A.3   Chapter 7 Graphs

SWAN validation
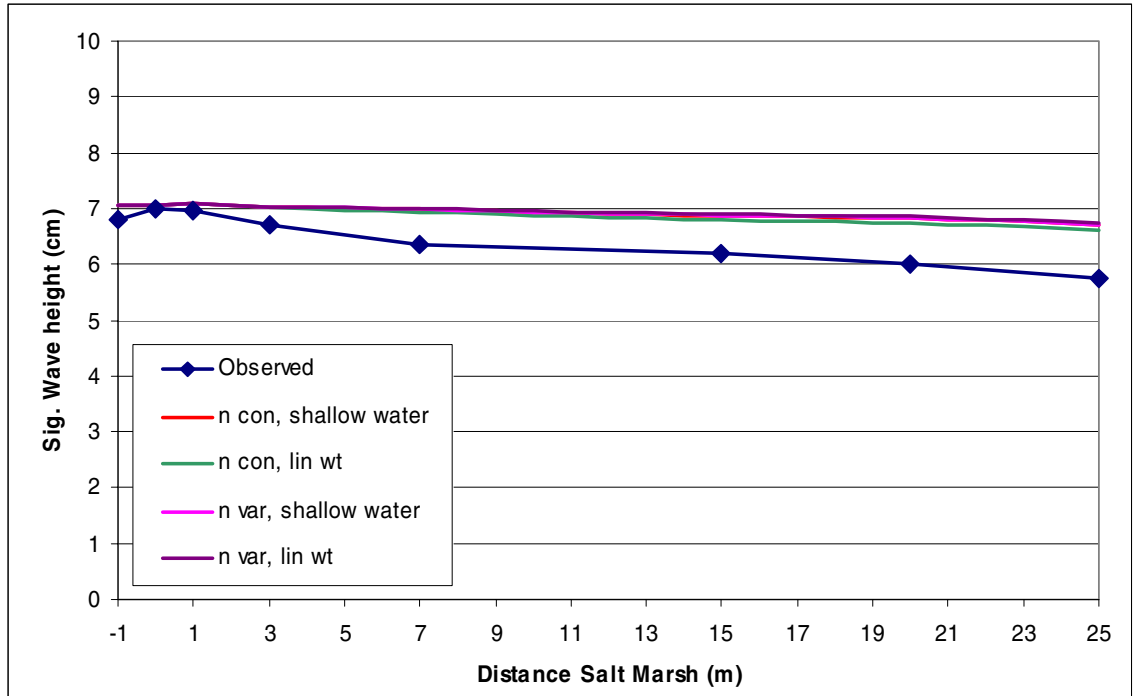
Graph 7.1: SWAN validation for August 10, 16:30
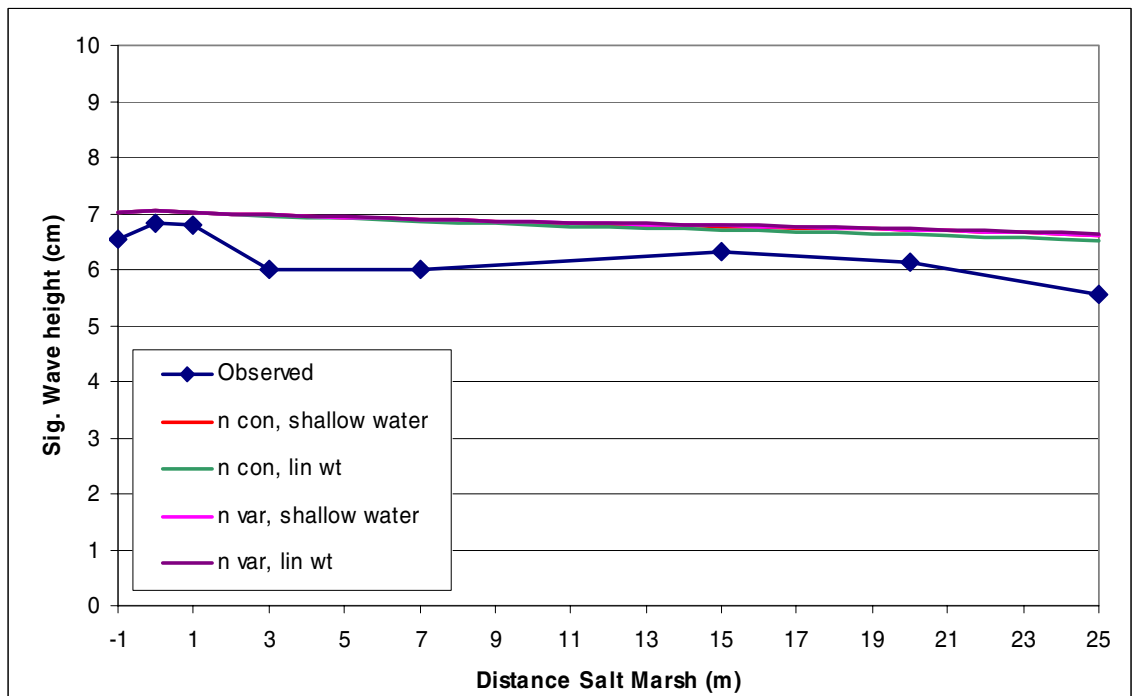
Graph 7.2: SWAN validation for August 10, 17:15
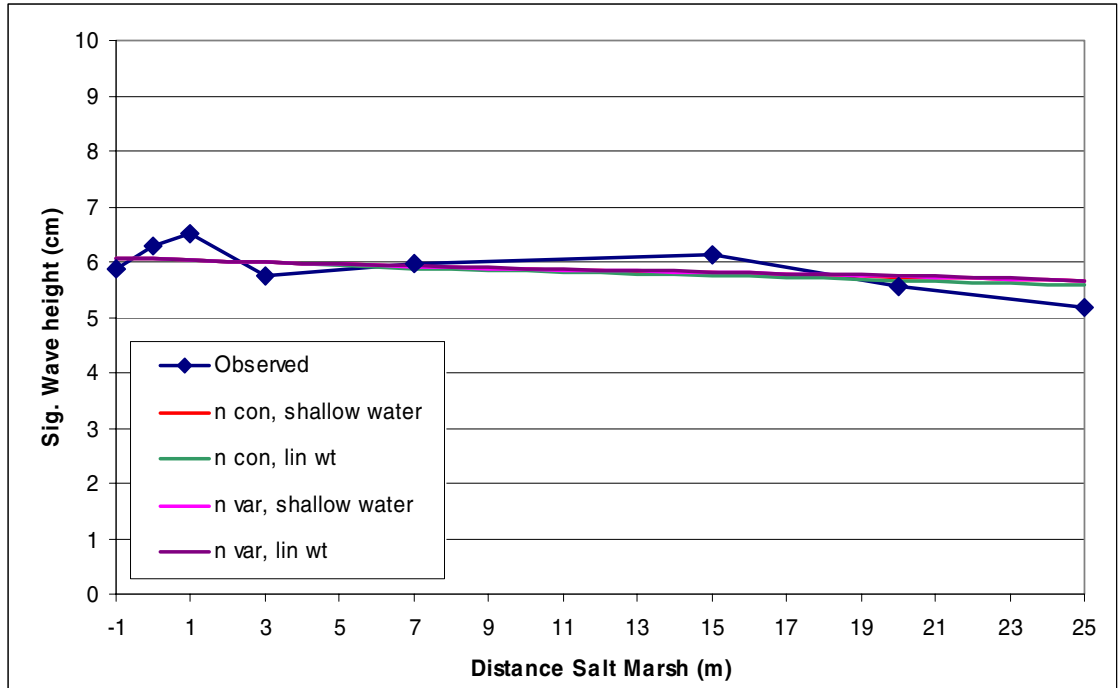
Graph 7.3: SWAN validation for August 10, 18:00
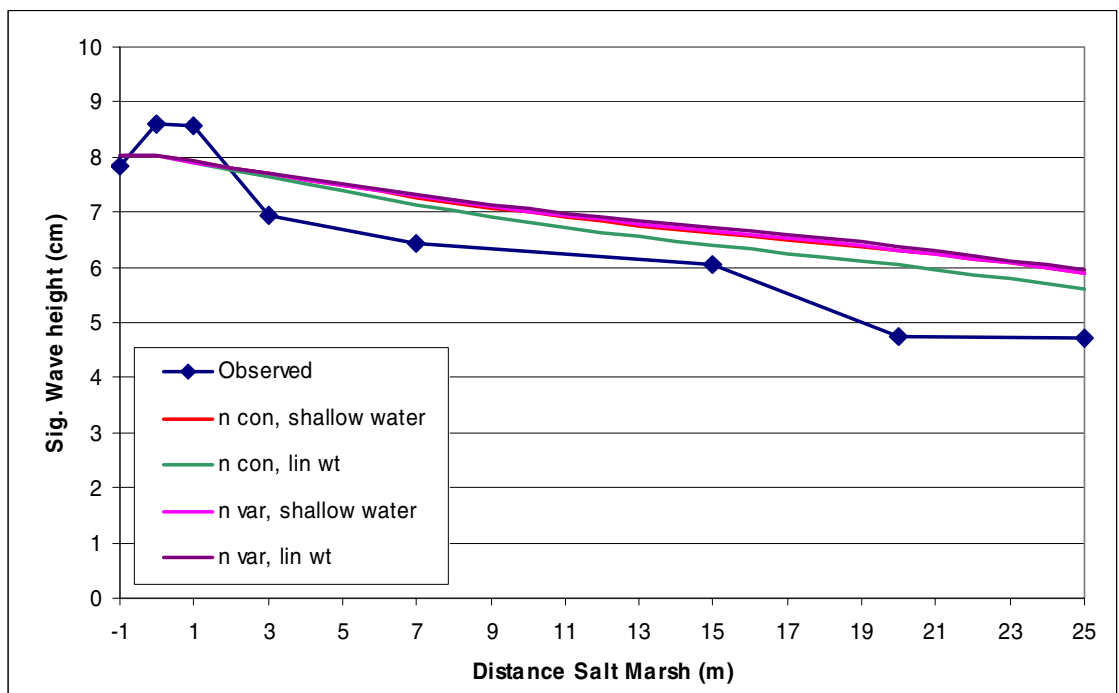
Graph 7.4: SWAN validation for August 10, 18:30
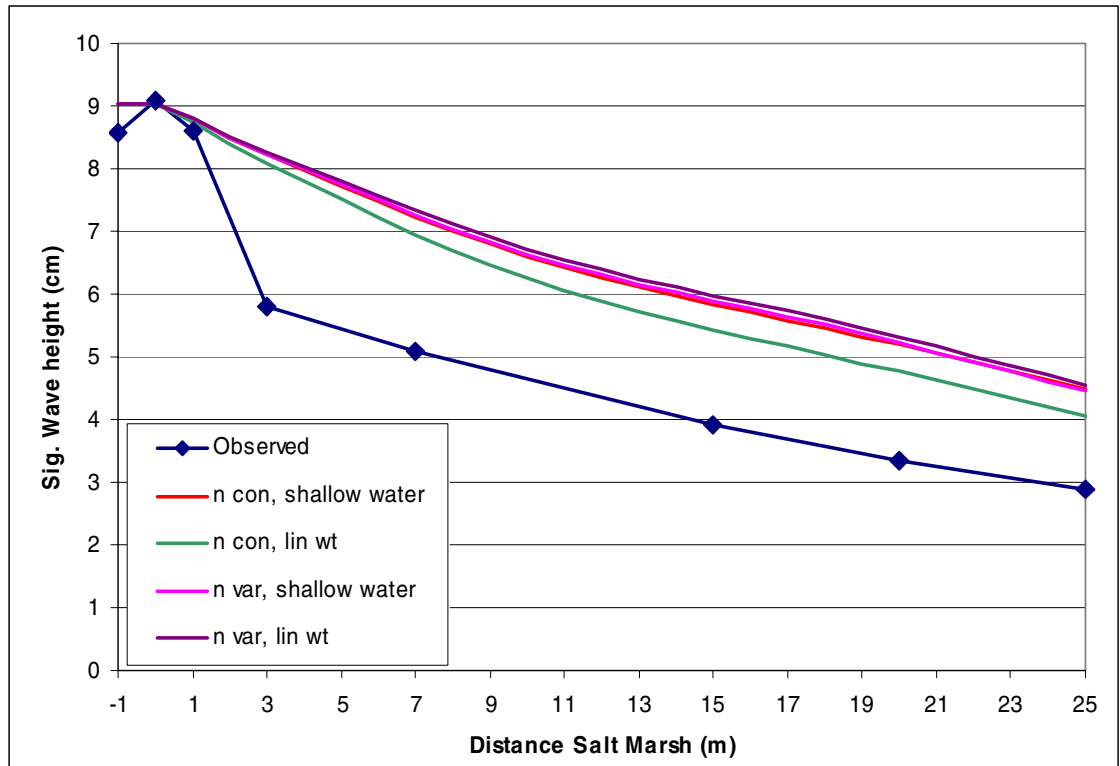
Graph 7.5: SWAN validation for August 10, 18:45
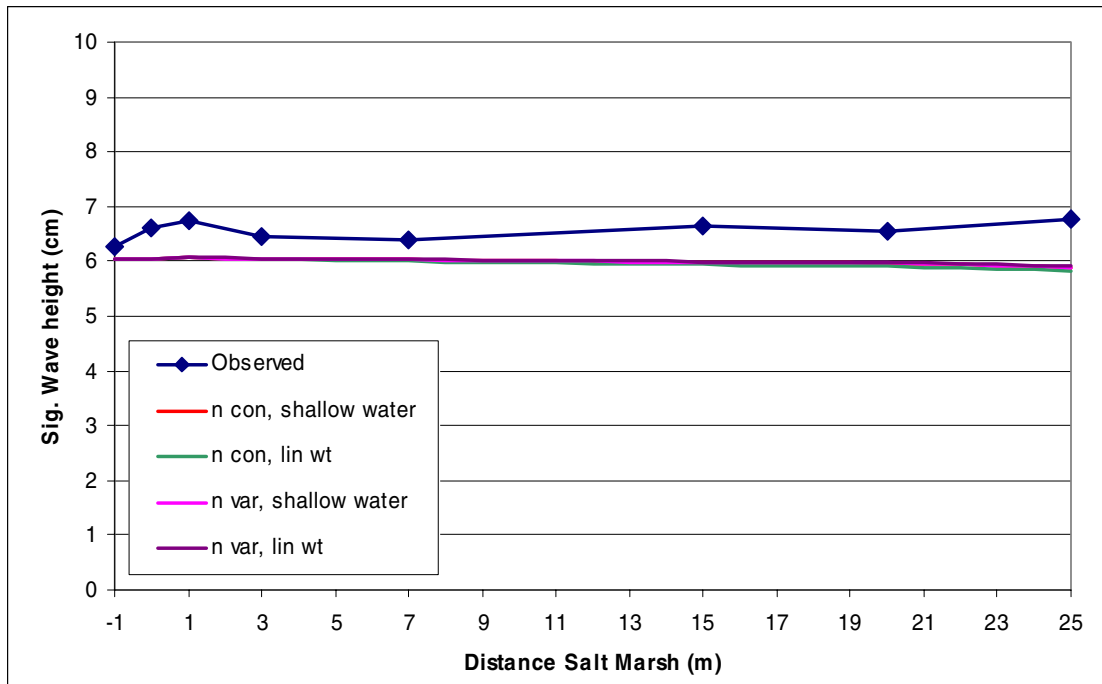
Graph 7.6: SWAN validation for August 12, 17:45
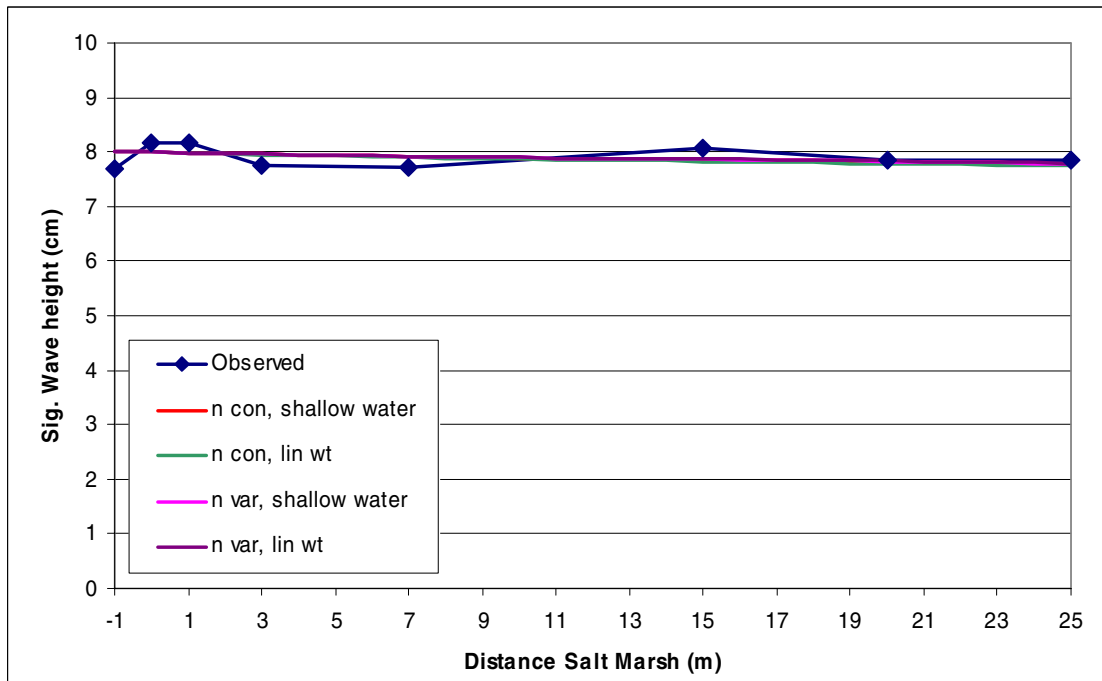
Graph 7.7: SWAN validation for August 12, 18:30
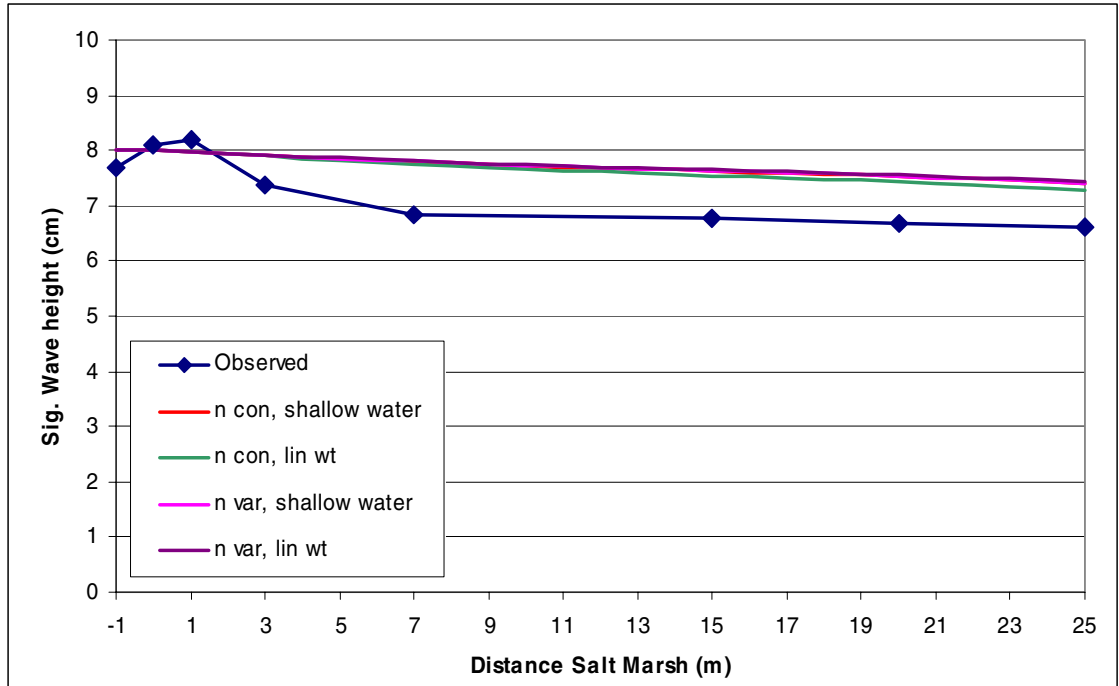
Graph 7.8: SWAN validation for August 12, 19:15
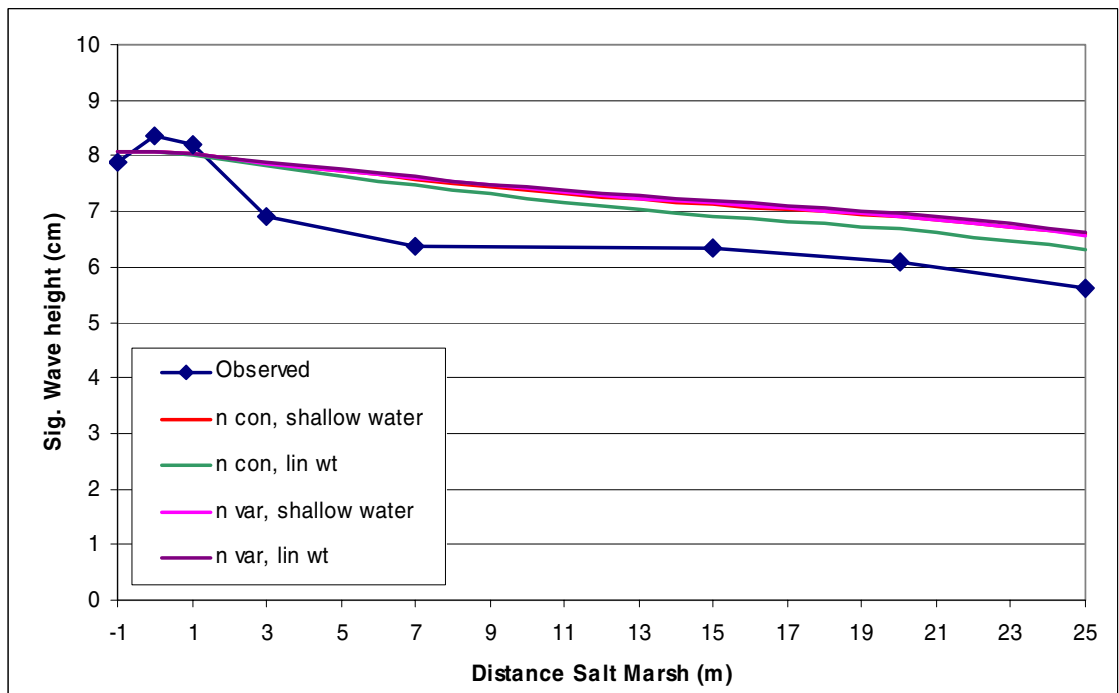
Graph 7.9: SWAN validation for August 12, 19:45
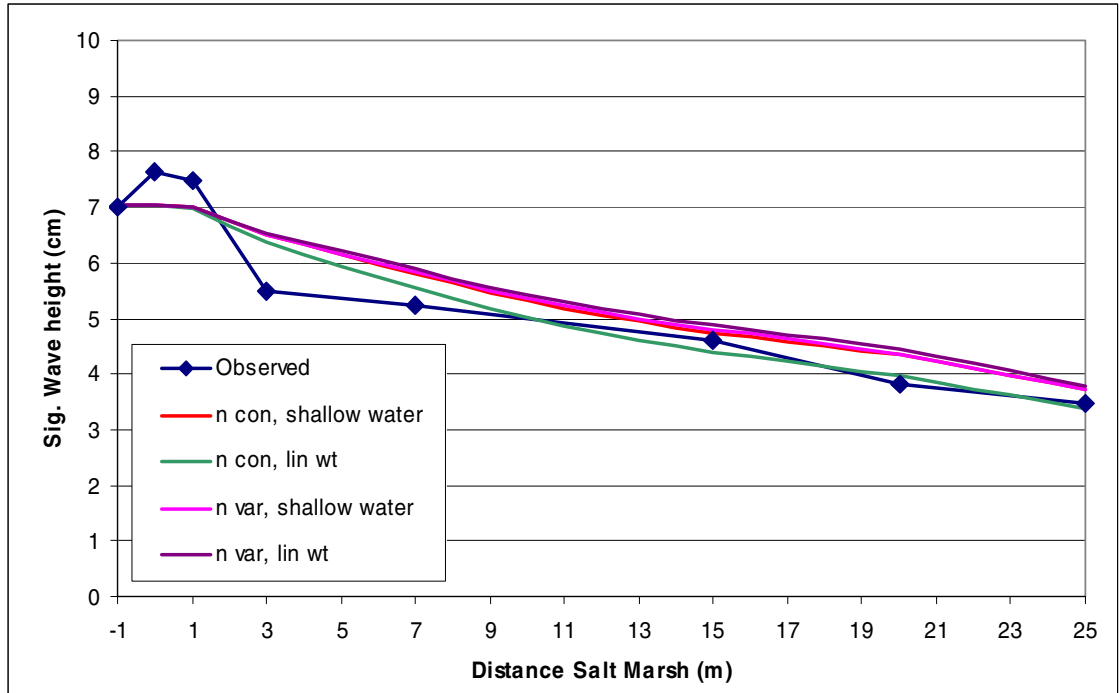
Graph 7.10: SWAN validation for August 12, 20:15
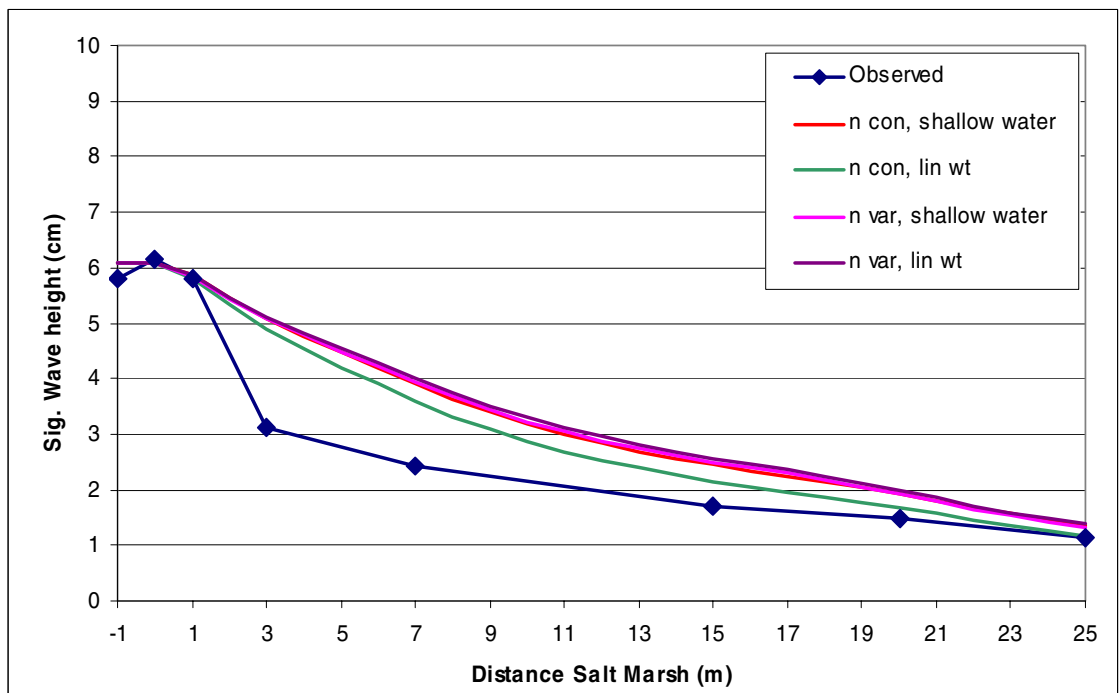
Graph 7.11: SWAN validation for August 12, 20:30
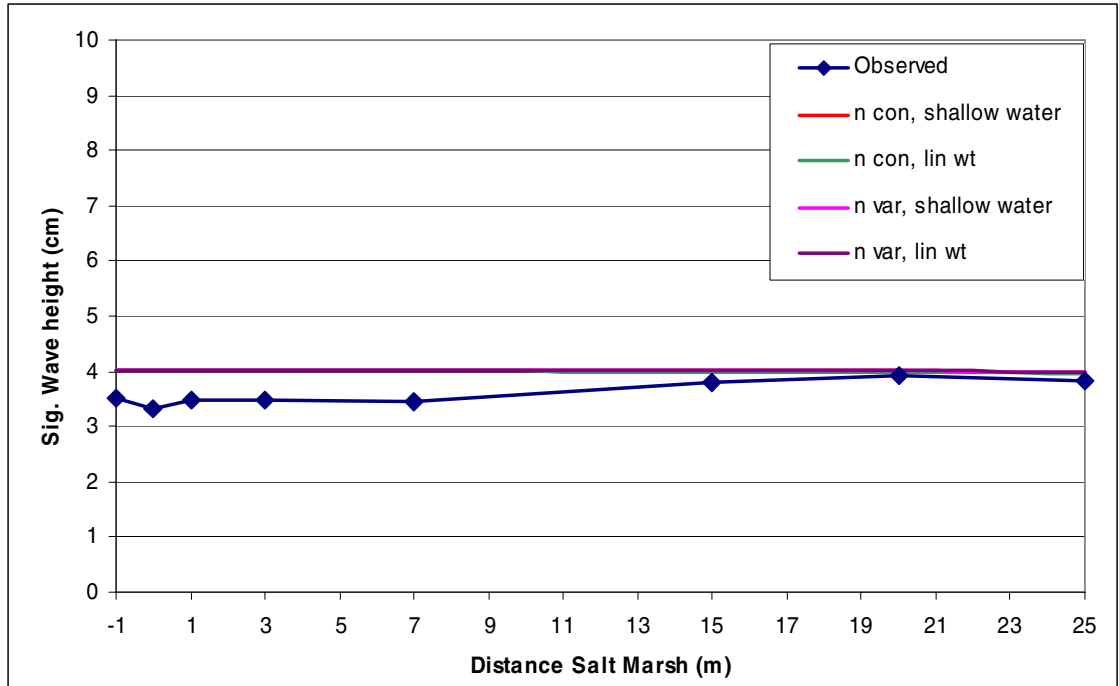
Graph 7.12: SWAN validation for September 10, 17:15
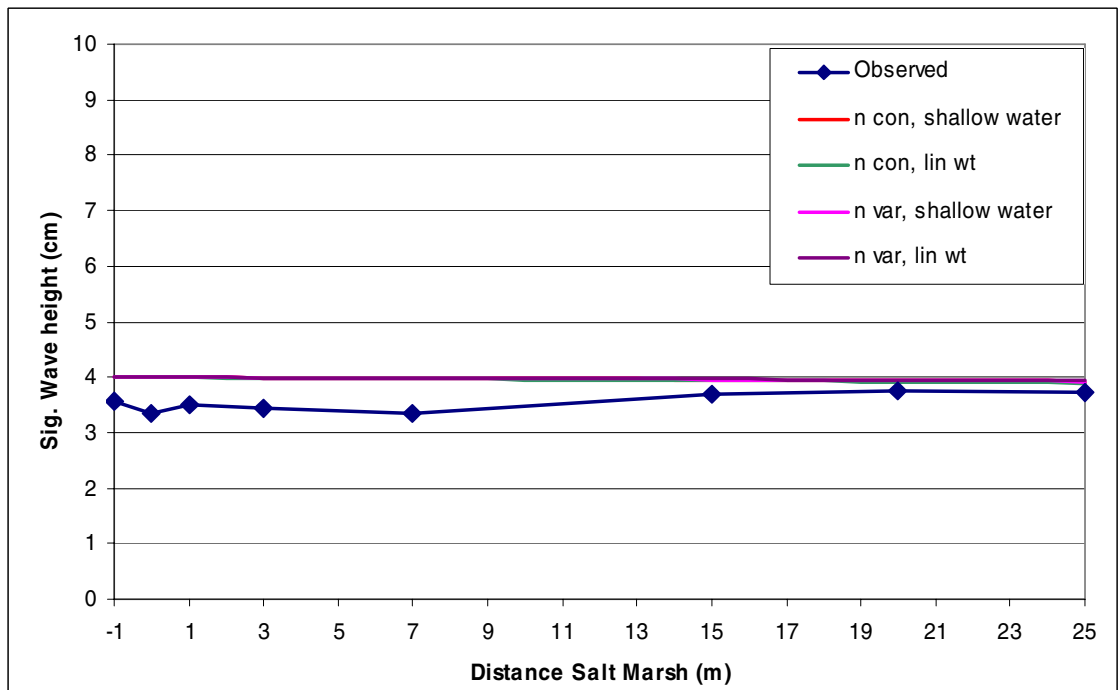
Graph 7.13: SWAN validation for September 10, 18:00
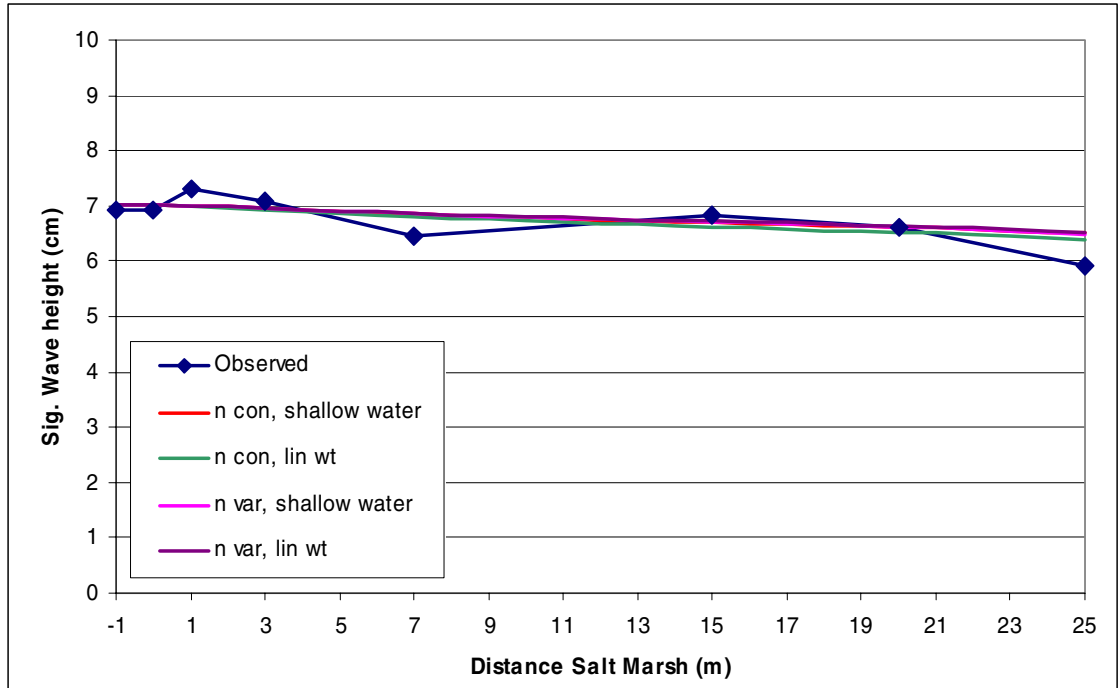
Graph 7.14: SWAN validation for September 10, 18:45
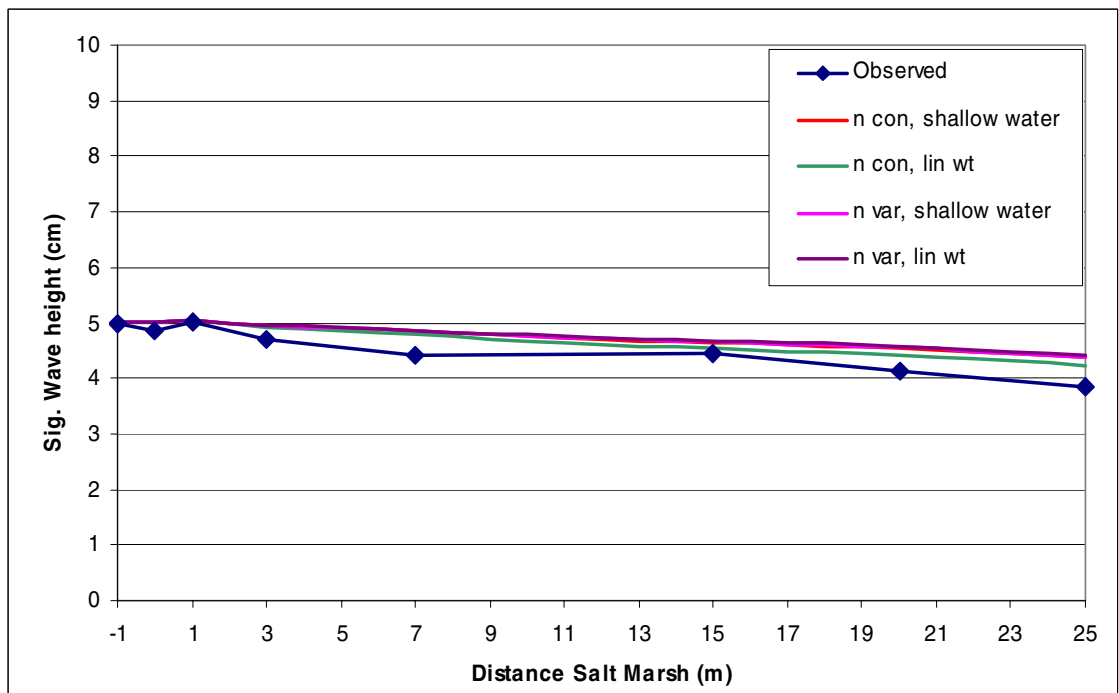
Graph 7.15: SWAN validation for September 10, 19:15
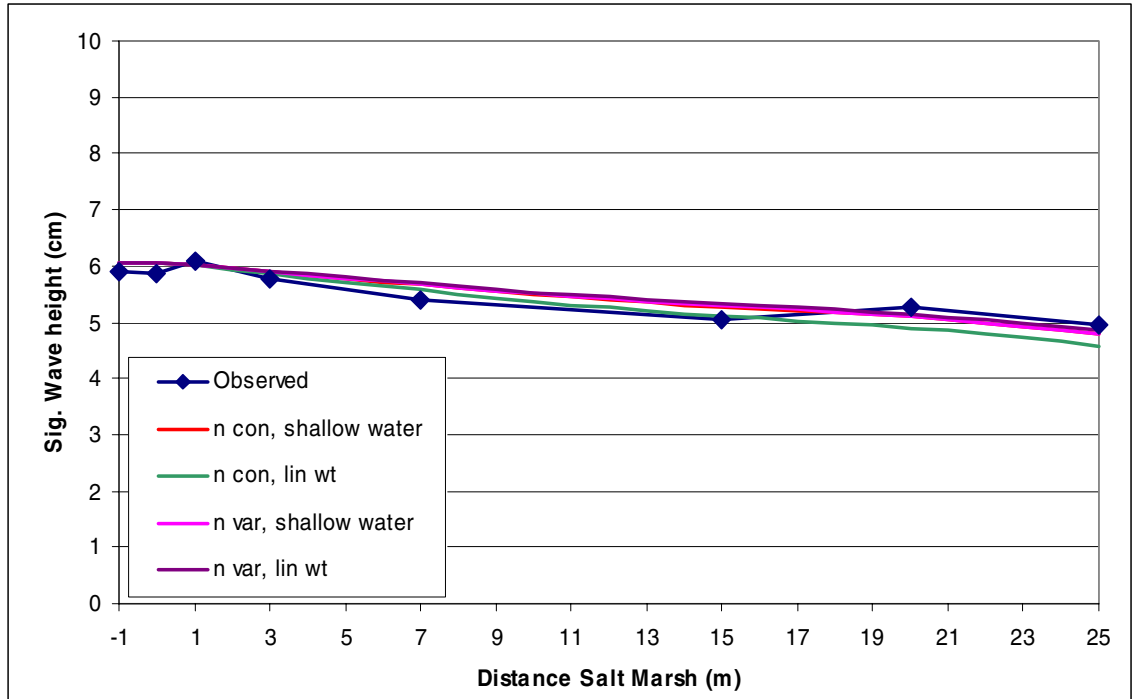
Graph 7.16: SWAN validation for September 10, 19:30
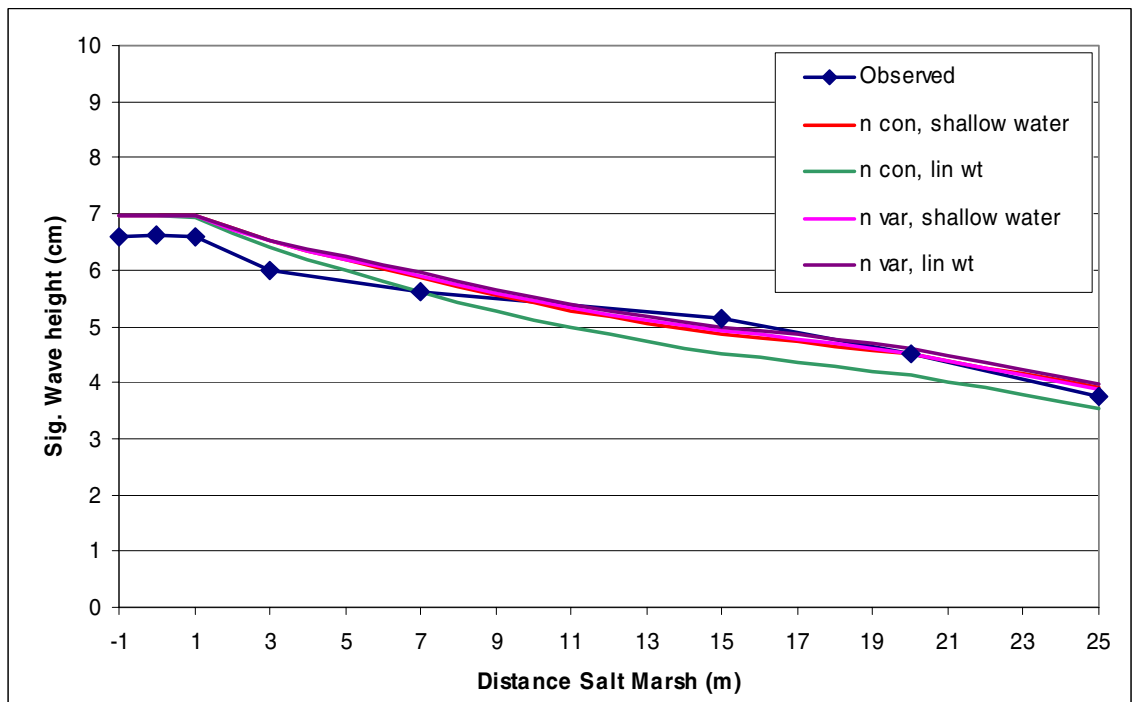
Graph 7.17: SWAN validation for September 10, 19:45
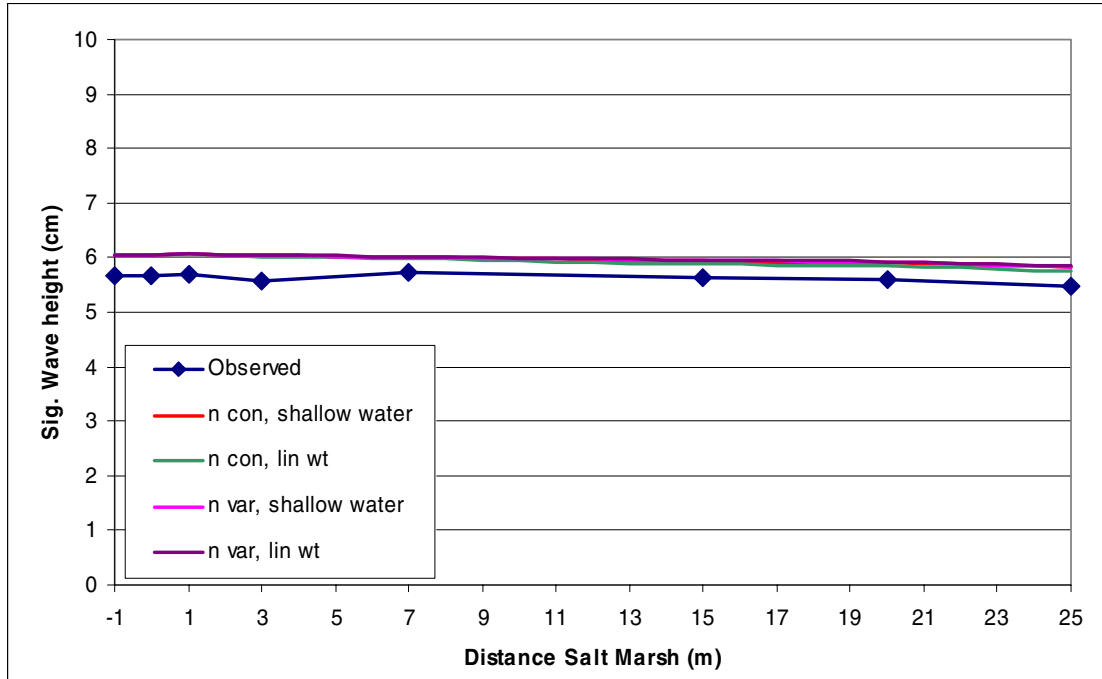
Graph 7.18: SWAN validation for September 11, 18:15
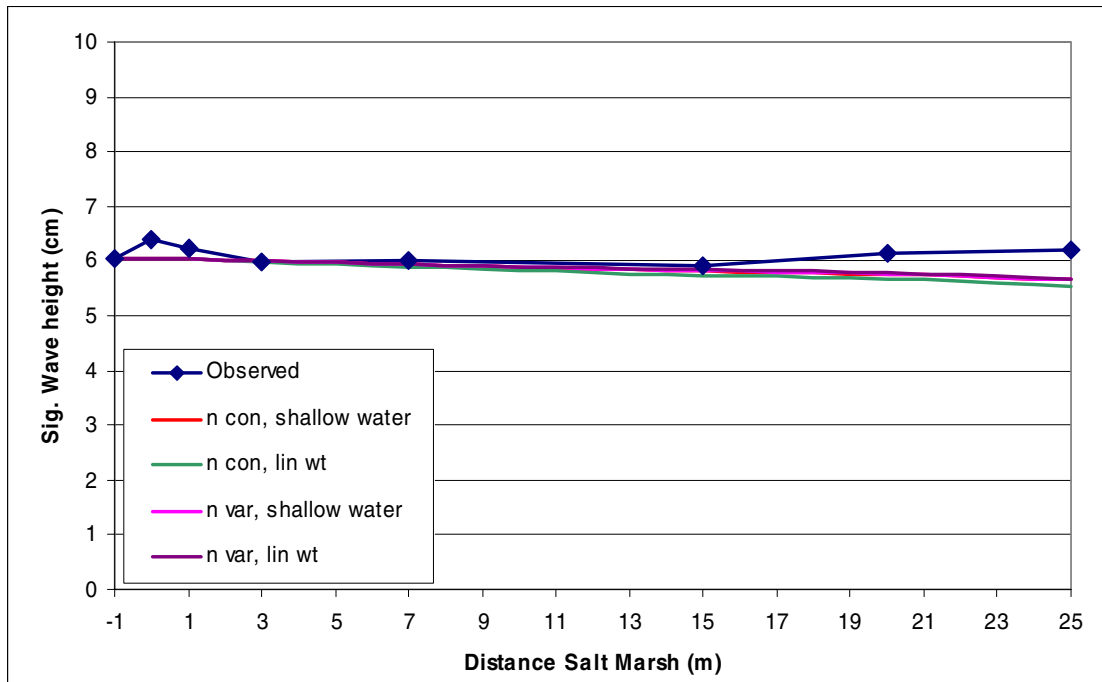
Graph 7.19: SWAN validation for September 11, 19:00
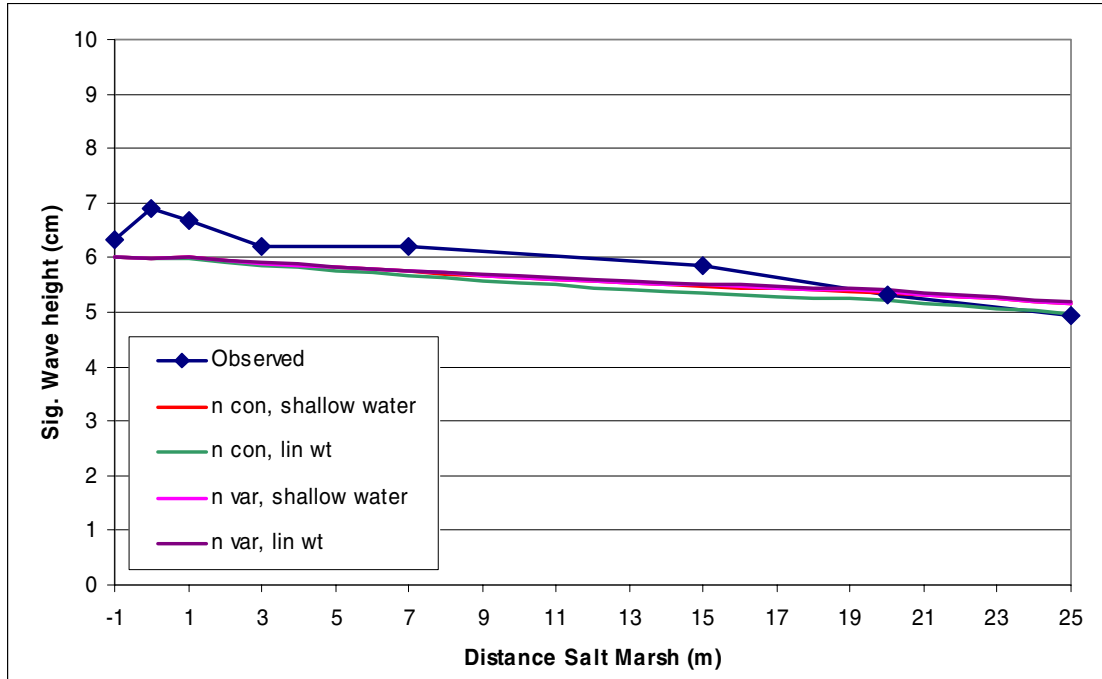
Graph 7.20: SWAN validation for September 11, 19:45
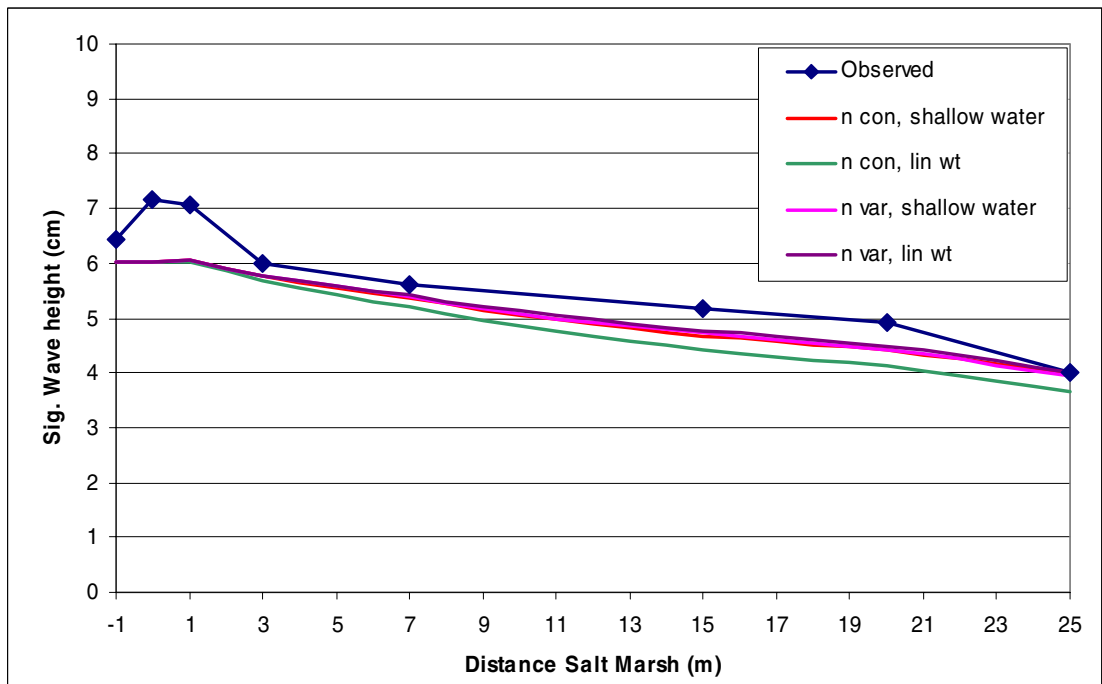
Graph 7.21 SWAN validation for September 11, 20:15
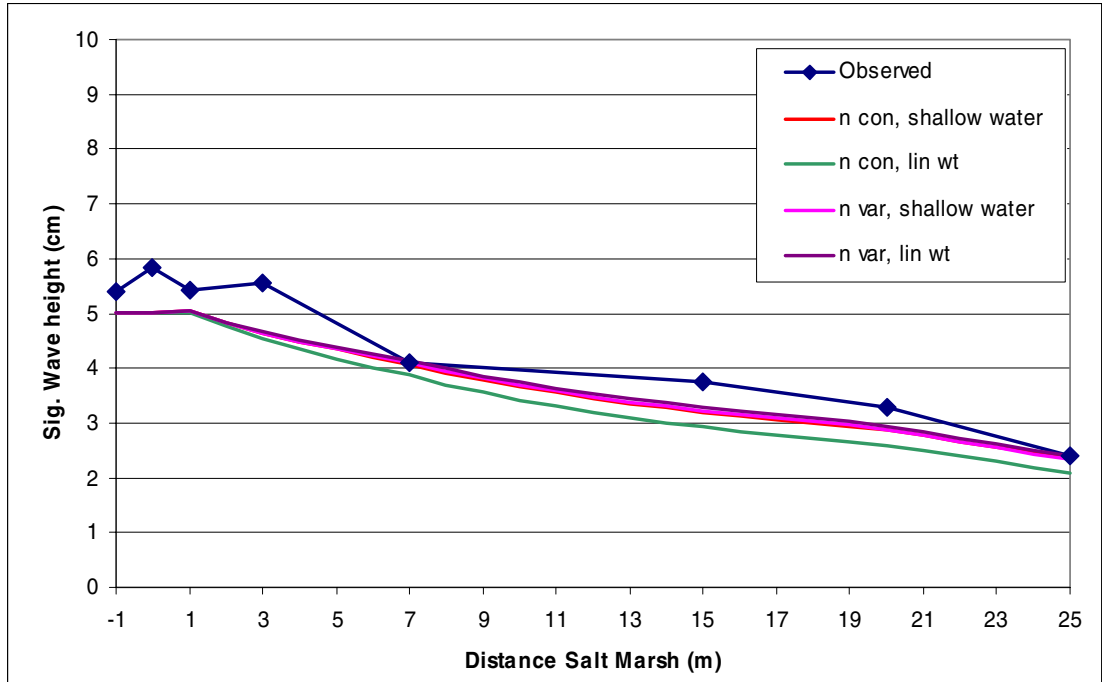
Graph 7.22: SWAN validation for September 11, 20:30
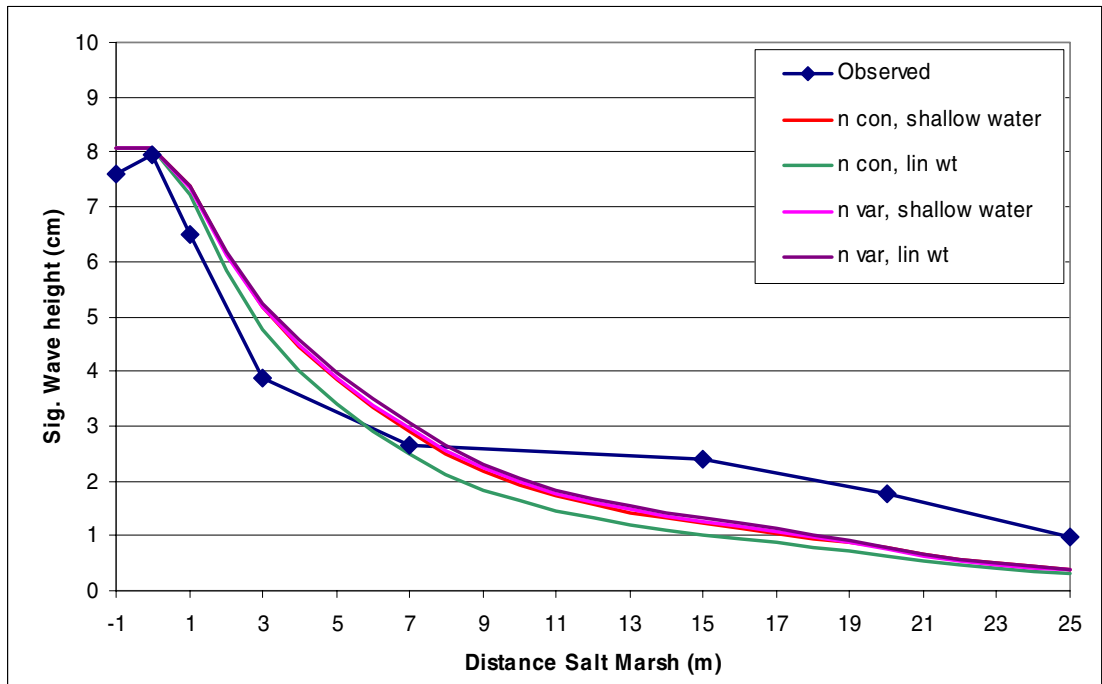
Graph 7.23: SWAN validation for September 11, 20:45

SWAN sensitivity analyses
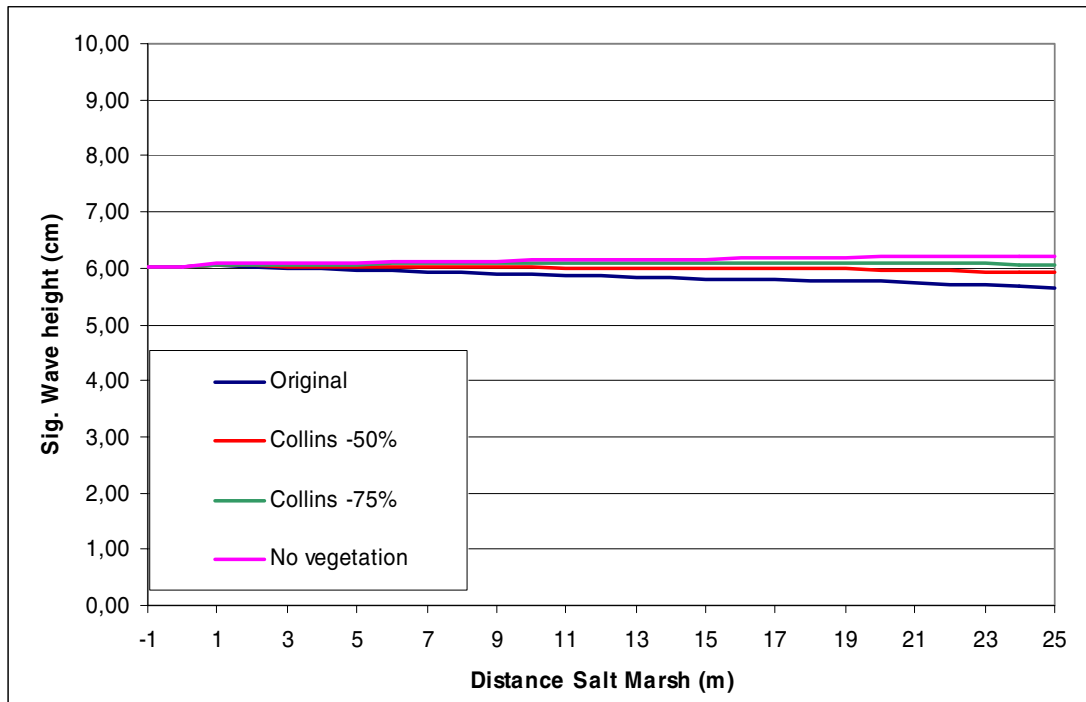
Graph 7.24: friction sensitivity, water level 2,21 m NAP (case 19:00)
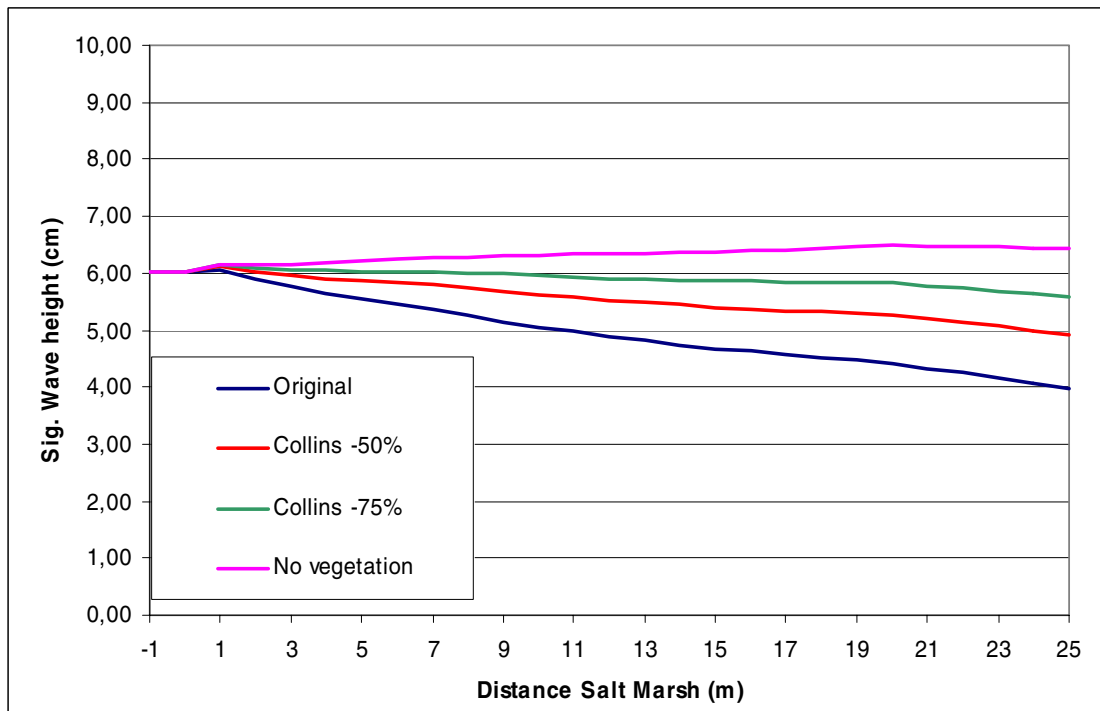
Graph 7.25: friction sensitivity, water level 1,46 m NAP (case 20:15)
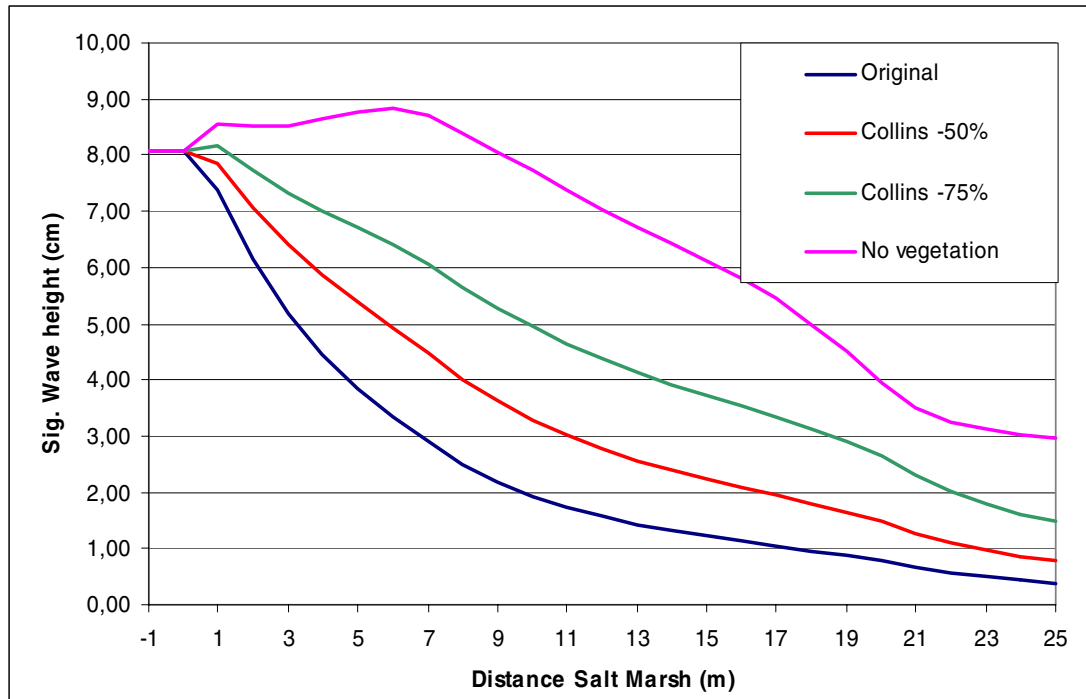
Graph 7.26: friction sensitivity, water level 1,03 m NAP (case 20:45)
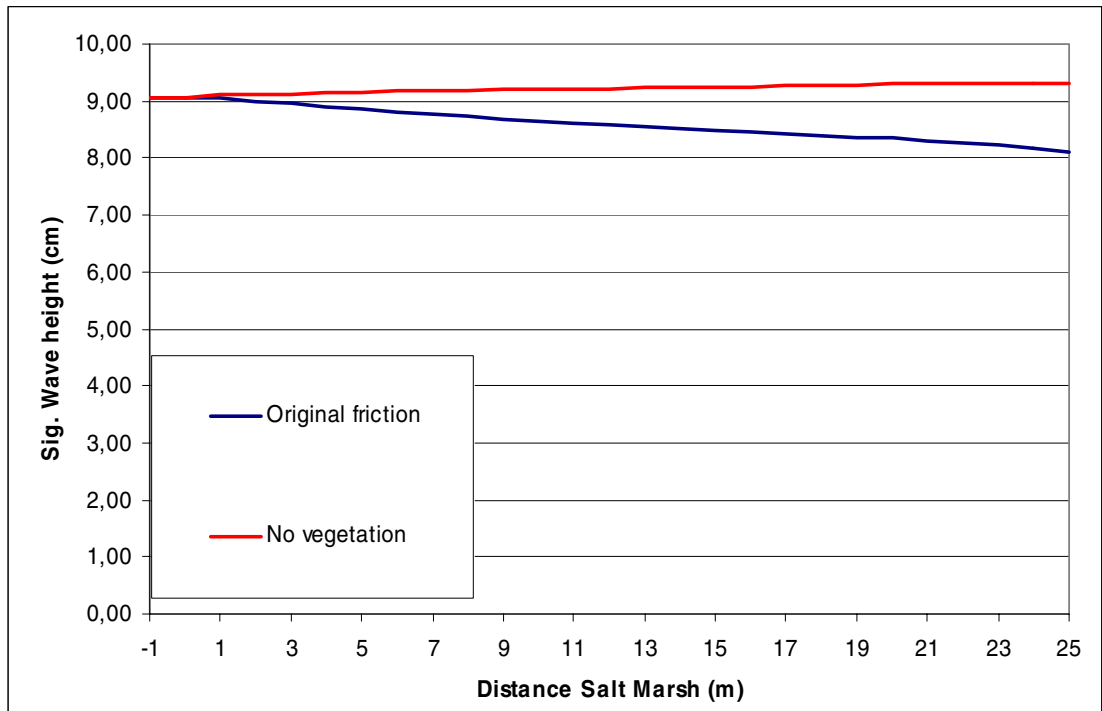
Graph 7.27: boundary wave height 150%, water level 2,21 m NAP (case 19:00)
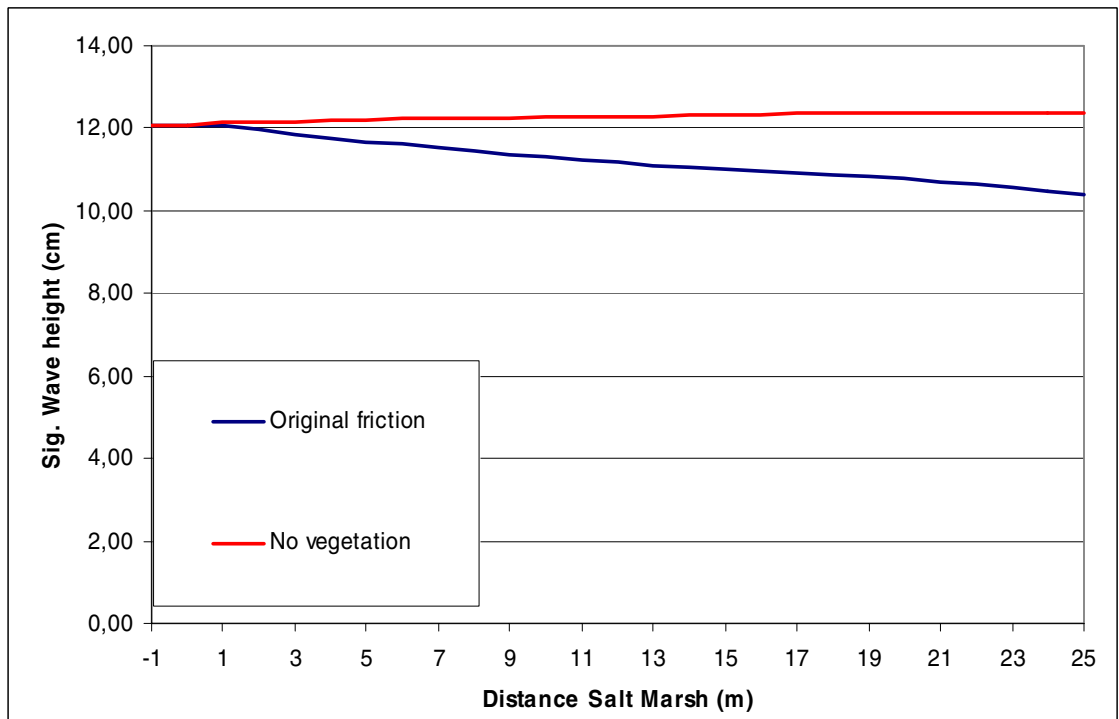
Graph 7.28: boundary wave height 200%, water level 2,21 m NAP (case 19:00)
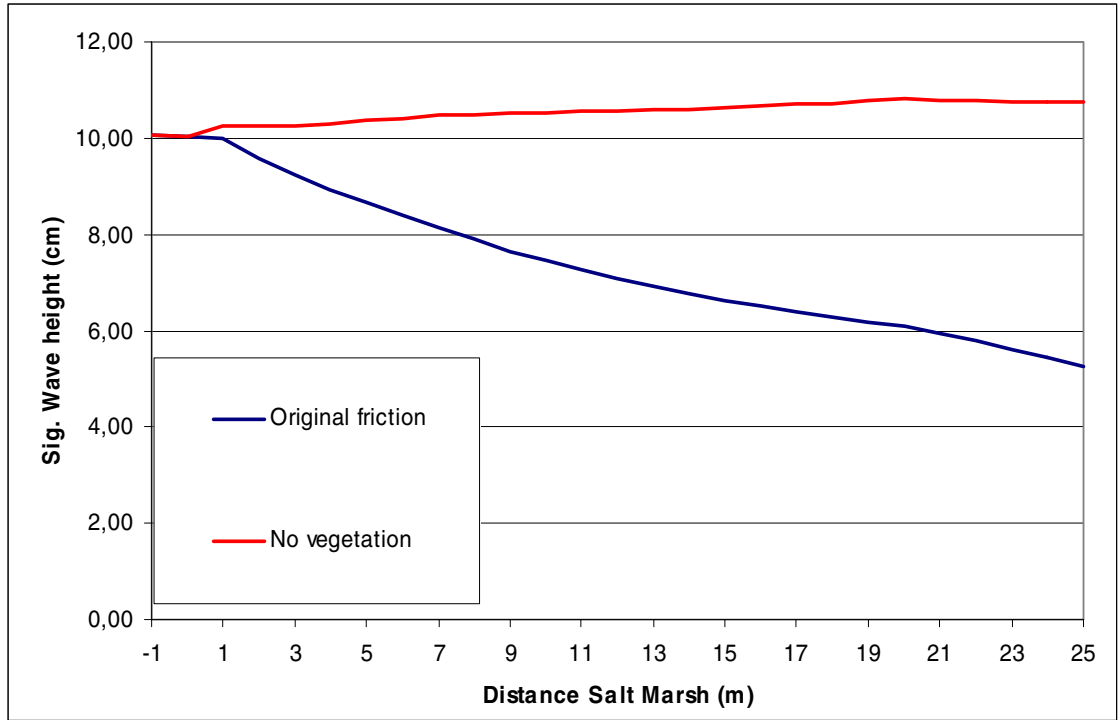
Graph 7.29: boundary wave height 150%, water level 1,46 m NAP (case 20:15)
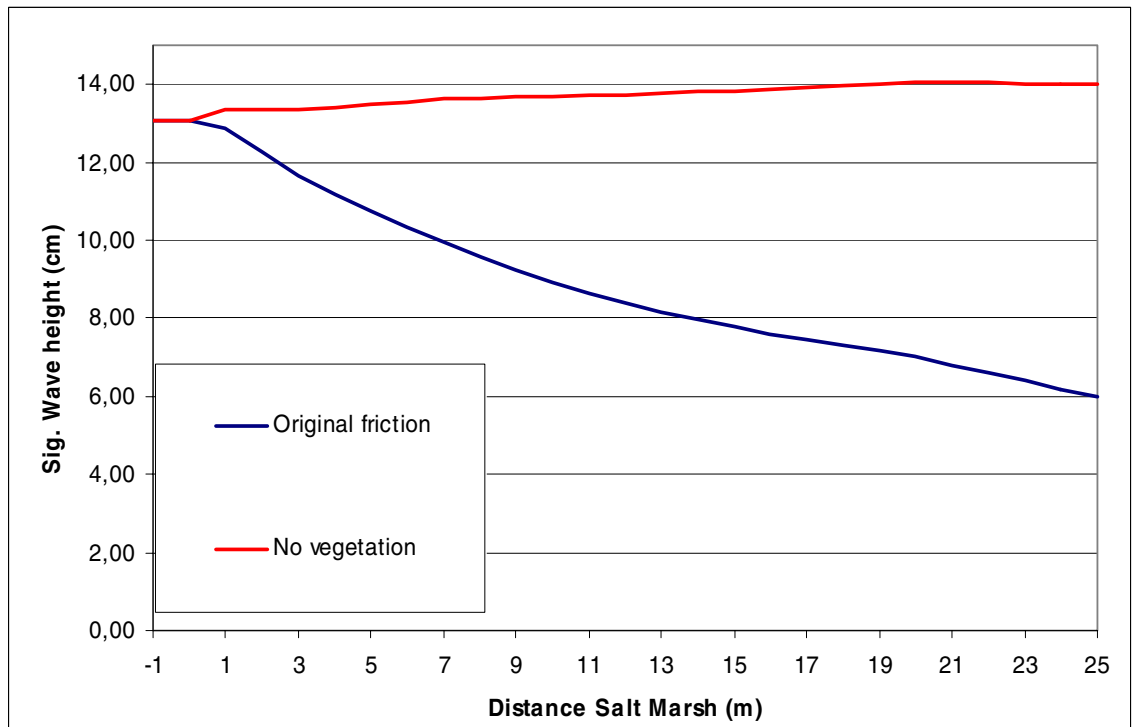
Graph 7.30: boundary wave height 200%, water level 1,46 m NAP (case 20:15)
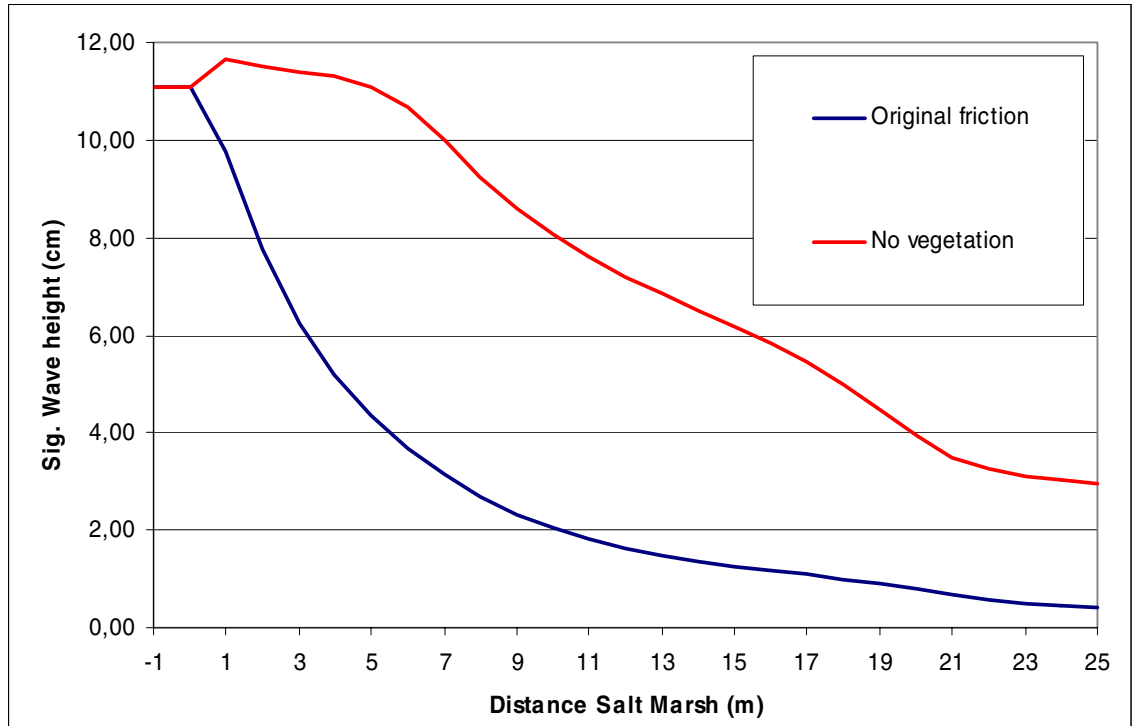
Graph 7.31: boundary wave height 150%, water level 1,03 m NAP (case 20:45)
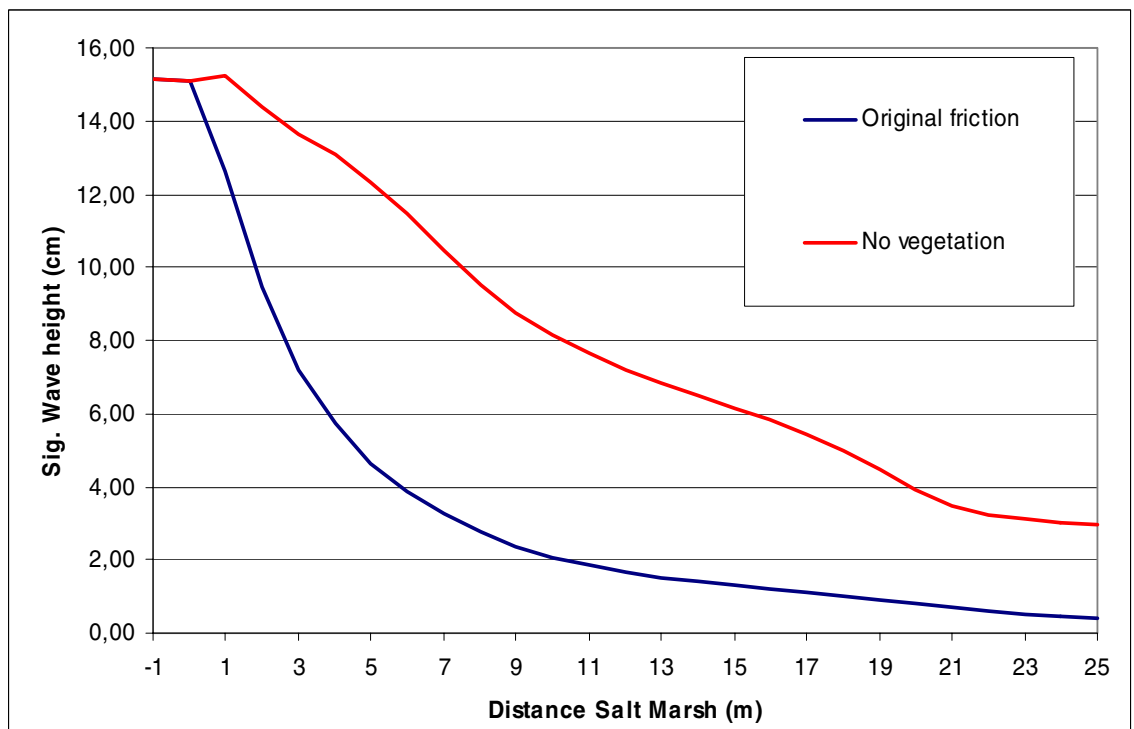
Graph 7.32: boundary wave height 200%, water level 1,03 m NAP (case 20:45)

B   Executive overview of ESTPROC

Project Inception Report, September 2002

Purpose

The DEFRA funded Estuary Process Research project (EstProc) started in December
2001 and has the following stated objectives:

- Innovative and fundamental research in estuarine hydrodynamics, sediments and biological interactions
- Improved underpinning knowledge and sound scientific results for the estuary research community and end users

The specific scientific objectives defined in the Terms of Reference were as follows,
subdivided under three technical headings (denoted Themes within the project)
namely, hydrodynamics, sediment processes and biology:

Hydrodynamics
1. To improve the modelling of waves in estuaries;
2. To improve the prediction of the impact of extreme events and major anthropogenic influences;
3. To investigate the interrogation of existing data to extract further information, interrelationships and correlations between parameters;
4. To improve the representation of near bed stresses.

Sedimentary Processes
1. To undertake further investigation into the transport of mixed sediments, where mixed sediments includes sand, mud, gravel or shell mixtures and dredged material with sizes upward of 5 microns;
2. To expand the understanding of the sediment transport profile;
3. To improve the understanding of general sedimentary processes.

Interactions Between Biological and Sedimentary Processes
1. To review and prioritise, at an early stage, the relevant biological process parameters that effect the stability, erodability and deposition of sediments;
2. To undertake investigations into the effect of biological processes on the stability; erodability and deposition of sediments. Format results for incorporation into existing models for morphological prediction and assess validity through use in different models;
3. To develop understanding of the impact of benthic life (primarily macrofauna) on performance of intertidal areas and the effect of the change in flow regime related to tidal stage.

Project Overview

A 3 year multi-disciplinary, integrated research project has been defined by the
EstProc project team, which comprises:

- HR Wallingford
- Proudman Oceanographic Laboratory
- Professor Keith Dyer / University of Plymouth
- St Andrews University, Gatty Marine Laboratory (Sediment Ecology Research Group)
- ABP Marine Environmental Research

- WL | Delft Hydraulics
- Plymouth Marine Laboratory
- University of Cambridge, Cambridge Coastal Research Unit
- University of Southampton, School of Ocean and Earth Sciences
- Digital Hydraulics Holland B.V.
- Centre for Environment, Fisheries and Aquaculture Science

The research is undertaken in an integrated fashion and each one of the themes has a designated Theme Leader to oversee the conduct and delivery of the research, which tackles key issues related to the delivery of:
- Improved understanding and modelling of hydrobiosedimentary processes
- Improved understanding and modelling of sediment erosion and deposition and the resulting changes in estuary morphology

The project is being run in 3 sequential stages:

Stage 1 – Improving focus and synergy (months 1 to 3)
A key activity in this Stage was the kick-off workshop which was attended by the entire project Consortium and Funders' representatives to brainstorm the detailed make-up of the project. The workshop clarified linkages between research topics and data sources, as well as identifying external links to other process based and engineering research. Activities completed in this Stage of the project led to the production of the Inception Report detailing the conduct of the programme in Stages 2 and 3.
Some secondary milestones have been defined in terms of some key integrating objectives:
- Tidal flat sedimentation – a key environment in which the research results must be demonstrated to operate in a harmonious fashion;
- Mudflat-saltmarsh interactions – a key area of the estuary fringe for fluxes of water and sediment, and a role as high water storage;
- Scales of interest – at what time and space scales should the assessment of various estuarine processes be made;
- Data task – interrogation of existing datasets for an improved understanding of hydrodynamic, sediment and biological processes and their interactions;
- Integrated morphological modelling – a key tool for implementing the new research findings and assessing their suitability in the subtidal and intertidal reaches of estuaries. The knowledge produced by the project can be used to improve the capability of predictive tools and methods and hence directly underpin their use in management activities.

Stage 2 – Delivering the science (months 4 to 30)
In this Stage of the programme all the technical work is planned for completion. The project team will participate in two workshops during this stage of the research at which the results will be presented and discussed. At these workshops progress will be facilitated by the secondary milestones defined in Stage 1 and by smaller technical meetings organised as required by the Task Leaders.

Stage 3 – Synthesis and outcomes (months 31 to 36)
The main effort in this Stage will be on documenting the scientific results from the previous 30 months in an integrated fashion, and to present them in such a way that they match the Quantifiable Deliverables associated with each of the Scientific Objectives defined in the Terms of Reference.

Dissemination and timetable

On completion of Stage 1

- Inception Report;
- Initiation of project web site through HR Wallingford which can be located at www.estproc.net ;

On completion of Stage 2

- Scientific Reports and Papers that have been produced by the partners;

On completion of Stage 3

- A workshop will be held as an open presentation to the scientific and engineering community concentrating on scientific and technical achievements and discussing the best ways for the audience to access them;
- Final report summarising in clear English the principal results and conclusions, and how the users of the research can pick up and implement the results;
- Specific reports and papers produced both individually and on a collaborative basis detailing technical aspects of the work undertaken;
- Improved methodologies or algorithms for representing processes and their interaction in estuaries;
- A data report detailing the data used in the project and how the data can be utilised in future projects; and,
- An update on future research requirements in the field of estuarine process research that will underpin the long-term goal of developing the Estuary Impact Assessment System.

Publicity for the project will be achieved through the web site as well as articles in the press, newsletters (including the DEFRA newsletter).

The deliverables and timetable for the project are described in more detail in the Inception Report. The two key events with respect to accessing the project results are:

1. An open scientific workshop to be held in July 2004; and,
2. The publication of the final deliverables, which is scheduled for November 2004.

Updates for these events will be published on the project web site as appropriate.

The project Inception Report report presents an appreciation of the main challenges and the scientific work proposed to achieve the above.

For more details please contact the EstProc Project Manager Richard Whitehouse (rjsw@hrwallingford.co.uk) or the Funders' Nominated Project Officer Jonathan Rogers (jonathan.rogers@mouchel.com).

C   Logger Connections

See figure 3.2 for corresponding locations

Period 1

logger #	logger location	sensor code	locatie	height (cm)
Logger 1	druk 1	8	8	2
Logger 1	druk 2	5	5	2
Logger 1	druk 3	4	4	2
Logger 1	druk 4	6	6	2
Logger 1	druk 5	9	9	2
Logger 1	EMS 1	E249	5	5
Logger 1	EMS 2	O63	4	5
Logger 1	EMS 3	D400	5	50
Logger 1	EMS 4	O20	7	5
Logger 1	EMS 5	D120	9	5
Logger 2	druk 1	7	7	2
Logger 2	druk 2	0	0	2
Logger 2	druk 3	1	1	2
Logger 2	druk 4	2	2	2
Logger 2	druk 5	3	3	2
Logger 2	EMS 1	O51	8	5
Logger 2	EMS 2	O17	1	50
Logger 2	EMS 3	D119	1	5
Logger 2	EMS 4	D115	3	5
Logger 2	EMS 5	O10	2	5

Period 2

logger #	logger location	sensor code	locatie	height (mm)
Logger 1	druk 1	**8**	8	20
Logger 1	druk 2	**5**	5	20
Logger 1	druk 3	**4**	4	20
Logger 1	druk 4	**6**	6	20
Logger 1	druk 5	**9**	9	20
Logger 1	EMS 1	**E249**	P4	1080
Logger 1	EMS 2	**O63**	P4	63
Logger 1	EMS 3	**D400**	P4	457
Logger 1	EMS 4	**O20**	P7	60
Logger 1	EMS 5	**D120**	P4	624
Logger 2	druk 1	**7**	7	20
Logger 2	druk 2	**0**	0	20
Logger 2	druk 3	**1**	1	20
Logger 2	druk 4	**2**	2	20
Logger 2	druk 5	**3**	3	20
Logger 2	EMS 1	**O51**	P7	1075
Logger 2	EMS 2	**O17**	P2	640
Logger 2	EMS 3	**D119**	P2	448
Logger 2	EMS 4	**D115**	P2	990
Logger 2	EMS 5	**O10**	P2	35

D   File Formats Loggers Paulinaschor

(parts are in Dutch)
AMF

ADMI
"TIMESTAMP","RECORD","Year","mmdd","hhmm","ss","DataCode","IDCode","RunInt
Min","BurstLength","SmplIntmSec","RawIntMin"
"TS","RN","","","","","","","","","",""
"","","Smp","Smp","Smp","Smp","Smp","Smp","Smp","Smp","Smp","Smp"
"2002-06-14 14:38:00",0,2002,614,1438,0,128,457,15,2048,250,15

PROC
"TIMESTAMP","RECORD","EMS1Vx_Avg","EMS1Vy_Avg","ECHO1_Avg","ECHO2_
Avg","OBS_Avg","Druk_Avg","EMS1Vx_Std","EMS1Vy_Std","ECHO1_Std","ECHO2_
Std","OBS_Std","Druk_Std"
"TS","RN","m/s","m/s","m","m","FTU","hPa","m/s","m/s","m","m","FTU","hPa"
"","","Avg","Avg","Avg","Avg","Avg","Avg","Std","Std","Std","Std","Std","Std"
"2002-06-14
14:53:37.5",0,0.157,0.037,0.634,0.956,44.4,163.1,0.019,0.016,0.003,0.004,2.696,3.561

RAW
"TIMESTAMP","RECORD","EMS1Vx","EMS1Vy","ECHO1","ECHO2","OBS","Druk"
"TS","RN","m/s","m/s","m","m","FTU","hPa"
"","","Smp","Smp","Smp","Smp","Smp","Smp"
"2002-07-02 07:07:53",1621837,0.294,0.05,0.584,0.954,1013,374.6

REF
"TIMESTAMP","RECORD","Year","mmdd","hhmm","ss","HEADING","TILTX","TILTY
","Druk","ExtVolt","Temp"
"TS","RN","","","","","deg","deg","deg","hPa","V","deg"
"","","Smp","Smp","Smp","Smp","Smp","Smp","Smp","Smp","Smp","Smp"
"2002-06-14 14:45:06.82",0,2002,614,1445,6.824,43.24,5.891,-4.756,157.7,13.95,22.38

DON

ID 100
Raw	EMF_1X
Raw	EMF_1Y
Raw	EMF_2X
Raw	EMF_2Y
Raw	OBS_1
Raw	OBS_2
Raw	Druksens

ID 200 :
Day	julday
Hour/Minute	hhmm
Average	Kompas

Average	Tilt_X
Average	Tilt_Y
Average	Batt__24V
Average	Batt_CR10
Average	Temp_CR10

ID 300 of ID 301

Day	julday
Hour/Minute	hhmm
Average	EMF_1X
Standard Deviation	EMF_1X
Average	EMF_1Y
Standard Deviation	EMF_1Y
Average	EMF_2X
Standard Deviation	EMF_2X
Average	EMF_2Y
Standard Deviation	EMF_2Y
Average	OBS_1
Standard Deviation	OBS_1
Average	OBS_2
Standard Deviation	OBS_2
Average	Druksens
Standard Deviation	Druksens

DON Snel
ID 103: 16Hz

Raw	EMF_1X
Raw	EMF_1Y
Raw	EMF_2X
Raw	EMF_2Y

ID 300 60 seconden
Year

Day	julday
Hour/Minute	hhmm
Seconds	ss.s
Average	OBS_1
Average	OBS_2
Average	Druksens

ID 500 (start van burst)
Year

Day	julday
Hour/Minute	hhmm
Average	Compass (Volt)
Average	Tilt1 (Volt)
Average	Tilt2 (Volt)

RAAI

Hierbij een paar kleine data files van de raai metingen, Paulina Polder. De indeling staat hieronder beschreven. Er zijn twee file soorten: Raai MASTER en Raai SLAVE. De SLAVE was uitgerust met een extra EMS (stroommeter)

en een extra drukopnemer. Elke regel bevat data van hetzelfde tijdstip. Regels die beginnen met 100 (M) / 101 (S) bevatten ruwe data en 200 (M) / 201 (S) bevatten datum / tijd en gemiddelde waarden.

De file raai1msm201lgr.dat behoort tot raai 1, de master unit, 2de meting, 01de file, van de logger (lgr)..
De file raai1ssm201lgr.dat behoort tot raai 1, de slave unit, 2de meting, 01de file, van de logger (lgr)..
De logger files bevatten gebufferde data en dienen als voorbeeld, de echte files zijn veel groter: tot ruim 41 Mbyte.

De data beginnen niet netjes aan het begin van een meetserie: zoek eerst het eind en tel dan terug of er 2048 meetwaarden zijn. Tussen opeenvolgende terminators moeten wel 2048 ruwe data regels staan

Raai   data   format
Het meetinterval was 250 ms.
Alle sensor waarden zijn in mV, met een lineaire verband zijn ze om te rekenen naar SI eenheden.
IJkgegevens EMS via Tjeerd Bouma te verkrijgen.
De druk opnemers geven 500 mV als ze droog staan (0 m WK) en 2500 mV bij 350 mbar (ongeveer 350 cm WK in zeewater).

Raai   MASTER
ID 100 0.25 Sec
EMS_1_Vx
EMS_1_Vy
EMS_2_Vx
EMS_2_Vy
Pres1
Pres2

ID 200 Output_Table, terminates each block of 2048 readings
Year_RTM
Day_RTM
Hour_Minute_RTM
Seconds_RTM
EMS_1_Vx_AVG
EMS_1_Vy_AVG
EMS_2_Vx_AVG
EMS_2_Vy_AVG
Pres1_AVG
Pres2_AVG

Raai   SLAVE
ID 100 0.25 Sec
EMS_1_Vx
EMS_1_Vy
EMS_2_Vx
EMS_2_Vy
EMS_3_Vx
EMS_3_Vy
Pres1
Pres2

Pres3

ID 200 Output_Table, terminates each block of 2048 readings
Year_RTM
Day_RTM
Hour_Minute_RTM
Seconds_RTM
EMS_1_Vx_AVG
EMS_1_Vy_AVG
EMS_2_Vx_AVG
EMS_2_Vy_AVG
EMS_3_Vx_AVG
EMS_3_Vy_AVG
Pres1_AVG
Pres2_AVG
Pres3_AVG

RIZA
ID 100
Raw   EMF_1X
Raw   EMF_1Y
Raw   Druksens
Raw   OBS_1

ID 200
Year, Day, Hour/Minute
Average   Kompas
Average   Tilt_X
Average   Tilt_Y
Average   Batt__24V
Average   Batt_CR10
Average   Temp_CR10

ID 300
Year, Day, Hour/Minute
Average   Kompas
Average   Tilt_X
Average   Tilt_Y
Average   Batt__24V
Average   Batt_CR10
Average   Temp_CR10
Average   EMF_1X
Standard Deviation   EMF_1X
Average   EMF_1Y
Standard Deviation   EMF_1Y
Average   Druksens
Standard Deviation   Druksens
Average   OBS_1
Standard Deviation   OBS_1

ID 400 (PC fout)
Year, Day, Hour/Minute

E   Description of Delft Auke Processes

(the description is copied from the Auke manual)

E.1 General information

1 Introduction
This chapter gives a first introduction to the use of the programs of DELFT-AUKE to compute wave generation signals and to perform wave generation. Another phrasing that will also be used for wave generation is wave board control because that is the essence of wave generation: control the wave board(s) in such a way that the wanted wave field is generated.
In section 1.1 *What is DELFT-AUKE PROCESS* it is explained in a general way how processing is performed just to give a good insight. Section 1.2 *How PROCESS is organized* shows how the process programs are organized. The following chapters tell more in detail how programs can be used. The programs use a set of commands which are described in detail in this manual. A more general description on commands and directives is presented in the FRAMEWORK manual.
1.1 What is DELFT-AUKE PROCESS
DELFT-AUKE is a set of programs for data acquisition and control of wave boards in experimental facilities for hydraulic research as well as processing of signals from instruments.
This manual deals with the part of DELFT-AUKE which provides the processing of series. The result of a program is always an output file which reflects the command file, gives information on the series file and on the series which are used. Some programs also create a new series file which can be processed again or plotted.
In a process program parameters are computed that describe some aspects of a series. Some of these parameter quantities can be stored in a parameter file. After that the parameters may be presented in a table or used to plot.
1.2 How PROCESS is organized
All processing programs use command files to instruct the program what to do. They also use the DEVICE.CNF configuration file for environment information.
A processing program has a simple structure:
series file   PROGRAM   *series file/parameter file*
where the data in an input series file is never changed. The output series file will always be created anew. An existing series file can only be overwritten with explicit permission. Parameter values in a parameter file will be overwritten without warning when a new computation is done for the same parameter. When the parameter is not yet stored it will be added.

The general plotting program AUKEPLOT uses always a series files as input. The result is a plot with one or more graphs and per graph one or more series. The series in one graph may come from various series files.
To be able to plot parameter values program PARPLOT is used to store these values in a series file according to the selection of the user.
Program GREDIT can be used to have a view to a series with an equidistant base. It is possible to scroll in the series. It is also used to edit series data for example pikes. Here too a new series file is created with the edited series stored.
In the directional case the use of (intermediate) files is somewhat different. It is explained in the section where the directional processing programs are described.
As a result the diagrams of the programs are:
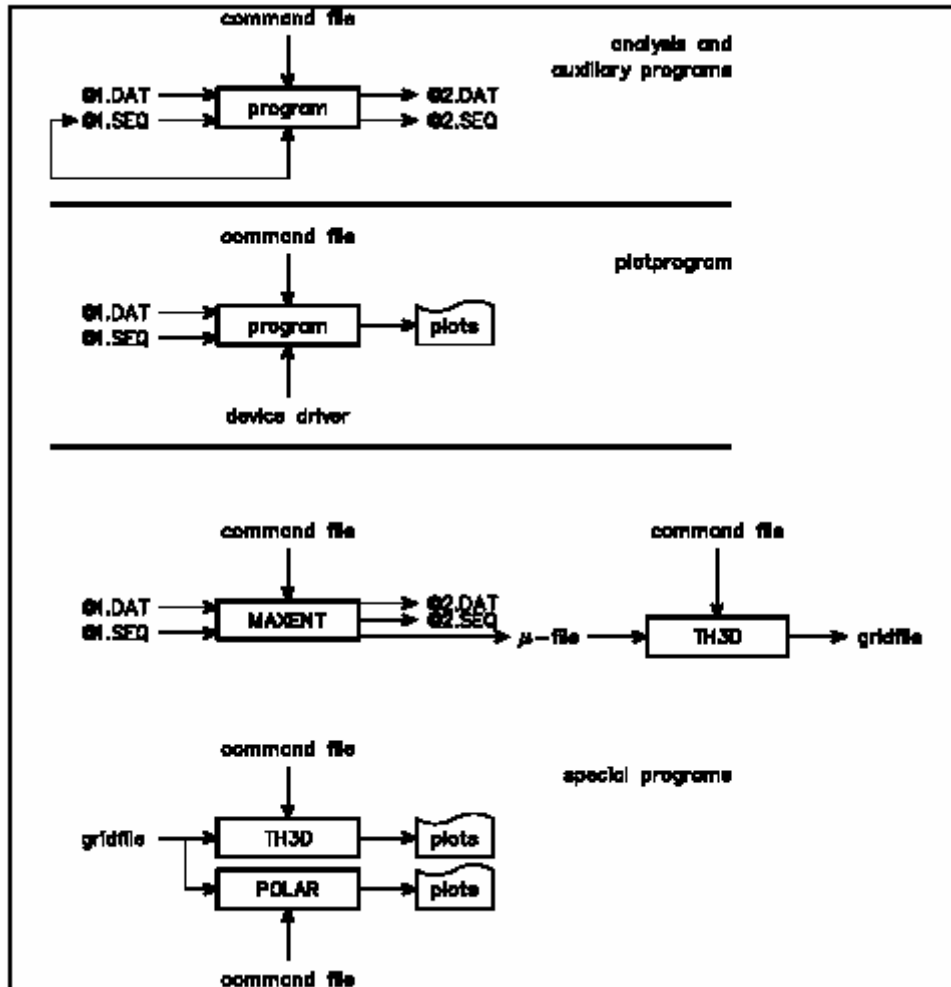
Structure diagram of process programs

The series files have two basic files:
. Data file with extension .DAT
. Information file with extension .SEQ
The parameter file has the extension .PAR and may have the name of the used series file or a name of its own supplied by the user.

1.3 Applying PROCESS

1.3.1 Applicability

The programs in PROCESS are in the first place used to process signals from hydraulic experiments. But any series may be processed no matter where they come from. The only restriction is that they fit in the DELFT-AUKE file system.

This way the processing programs can also be used to process data from measurements that are done outside an experimental facility. For instance, measurements in rivers or at the coast done by other systems can be processed.

When data does not meet the DELFT-AUKE standards it may be easy to transform the structure of the file, sometimes just by adding an SEQ information file. Please refer to the FRAMEWORK manual to see what can be done.

The programs can be used by everyone. Sometimes some theoretical background is needed which can be found in the description of that program. A working procedure will be that the project manager decides what must be computed and how the results must be presented. a project staff member than will make the command files for the various programs. A staff member will also develop the script files for a special work flow.

1.3.2 Limitations

Each processing program will have its own limitations. Therefore they are not given here but

with the description of the programs. For instance, program SPECTRUM has a limitation in the size of the sub-series that are used to compute spectral energy but there is no limitation to the size of the total series. Program FILTER on the other hand is restricted to a maximum number of data from a series. Only thinning can enlarge the part that can be used.

The computation time of the various programs will also differ and will even depend on the parameter setting in the command file. In general there is no computation time given for a program.

4 Programs description

In section 1.2 *How PROCESS is organized* diagrams are presented for a computation program and the plotting program. The diagram holds for all computing programs.

According to the license agreement the next sets of programs are purchased:

. Auxiliary programs.

. Non directional processing.

. Directional processing.

where the auxiliary programs will always be purchased. The types are described in separate sections of this chapter.

Each program is described in a separate subsection. A subsection has minimal three parts:

. The *introduction* part, a short summary of the task of the program.

. The *theory* part, the theoretical description of a process, if appropriate.

. The *commands* part, an overview and description of commands the program uses.

Among the subjects described in the theory part we explain how to use the program correctly. We also go into the theoretical limitations and possible settings. If appropriate a mathematical description is added. If necessary reference is made to the mathematics which can be found in Part 1 of this manual. Supplement to Bulletin N° 52 (1986) "List of sea state parameters" from the IAHR has been used for the notation of parameters and their descriptions.

When parameters are computed and stored to a parameter file they are described in the *theory* part.

The commands description part describes how all the offered options of a program offers may be applied with the help of commands and their parameters. Here also an overview is presented of the parameters that are stored in the parameter file and what identification is used.

In the commands part first a summary is presented of all commands that can be used by the program. The summary is divided into commands which are explained in section 4.3 *General commands*, and those commands specific for a program which are explained in the subsection of that program. The parameter commands follow the general commands and than the remaining commands will follow. Only the general commands relevant to the specific programs have been included in the review and when needed some additional information is given for that type of commands.

In the description of a program we will also indicate what files are used, both for input and output. We did not present these files again in a structure diagram as this is already done in chapter 1. Additional information on used file types is presented in the *Directional programs* subsection. Series that may be used are described as in some cases the type of series or the set of series to be used is fixed. Different file types may be performed as an outcome of a processing program. These file types are described in the separate program chapters.

The layout of all chapters is the same for each program description and they can easily be grasped. For this reason we did not include this program layout each time as it would make the table of contents unnecessarily lengthy.

Error messages are self-explaining and are therefore not mentioned in the User's Manual.

In the *Examples* document, the output of the programs for one or more runs is presented. The necessary command files and all related resulting files for that example runs can be found in the standard **DELFT-AUKE** kit. By doing so runs can be simulated and you, the user, may observe the effects when you change parameters and parameter values.

Before any program is described some general aspects which may concern all or part of the processing programs are described.

The first aspect is the *USE setting*: some parameters can be computed and used in a general way by each processing program.

The second aspect is some general mathematics: a set of programs may use the same fundamental mathematics. This will be described in a separate section *Mathematics* before the sections with the programs description.

Throughout the programs description and at output the notation for parameters is used which is presented in *IAHR, List of sea state parameters* [2].

4.1 The USE setting

Each series in a series file has a SERIES block. In such a block the information of a series may be stored. The directives that can be used are described in the FRAMEWORK manual in sub-section 3.3.6. This is not repeated here.

Another type of information are the *USE parameters*. These parameter values give some statistical information which can be used by the processing programs. They are computed by program STATIST that also stores them in the SERIES block or by the process program itself. In the latter case the USE parameter values are not stored.

From heron the directives that are stored are described.

MAXIMUM,$value$
MINIMUM,$value$

The extremes of the series are stored in $value$. The values hold for the part of the series that is selected the moment the computation was performed. Most of the time the complete series will be used.

VARIANCE,$value$

The variance of the series data values is stored in $value$ and is computed according to

$$\left[\sum_{i=1}^{n} (\bar{x} - x_i)^2 \right] / (n-1)$$

POLY0,C0=$c0$
POLY1,C0=$c0$**,C1=**$c1$
POLY2,C0=$c0$**,C1=**$c1$**,C2=**$c2$
POLY3,C0=$c0$**,C1=**$c1$**,C2=**$c2$**,C3=**$c3$

Data values can be related to a level that is defined by a polynomial. A polynomial has the general formula

$$y(j) = \sum_{k=0}^{3} c_k x^k (j)$$

with j the ordering number of the data values in the series. The computed level value for a data value according to the used polynomial is subtracted from the calibrated series value. This way a possible trend in the series is removed.

The number that is attached to **POLY** gives the order of the polynomial.

All polynomial coefficients are computed by program STATIST and stored in the series block or computed in the processing program which is used. Here too it must be decided whether the total series or just a part is used for the computation of the coefficients.

The polynomial coefficients hold up to the part that is used for the computation.

The **POLY0** polynomial equals the mean of the selected series part. For that reason no mean value is stored.

Refer to the description of program STATIST in the section of the non directional process programs how these parameters are computed and stored in a series file. After this such a parameter value can be used by any other processing program.

In a processing program there are two options how a USE parameter can be used in a computation:

1. Use the parameter value that is computed and stored with STATIST.

2. Compute the parameter value in the processing program for the selected series part.

The USE parameters that must be used must be set in the USE block in the command file for a processing program:

USE

..

END:USE

If it is not positioned in this block it will not be made active.

A parameter is selected with

parameter, {**CALCULATE**|}

with possible *parameters*:

MAXIMUM
MINIMUM
VARIANCE
POLY0
POLY1
POLY2
POLY3

When parameter **CALCULATE** is added the value of the USE parameter is computed by the processing program. When the parameter field is empty or another text is given the processing program uses the parameter value that is stored in the SERIES block in the SEQ information file. If the parameter is not found there the parameter value that is used is zero.

4.2   Mathematics

In several programs the same mathematics is used. In this section we describe the various aspects of the relevant equations.

4.2.1   Discrete Fourier Transform

A complete series or a subseries of the selected series can be analyzed by using discrete Fourier transform (DFT).
The general equation used for a single series is:

$$\hat{Z}(k) = \sum_{n=0}^{N-1} z(n) e^{-i\frac{2\pi}{N}nk} \tag{4.1}$$

with $\hat{Z}(k)$ complex and k=0,1,..,N/2. Z(n) represents the series data value with n=0,1,..,N where N is a power of 2.
A fast DFT procedure (FFT) is used for solving this equation.

The required frequency step Δf is derived from the used frequency window used. This window is defined as $f_{Nyq} = \frac{1}{2\Delta t}$ in which f_{Nyq} is the Nyquist frequency and Δt the selected time step or other equidistant unit. The frequency step Δf which is applied can be found from $\frac{1}{N \cdot \Delta t}$.

Three parameters are used to inform the user what the accuracy of the spectral analysis is:

- Frequency resolution $Be = 2 \cdot \frac{c_1}{c_2} f_{Nyq} \frac{1}{N+1}$ (4.2)

- Degrees of freedom $\upsilon = 2 c_1 M$ (4.3)

- Relative error estimate $\varepsilon_r = \sqrt{\frac{2}{\upsilon}}$ (4.4)

In these equations M is the number of subseries used and c_1 and c_2 are coefficients with values depending on tapers used. The tapers used with the values for the coefficients are explained in the descriptions of the programs SPECTRUM and CROSS.

The spectral densities for a subseries are computed with equation:

$$\hat{S}(k.\Delta f) = \beta \frac{2\Delta f}{N} |\hat{X}(k)|^2$$

(4.5)

In this equation β is a factor depending on the taper type used for the subseries.
The resulting spectral densities are given with equation:

$$\tilde{S}(k.\Delta f) = \frac{1}{M} \sum_{i=1}^{M} \hat{S}_i(k.\Delta f)$$

(4.6)

A new series is computed with an inverse FFT procedure according to equation:

$$\tilde{z}(k) = \frac{1}{N} \sum_{n=0}^{N-1} \tilde{Z}(n) \, e^{j\frac{2\pi}{N}nk}$$

(4.7)

where, for instance, the $\tilde{Z}$ series is the transformed $\hat{Z}$ series from Eq. 1 according to any user-supplied transformation.

4.2.2 Spectral information

When a spectrum is computed from a series spectral parameters become available. They are computed in several programs. We explain them in this subsection.

Some of these parameters use spectral moments, indicated with m_i where i is a figure. The general equation for the moments is:

$$m_i = \int_{f_1}^{f_2} f^i \, S(f) \, df \quad i = 0,1,2...$$

(4.8)

with f_1 and f_2 the lower and upper frequency limit of the area containing energy.

As the spectral density values are computed at discrete intervals the above equation is realised with a numerical integration procedure.

The parameters at output are:

The moments
Computed are m_0, m_2 and m_4 according to Eq. 4.8.

The peak frequency
f_p The frequency where the spectral energy is at a maximum and forms the spectrum peak. The peak period here is $T_p=1/f_p$.
f_{pD} The spectral peak frequency as computed by the centroid of the spectral band between the lower and upper intercepts (f_1 and f_2) of the spectral density and the threshold which is 80% of $S_\eta(f_p)$

$$f_{pD} = \frac{\int_{f_1}^{f_2} f\, S_\eta(f)\, df}{\int_{f_1}^{f_2} S_\eta(f)\, df}$$

(4.9)

Average periods from spectral moments

$$T_{0,1} = m_0 / m_1$$

(4.10a)

$$T_{0,2} = \sqrt{m_0 / m_2}$$

(4.10b)

equals the average period between two positive zero crossings

$$T_{2,4} = \sqrt{m_2 / m_4}$$

(4.10c)

equals the average interval between two successive local maximum values. A local maximum is the value where the first derivative of the signal changes from a positive value to a negative value.

Narrowness Parameter

$$\varepsilon_2 = \sqrt{m_0 m_2 / m_1^2 - 1}$$

(4.11)

this is the ν parameter from Longuet-Higgins.

Broadness Factor

$$\varepsilon_4 = \sqrt{1 - m_2^2 / (m_0 m_4)}$$

(4.12)

Correlation between successive wave heights

In *van Vledder, Statistics of wave group parameters* [7] a statistical analysis of random wave groups is presented. Formulae presented there are used to give an estimate of correlations in a random wave signal.

A correlation value is the κ value. The general equation for this parameter:

$$m_0^2 \kappa^2(\tau) = \left(\int_0^\infty E(\omega) \cos[\omega - \overline{\omega}]\, d\omega \right)^2 + \left(\int_0^\infty E(\omega) \sin[\omega - \overline{\omega}]\, d\omega \right)^2$$

(4.13)

Taking for the separation τ an integer number of mean wave periods, $\tau = \alpha \overline{\tau} = \alpha . 2\pi / \overline{\omega}$ where $\alpha = 1,2,3......$ The above expression can be simplified to (H228, 1B, app. G):

$$m_0^2 \kappa^2(\tau) = \left(\int\limits_0^\infty E(\omega)\cos\omega\tau d\omega \right)^2 + \left(\int\limits_0^\infty E(\omega)\sin\omega\tau d\omega \right)^2$$

The τ value in Eq. 4.13 can be chosen freely. In the DELFT-AUKE programs $T_{0,2}$ is used to compute the κ correlation value for output.

The relation between the correlation value κ and the coefficient of linear correlation ρ_{HH} is given by

$$\rho_{HH} = \frac{\pi}{16-4\pi}\left(\kappa^2 + \frac{\kappa^4}{16} + \frac{\kappa^6}{64} \right)$$

Van Vledder [7] found an improved computation of the coefficient of linear correlation:

$$\rho_{HH} = \frac{\rho_{HH}\left(\frac{1}{2}T\right) + 2\rho_{HH}(T) + \rho_{HH}\left(\frac{3}{2}T\right)}{2 + 2\rho_{HH}\left(\frac{1}{2}T\right)} \tag{4.14}$$

with T the period $T_{0,2}$. This linear correlation coefficient is sent to output.

Significant wave height

$$H_{m0} = 4\sqrt{m_0} \tag{4.15}$$

E.2 A description of Conasc

Program CONASC converts an ASCII data file to an DELFT-AUKE series file. The program is useful when the data are stored in an ASCII file and you want to do some processing with DELFT-AUKE programs.

The layout of the ASCII file is explained in the description of the **FILE-TYPE** command. All series must have the same number of samples. In the resulting DELFT-AUKE series file the series are stored according to the EQ option. In the EQ directive the LOW parameter is set to 1, the HIGH parameter to the number of samples found and the STEP parameter to 1. So, if there is an equidistant time series this will be stored as a series and not in the EQ directive. How the program works is best explained with the description of the commands.

E.3 Description of Waves

SPECTRUM

Introduction

With the program SPECTRUM the spectral densities of series are computed. A number of series may be selected, up to the number of series available in the data file. Together with the densities a set of parameters is computed and sent to the chosen output device.
The spectral density series can be sent to a new series file after which this file can be applied for plotting or for further post processing.
The theoretical aspects of spectral analysis are dealt with in Chapter 4 *Mathematics*.

Theory

With the general commands the whole data set or a part of a series is selected. The spectral analysis is executed on that specific selected part.
If the USE mechanism is used and, for instance, a POLYi directive is selected the series data values will be related to this base for spectral analysis.

When a reference is made in this chapter to a particular equation number, this equation is incorporated in Chapter 4.

With special commands the total data part is divided into smaller parts, the sub-series. There are two possible ways in selecting subseries:

1. The subseries are linked up so that a new subseries starts immediately after ending of the previous subseries.
2. The subseries partly overlap one another, each subseries starts halfway of the previous subseries. This means that most of the data values will be used twice.

These two modes are visualised below:

where # i is the selected subseries number
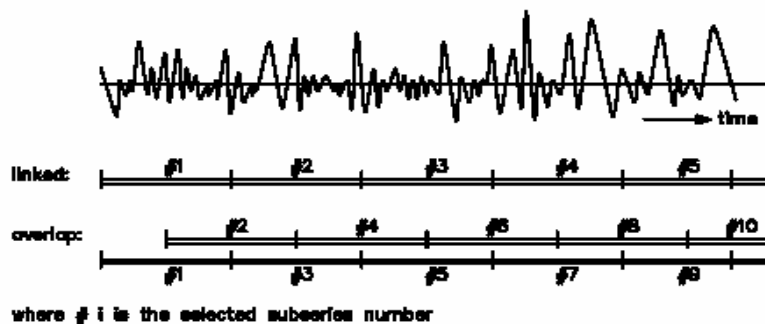
When a subseries is selected the spectral analysis is performed with an FFT according to Eq. 4.1 for that subseries data values. The series must be time-based with an equidistant

step. The spectral densities are computed according to Eq. 4.5 where the value for β is set according to the table in this section.

The three parameters Be (Eq. 4.2), υ (Eq. 4.3) and $\_{r}$ (Eq. 4.4) are used to indicate what the accuracy of the analysis is. An overview of the values for coefficients c_i in these equations is given in the table in this chapter.

The completed spectral density values are eventually averaged according to Eq. 4.6.

Three types of data tapering may be applied, two of them in the frequency domain and one in the time domain.

1. COSINE taper (Welch;1967), used in the frequency domain on each subseries result:

$$\tilde{X}(k) = -\tfrac{1}{4}\hat{X}(k-1) + \tfrac{1}{2}\hat{X}(k) - \tfrac{1}{4}\hat{X}(k+1) \quad k = 1,\ldots\frac{N}{2}-1$$

$$\tilde{X}(0) = \tfrac{1}{2}\hat{X}(0) - \tfrac{1}{2}\hat{X}(1)$$

$$\tilde{X}(\frac{N}{2}) = -\tfrac{1}{2}\hat{X}(\frac{N}{2}-1) + \tfrac{1}{2}\hat{X}(\frac{N}{2})$$

2. SINE taper, used in time domain on a subseries:

$$\hat{x}(n) = x(n)\tfrac{1}{2}[\mathrm{SIN}\{(\frac{n}{\frac{N}{10}}-1)\frac{\pi}{2}\} + 1] \quad n = 0,1,\ldots,\tfrac{N}{10}$$

$$\hat{x}(n) = x(n)\tfrac{1}{2}[\mathrm{SIN}\{(1+\frac{n}{\frac{N}{10}})\frac{\pi}{2}\} + 1] \quad n = N - \tfrac{N}{10},\ldots,N$$

and the remaining values

$$\hat{x}(n) = x(n)$$

Illustration of the SINE taper:

3. The Hanning (or Tukey) window, used in the frequency domain, is a frequency-smoothing filter. After the spectral densities are averaged over all the subseries this taper can be expressed as follows:

$$S(k) = \tfrac{1}{4}\tilde{S}(k-1) + \tfrac{1}{2}\tilde{S}(k) + \tfrac{1}{4}\tilde{S}(k+1) \quad k = 1, \ldots, \tfrac{N}{2} - 1$$

$$S(0) = \tfrac{1}{2}\tilde{S}(0) + \tfrac{1}{2}\tilde{S}(1)$$

$$S(\tfrac{N}{2}) = \tfrac{1}{2}\tilde{S}(\tfrac{N}{2}-1) + \tfrac{1}{2}\tilde{S}(\tfrac{N}{2})$$

When there is no window used in the time domain it is called a RECTANGULAR window.

An overview of the possible combinations of subseries selection and tapering is given below, with values for the coefficients c_1, c_2 and β.

#	overlap	taper type COSINE	SINE	HANNING	c_1	c_2	β
1	No	No	No	No	1.	1.	1.
2	No	No	No	Yes	1.3	1.	1.
3	No	Yes	No	No	1.	.5	8/3
4	No	No	Yes	No	1.	.9	8/7
5	No	Yes	No	Yes	1.3	.5	8/3
6	No	No	Yes	Yes	1.3	.9	8/7
7	Yes	Yes	No	No	1.	.5	8/3
8	Yes	Yes	No	Yes	1.3	.5	8/3

In the resulting output a set of parameters is presented. The used equations are Eq. 4.8 to Eq. 4.15.

The parameters are the spectral moments m_i, the peak frequency f_p and period T_p, the average periods $T_{0,1}$, $T_{0,2}$ and $T_{2,4}$. Some more parameters are the narrowness parameter ε_2, the broadness factor ε_4, the κ kappa value, the coefficient of linear correlation ρ and the significant height H_{m_0}.

Note that β from the table is only a mean estimate. The precise value in reality depends on the time series (see R680-II).

E.4: A description of Waves

WAVES

Introduction

With WAVES the development of series values between two positive zero crossings is determined. Some of the results can be stored in a new series file. In the description the term waves and wave signal is used. However, any signal that acts such as a wave signal may be used.

Theory

A definition of the various quantities in a wave series, or in any series with the behaviour like in a wave signal, is presented by the next illustration, derived from the 'List of sea state parameters' from IAHR.
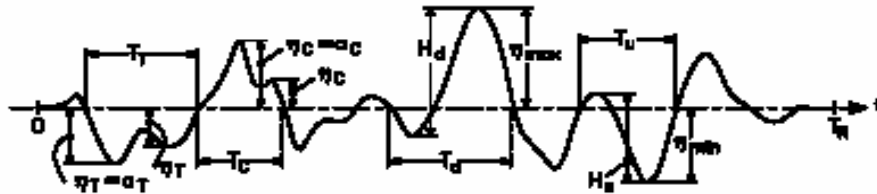
The wave parameters in the illustration are:

η The distance to a base line, normally zero.

H   The height between the minimum and maximum values found between two base line crossings with the same direction.

T   The difference of the values of two base line crossings with the same direction.

a   The amplitude being the greatest η between two successive base line crossings, so with different direction.

Subscripts indicate a differentiation of the parameters:

- $_C$ The given parameter is related to a crest.
- $_T$ The given parameter is related to a trough.
- $_u$ A value between two upwards base-line crossings.
- $_d$ A value between two downwards base-line crossings.

Possible base lines are:

- The zero value
- The ZEROLEVEL value from a SERIES block
- The level described by one of the POLYi functions

In program WAVES the following parameters are computed and sent to output:

- The number of waves between the upward crossings.
- The average wave period Tm.
- Average of the highest one-third upward crossings:

  H1/3u   the total height
  aC1/3,u   the crest amplitude
  aT1/3,u   the trough amplitude

Average of the highest one-tenth upward crossings:

  H1/10u   the total height
  aC1/10,u   the crest amplitude
  aT1/10,u   the trough amplitude

The u index from "upwards" can also be d from "downwards". The index type indicates whether an upwards or a downwards zero crossing for the wave detection is used.

- Correlation values, with the general formula for the linear correlation coefficient:

$$r(\bar{Z}) = \frac{N}{N-1} \frac{\sum\limits_{i=1}^{N-1} (Z_i - \bar{Z})(Z_{i+1} - \bar{Z})}{\sum\limits_{i=1}^{N} (Z_i - \bar{H})^2}$$

In WAVES two parameter types are computed with the correlation function:

1. Kappa $\kappa = \sqrt{r(X^2)}$
2. Gamma $\gamma = r(X)$

For X the H, a_C or a_T parameter can be selected.

- The gamma value, being the linear correlation coefficient, computed from the κ value for one of the three possible wave parameters:

$$\gamma(\kappa) = \frac{E(\kappa) - \frac{1}{2}(1-\kappa^2)K(\kappa) - \frac{\pi}{4}}{1 - \frac{\pi}{4}}$$

with

$$K(\kappa) = \int\limits_{0}^{\pi/2} \frac{d\theta}{\sqrt{1-\kappa^2\sin^2\theta}}$$

and

$$E(\kappa) = \int_{0}^{\pi/2} \sqrt{1 - \kappa^2 \sin^2\theta} \, . \, d\theta$$

Output in the form of a table presents the minimum and maximum values of H_u, a_c and a_T together with the position (time) in the series of the related wave. As each of these parameters may be derived from another location, the values of the other parameters for that wave are also presented together with their position. Also T_u of the related wave is presented for each parameter.
The location of H_u is the position where the wave starts, so the upward base-line crossing. The location of a_c and a_T is the position of the value itself.

The values H_u, a_c and a_T can be presented for various percentage values Z_i being the probability of exceedance. This is according to the Rayleigh probability distribution function $P(x > Z_i) = e^{-\left(\frac{Z_i}{Z_{rms}}\right)^2}$ with $P(x > Z_i)$ the number of waves n larger than Z_i divided by the total number N of waves. So P has the form n/N.

Also on output is the root mean square of a height $Y_{rms} = \sqrt{\frac{1}{N} \sum_{j=1}^{N} Y_j^2}$, where Y can be H_u,

a_c and a_T.

Information can be retrieved of maximum 50 highest values of H_u, a_c and a_T together with their location. This information is sent to output.
For further use the series of all values of H_u, a_c and a_T can be stored together with their location in a new series file. By doing so it is for instance possible to make a H-T correlation graph with AUKEPLOT.

E.5 Output parameters

Spectrum:

Parameters

NAME	UNIT	DESCRIPTION	
m-1	$\diamond^{\wedge}2s$	Spectral moment m_{-1}	Gen.Eq. 4.8
m0	$\diamond^{\wedge}2$	Spectral moment m0	Gen.Eq. 4.8
m1	$\diamond^{\wedge}2/s$	Spectral moment m1	Gen.Eq. 4.8
m2	$\diamond^{\wedge}2/s2$	Spectral moment m2	Gen.Eq. 4.8
m4	$\diamond^{\wedge}2/s4$	Spectral moment m4	Gen.Eq. 4.8
TpD	s	Dominant peak period for total spectrum	Gen.Eq. 4.9
fpD	Hz	Dominant peak frequency for total spectrum	Gen.Eq. 4.9
Tp	s	Period of the largest density	
fp	Hz	Frequency of the largest density	
Maxden	$\diamond^{\wedge}2s$	Maximum spectral density anywhere in the spectrum	
T01	s	Average period $T_{0,1}$	Gen.Eq 4.10a
T02	s	Average period $T_{0,2}$	Ge.Eq. 4.10b
T24	s	Average period $T_{2,4}$	Ge.Eq. 4.10c
Hm0	$\diamond$	Significant wave height	Gen.Eq. 4.15
eps2	--	Narrowness parameter (ν from Longuet-Higgins)	Gen.Eq. 4.11
eps4	--	Broadness parameter	Gen.Eq. 4.12
kappa(f)	--	The κ correlation value	Gen.Eq. 4.13
gamma(f)	--	The linear correlation coefficient for wave heights	Gen.Eq. 4.14

Waves:

Parameters

NAME	UNIT	DESCRIPTION	
H1/3*	$\diamond$	Mean of the highest 1/3 of the waves	
T1/3*	s	Mean of the highest 1/3 of the periods	
H1/10*	$\diamond$	Mean of the highest 1/10 of the waves	
T1/10*	s	Mean of the highest 1/10 of the periods	
Tm*	s	The average wave period	
Hmax*	$\diamond$	The maximum of all wave heights	
Tmax*	s	The maximum of all wave periods	
Hm*	$\diamond$	The average wave height	
Hrms*	$\diamond$	The root mean square wave height	
kappa(t)*	--	The κ correlation value	Gen.Eq. 4.13
gamma*	--	The linear correlation coefficient for wave heights	Gen.Eq. 4.14
N*	--	The number of waves found	
Hx%*	$\diamond$	The $x\%$ exceeded wave height	
HGT*hhh*	%	Find the exceedance percentage for the height hhh	

F   Matlab Script

This script has been used for the calculation of wave number k

```
function [k,omega,c,cg,D,Dr]=wavenr(h,t,E,beta,Er)
g=9.81;
rho=1025;
fac=8/rho/g;
n=10;
alfa=1;
gamma=.55;

H=sqrt(fac*E);
a1 = 5.060219360721177D-01; a2 = 2.663457535068147D-01;
a3 = 1.108728659243231D-01; a4 = 4.197392043833136D-02;
a5 = 8.670877524768146D-03; a6 = 4.890806291366061D-03;
b1 = 1.727544632667079D-01; b2 = 1.191224998569728D-01;
b3 = 4.165097693766726D-02; b4 = 8.674993032204639D-03;

pi   = 4.0 .* atan ( 1.0);
ome2 = (2.0 .* pi ./ t).^2 .*  (h) ./  (g);

num  = 1.0 + ome2.*(a1+ome2.*(a2+ome2.*(a3+ome2.*(a4+ome2.*(a5+ome2.*a6)))));
den  = 1.0 + ome2.*(b1+ome2.*(b2+ome2.*(b3+ome2.*(b4        +ome2.*a6 ))));
k    = sqrt ( ome2 .* num ./ den) ./  h;

omega=2*pi./t;
c=omega./k;
kh=k.*h;
tkh=tanh(kh);
cg=g/2./omega.*(tkh+kh.*(1.-tkh.*tkh));
D=2*alfa./t.*E.*(1-exp(-(H/gamma./h).^n));
Dr=2*beta*g*Er./c;
end
```

G   Theory of SWAN

The following part has been copied out of the Swan manual (short version)

In SWAN the waves are described with the two-dimensional wave action density spectrum $N(\sigma,\theta)$ equal to the energy density divided by the relative frequency: $N(\sigma,\theta)=E(\sigma,\theta)/\sigma$.

<u>Action balance equation</u>
In SWAN the evolution of the wave spectrum is described by the spectral action balance equation which for Cartesian coordinates is

$$\frac{\partial}{\partial t}N+\frac{\partial}{\partial x}c_x N+\frac{\partial}{\partial y}c_y N+\frac{\partial}{\partial \sigma}c_\sigma N+\frac{\partial}{\partial \theta}c_\theta N=\frac{S}{\sigma} \tag{A1a}$$

The first term in the left-hand side of this equation represents the local rate of change of action density in time, the second and third term represent propagation of action in geographical space (with propagation velocities c_x and c_y in x- and y-space, respectively). The fourth term represents shifting of the relative frequency due to variations in depths and currents (with propagation velocity c_σ in σ-space). The fifth term represents depth-induced and current-induced refraction (with propagation velocity c_θ in θ-space). The expressions for these propagation speeds are taken from linear wave theory. The term S $(=S(\sigma,\theta))$ at the right hand side of the action balance equation is the source term in terms of energy density representing the effects of generation, dissipation and nonlinear wave-wave interactions.

<u>Wind input</u>
Transfer of wind energy to the waves is described in SWAN with a resonance mechanism and a feed-back mechanism. The corresponding source term for these mechanisms is commonly described as the sum of linear and exponential growth:

$$S_{in}(\sigma,\theta)=A+B\ E(\sigma,\theta) \tag{A2}$$

in which A and B depend on wave frequency and direction, and wind speed and direction.
<u>Dissipation</u>
The dissipation term of wave energy is represented by the summation of three different contributions: whitecapping $S_{ds,w}(\sigma,\theta)$, bottom friction $S_{ds,b}(\sigma,\theta)$ and depth-induced breaking $S_{ds,br}(\sigma,\theta)$.

Whitecapping is primarily controlled by the steepness of the waves. In presently operating third-generation wave models (including SWAN) the whitecapping formulations are based on a pulse-based model (Hasselmann, 1974), as adapted by the WAMDI group (1988):

$$S_{ds,w}(\sigma,\theta)=-\Gamma\ \tilde{\sigma}\frac{k}{\tilde{k}}E(\sigma,\theta) \tag{A3}$$

where Γ is a steepness dependent coefficient, k is wave number and $\tilde{\sigma}$ and $\tilde{k}$ denote a mean frequency and a mean wave number, respectively (cf. the WAMDI group, 1988
Depth-induced dissipation may be caused by bottom friction, which can generally be represented as:

$$S_{ds,b}(\sigma,\theta)=-C_{bottom}\frac{\sigma^2}{g^2\sinh^2(kd)}E(\sigma,\theta) \tag{A4}$$

in which C_{bottom} is a bottom friction coefficient. JONSWAP suggested to use an empirically obtained constant. It seems to perform well in many different conditions as long as a suitable value is chosen (typically different for swell and wind sea

The process of depth-induced wave-breaking is still poorly understood and little is known about its spectral modelling. In contrast to this, the total dissipation (i.e., integrated over the spectrum) due to this type of wave breaking can be well modelled with the dissipation of a bore applied to the breaking waves in a random field the expression that is used in SWAN is:

$$S_{ds,br}(\sigma,\theta) = \frac{D_{tot}}{E_{tot}} E(\sigma,\theta) \qquad \text{(A5)}$$

in which E_{tot} is the total wave energy and D_{tot} (which is negative) is the rate of dissipation of the total energy due to wave breaking.

Nonlinear wave-wave interactions

In deep water, quadruplet wave-wave interactions dominate the evolution of the spectrum. They transfer wave energy from the spectral peak to lower frequencies (thus moving the peak frequency to lower values) and to higher frequencies (where the energy is dissipated by whitecapping). In very shallow water, triad wave-wave interactions transfer energy from lower frequencies to higher frequencies often resulting in higher harmonics (low-frequency energy generation by triad wave-wave interactions is not considered here). In SWAN the computations are carried out with the Discrete Interaction Approximation (DIA): the Lumped Triad Approximation (LTA).

  a. first-order (stationary and non-stationary cases) backward space-backward time: the BSBT scheme,

  b. second-order (non-stationary cases) with third-order diffusion: the S&L-scheme (Stelling and Leedertse, 1992) and

  c. second-order (stationary cases) with second-order diffusion: the SORDUP scheme

The BSBT scheme (not default in SWAN) will be discussed first and then the extension to the higher order schemes which are default in SWAN. The first-order upwind scheme (BSBT= backward space, backward time) is a sequence of four forward-marching sweeps (one per quadrant). To properly account for the boundary conditions between the four quadrants, the computations are carried out iteratively at each time step. The integration in time is a simple backward finite difference, so that the discretization of the action balance equation is (for positive propagation speeds; including the computation of the source terms but ignoring their discretization):

$$\left[\frac{N_{i_t,n} - N_{i_t-1}}{\Delta t} \right]_{isubx, i_y, i_\sigma, i_\theta} +$$

$$\left[\frac{[c_x N]_{i_x} - [c_x N]_{i_x-1}}{\Delta x} \right]_{i_t, n\, i_y, i_\sigma, i_\theta} + \left[\frac{[c_y N]_{i_y} - [c_y N]_{i_y-1}}{\Delta y} \right]_{i_t, n\, i_x, i_\sigma, i_\theta} +$$

$$\left[\frac{(1-v)[c_\sigma N]_{i_\sigma+1} + 2v[c_\sigma N]_{i_\sigma} - (1+v)[c_\sigma N]_{i_\sigma-1}}{2\Delta\sigma} \right]_{i_t, n\, i_x, i_y, i_\theta} +$$

$$\left[\frac{(1-\eta)[c_\theta N]_{i_\theta+1} + 2\eta[c_\theta N]_{i_\theta} - (1+\eta)[c_\theta N]_{i_\theta-1}}{2\Delta\theta} \right]_{i_t, n\, i_x, i_y, i_\sigma} = \left[\frac{S}{\sigma} \right]_{i_t, n^*\, i_x, i_y, i_\sigma, i_\theta}$$

$$\text{(C1)}$$

where i_t is the time-level index and i_x, i_y, i_σ and i_θ are grid counters and Δt, Δx, Δy, $\Delta \sigma$ and $\Delta \theta$ are the increments in time, geographic space and spectral space respectively. The iterative nature of the computation is indicated with the iteration index n (the iteration index for the source terms n[*] is equal to n or n-1, depending on the source term, see below). Because of these iterations, the scheme is also approximately implicit for the source terms. For negative propagation speeds, appropriate + and - signs are required in Eq. (C1).

The coefficients ν and η determine the degree to which the scheme in spectral space is upwind or central. They thus control the numerical diffusion in frequency and directional space, respectively. A value of $\nu=0$ or $\eta=0$ corresponds to central schemes which have the largest accuracy (numerical diffusion≈0). Value of $\nu=1$ or $\eta=1$ correspond to upwind schemes which are somewhat more diffusive and therefore less accurate but more robust. If large gradients of the action density in frequency space or directional space are present, numerical oscillations can arise (especially with the central difference schemes) resulting in negative values of the action density. In each sweep such negative values are removed from the two-dimensional spectrum by setting these values equal to zero and rescaling the remaining positive values such that the frequency-integrated action density per spectral direction is conserved. The depth derivatives and current derivatives in the expressions of c_σ and c_θ are calculated with a first-order upwind scheme. For very strong refraction the value of c_θ is reduced in each grid point and for each wave component individually with the square of the fraction of the grid spacing over which $k d$ <3.0.

For stationary conditions SWAN can be run in stationary mode. Time is then removed as a variable but the integration (in geographic space) is still carried out iteratively. The propagation scheme is still implicit as the derivatives of action density (in x or y) at the computational level (i_x or i_y, respectively) are formulated at that level except in the integration dimension (x or y; depending on the direction of propagation) where also the upwave level is used. The values of Δx and Δy are therefore still mutually independent.

For the stationary second-order upwind scheme (Rogers et al., 2000; SORDUP = second-order upwind) which is the <u>default scheme for **stationary** computations</u>, the two terms in equation (C1) representing x- and y-derivatives are replaced by:

$$\left[\frac{1.5\ [\ c_x N\ ]i_x - 2\ [\ c_x N\ ]i_x - 1 + 0.5\ [\ c_x N\ ]i_x - 2}{\Delta x} \right] i_t,\ n\ i_y,\ i_\sigma,\ i_\theta\ +$$

(C1a)

$$\left[\frac{1.5\ [\ c_y N\ ]i_y - 2\ [\ c_y N\ ]i_y - 1 + 0.5\ [\ c_y N\ ]i_y - 2}{\Delta y} \right] i_t,\ n\ i_x,\ i_\sigma,\ i_\theta$$

For the nonstationary second-order upwind scheme (Rogers et al., 2000; S&L = Stelling and Leendertse), which is the <u>default scheme for **nonstationary** computations</u>, the two terms in equation (C1) representing x- and y-derivatives are replaced by:

$$\left[\frac{\frac{5}{6} [\ c_x N\ ]i_x - \frac{5}{4} [\ c_x N\ ]i_x - 1 + \frac{1}{2} [\ c_x N\ ]i_x - 2 - \frac{1}{12} [\ c_x N\ ]i_x - 3}{\Delta\ x} \right] i_t\ ,\ n\ i_y\ ,\ i_\sigma\ ,\ i_\theta\ +$$

$$\left[\frac{\frac{5}{6} [\ c_y N\ ]i_y - \frac{5}{4} [\ c_y N\ ]i_y - 1 + \frac{1}{2} [\ c_y N\ ]i_y - 2 - \frac{1}{12} [\ c_y N\ ]i_y - 3}{\Delta\ y} \right] i_t\ ,\ n\ i_x\ ,\ i_\sigma\ ,\ i_\theta\ +$$

$$\left[\frac{\frac{1}{4} [\ c_x N\ ]i_x + 1 - \frac{1}{4} [\ c_x N\ ]i_x - 1}{\Delta\ x} \right] i_t - 1\ i_y\ ,\ i_\sigma\ ,\ i_\theta\ +$$

$$\left[\frac{\frac{1}{4} [\ c_y N\ ]i_y + 1 - \frac{1}{4} [\ c_y N\ ]i_y - 1}{\Delta\ y} \right] i_t - 1\ i_x\ ,\ i_\sigma\ ,\ i_\theta$$

(C1b)

To explain the above numerical solution technique in terms of matrix solutions, first ignore the decomposition in quadrants. The propagation of the waves in both geographic and spectral space would then be described with one large basic matrix which can be solved in several ways. Removing refraction, frequency shifting and nonlinear source terms from this basic matrix permits a matrix solution with a Gauss-Seidel technique (e.g., Golub and van Loan, 1986) in which the matrix is decomposed in four sections (the above four directional quadrants) which are each solved in one step (super-convergence). Restoring refraction and frequency shifting to the matrix requires the solution of a submatrix for each geographic grid point. If no currents are present and the depth is stationary, this is readily done with a Thomas algorithm (e.g., Abbott and Basco, 1989; c_σ =0 and the sub-matrix is a simple tri-diagonal matrix). If currents are present or the depth is not stationary, the sub-matrix is a band matrix. It is solved with an iterative ILU-CGSTAB method (Vuik, 1993; Van der Vorst, 1992). Restoring refraction and frequency-shifting also introduces coefficients in each matrix section (directional quadrant) that cause dependency between the matrix sections. The same happens when nonlinear source terms are added to the matrix. The basic matrix as a whole needs therefore to be solved iteratively until some break-off criteria are met. To reduce the number of iterations in stationary mode with wind generation, SWAN starts with a reasonable first-guess of the wave field (a "quick-start" based on the second-generation source terms of Holthuijsen and De Boer, 1988, adapted for shallow water). It reduces the number of iterations typically by a factor two. In nonstationary mode, a very reasonable first-guess per time step is available from the previous time step and the number of iterations is expected to be small. If no iterations are used in nonstationary mode (as in most phase-averaged wave models), the computations of propagation are still implicit and therefore still unconditionally stable.

In the neighbourhood of grid points which represent open boundaries, land boundaries and obstacles (i.e., the last two grids adjoining such grid points for the SORDUP scheme and the last three grids adjoining such grid points for the S&L scheme), SWAN will revert to the first-order BSBT scheme. This scheme has a larger numerical diffusion but that is usually acceptable over the small distances involved.

The numerical diffusion of the S&L scheme is so small that the so-called garden-sprinkler effect (GSE) may show up if propagation over very large distances is considered. This effect is due to the spectral resolution (see Booij and Holthuijsen, 1987). It can be counteracted by a diffusion term that has been explicitly added to the numerical scheme (not default in SWAN). Its value depends on the spectral resolution and the propagation time of the waves (see the input variable [wave age] in the SCHEME command).

The diffusion applied in the propagation direction is:

$$D_{ss} = \Delta c^2 T/12 \tag{C2}$$

where T is the wave age.
The diffusion normal to the propagation direction is:

$$D_{nn} = c^2 \Delta\theta^2 T/12 \tag{C3}$$

From these diffusion coefficients (in terms of x and y) are calculated as:

$$D_{xx} = D_{ss}\cos^2\theta + D_{nn}\sin^2\theta,$$

$$D_{yy} = D_{ss}\sin^2\theta + D_{nn}\cos^2\theta \text{ and} \tag{C4}$$

$$D_{xy} = (D_{ss} - D_{nn})\cos\theta\sin\theta.$$

The diffusion terms are computed at the time level $i_t - 1$. The diffusion terms are computed as follows:

$$D_{xx}\left[\frac{[N]i_x + 1 - 2[N]i_x + [N]i_x - 1}{\Delta x^2}\right] i_t - 1 \ i_y \ , \ i_\sigma \ , \ i_\theta$$

$$D_{yy}\left[\frac{[N]i_y + 1 - 2[N]i_y + [N]i_y - 1}{\Delta y^2}\right] i_t - 1 \ i_x, \ i_\sigma \ , \ i_\theta$$

$$D_{xy}\left[\frac{[N]i_x,i_y - [N]i_x - 1,i_y - [N]i_x,i_y - 1 + [N]i_x - 1,i_y - 1}{\Delta x \ \Delta y}\right] i_t - 1 \ i_\sigma \ , \ i_\theta \tag{C5}$$

This explicit finite differencing is fast (having little impact on computation time) but only conditionally stable. Through mathematical analysis (not shown) it can be shown that a likely stability condition for the one-dimensional S&L scheme with this GSE correction is $D\Delta t/(\Delta x^2) \le 0.5$ which corresponds to the two-dimensional stability criterion of Tolman (1995; based on Fletcher, 1988, Part I, section 7.1.1):

$$Q = \frac{\max(D_{xx}, D_{yy}, D_{xy})\Delta t}{\min(\Delta x, \Delta y)^2} \le 0.5 \tag{C6}$$

Thus it is credible that Eq. (C6) holds true for the two-dimensional S&L scheme with this GSE correction. In experiments, it was found that for all experiments which satisfy the slightly more restrictive $Q \le 0.48$ no instability was observed. In short, by adding the GSE correction, the unconditionally stable advection scheme of SWAN becomes a (likely) conditionally stable advection-

diffusion scheme. It is readily shown that for typical ocean applications D_{nn} dominates the diffusion and Q can be written as:

$$Q = \overline{C} \, T \, / \, \Delta x \, . \, \overline{C} \, \Delta t \, / \, \Delta x \, . \, \Delta \theta^2 \, / \, 12 \tag{C7}$$

The variable wave age $\overline{T}$ could be computed during the computations of SWAN (Booij and Holthuijsen, 1987) but it requires the same order of magnitude of computer memory as integrating the action balance equation. Instead a constant wave age $\overline{T}$ can be used as an approximation, so that Eq.(C7) becomes

$$Q = \overline{L} \, / \, \Delta x \, . \, \mu \, . \, \Delta \theta^2 \, / \, 12 \tag{C8}$$

where the characteristic travel distance of the waves is $\overline{L} = \overline{C} \, \overline{T}$ (e.g., the dimension of the ocean basin). For oceanic applications the Courant number is typically $\mu \approx 1/2$ so that $Q \leq 0.25$ for typical values of $\Delta \theta$ and $\overline{L} / \Delta x$ (the number of grid point in one direction of the grid). This implies that the S&L scheme with this GSE correction is stable for typical ocean cases. For shelf sea (regional) applications the value of $\mu = O(1)$ but the garden-sprinkler effect tends to be small on these scales and the diffusion can and should not be used to avoid the stability problem. For small-scale (local) applications typically $\mu = O(10 \text{-} 100)$. But such cases are usually treated as stationary and the SORDUP scheme should be used (no GSE correction is included in this scheme).

The boundary conditions in SWAN, both in geographic space and spectral space are fully absorbing for wave energy that is leaving the computational domain or crossing a coast line. The incoming wave energy along open geographic boundaries, needs to be prescribed by the user. For coastal regions such incoming energy is usually provided only along the deep-water boundary and not along the lateral geographic boundaries (i.e., the spectral densities are assumed to be zero). This implies that such erroneous lateral boundary conditions are propagated into the computational area. The affected areas are typically triangular regions with the apex at the corners between the deep-water boundary and the lateral boundaries, spreading towards shore at an angle of 30° to 45° (for wind sea conditions) on either side of the deep-water mean wave direction (less for swell conditions; this angle is essentially equal to the one-sided width of the directional distribution of the incoming wave spectrum). For this reason the lateral boundaries should be sufficiently far away from the area of interest to avoid the propagation of this error into the area.

Generation, wave-wave interactions and dissipation
The numerical estimations of the source terms in SWAN are essentially implicit. This is achieved with explicit or implicit approximations of the source terms which in the limit of a large number of iterations, always result in an implicit estimation. In actual computations final convergence is obviously never achieved and the estimations of the source terms are therefore strictly speaking only approximately implicit. In the following the adjectives "explicit" and "implicit" refer to the approximations of the source terms within each iteration.

The linear growth term A is independent of integral wave parameters and of the energy density and can therefore be readily computed. All other source terms depend on energy density and they can be described as a (quasi-)linear term: $S = \phi \, E$, in which ϕ is a coefficient that depends on (integral) wave parameters (e.g., E_{tot}, $\tilde{\sigma}$, $\tilde{k}$, σ, k, etc.) and action densities of other spectral components. Since these are only known at the previous iteration level n-1, the coefficient ϕ is determined at that iteration level: $\phi = \phi^{\, n \text{-} 1}$.

For positive source terms (wind input and the triad wave-wave interactions if positive) the integration is generally more stable if an explicit formulation is used (i.e., the source term depends on $E^{\, n \text{-} 1}$

and not on E^n) rather than an implicit formulation (i.e., the source term depends also on E^n). The explicit formulation for these source terms in SWAN is therefore:

$$S^n \approx \phi^{n-1} E^{n-1} \qquad (C9)$$

For reasons of economy this explicit approximation is also used for the formulation of the quadruplet wave-wave interactions (for both the positive and negative contributions). This is considered reasonable since Tolman (1992a) has shown that using an explicit formulation in combination with a limiter (see below) gives similar results as the use of a more expensive implicit scheme (this implicit formulation is also optionally available in SWAN; in the WAM model it is indicated as the semi-implicit scheme, the WAMDI group, 1988; Komen et al, 1994).

For negative source terms the integration is generally more stable if an implicit scheme is used. The strongly nonlinear, negative source term of depth-induced wave breaking at iteration level n is accordingly estimated with a linear approximation:

$$S^n \_ \Phi^{n-1} E^{n-1} + \left(\frac{\partial S}{\partial E} \right)^{n-1} (E^n - E^{n-1}) \ . \qquad (C10)$$

However, to achieve even more stable computations for this source term, the term $\phi^{n-1} E^{n-1}$ in this formulation has been replaced by $\phi^{n-1} E^n$ (making the formulation somewhat more implicit and thus more robust; note that in the limit the solution is the same). Since this process of depth-induced wave breaking has been formulated such that $S = a \ S_{tot}$ and $E = a \ E_{tot}$, the derivative $\partial S / \partial E$ is analytically determined as $\partial S_{tot} / \partial E_{tot}$ (where a is identical in both expressions and the total energy E_{tot} and the total source S_{tot} are the integrals over all frequencies and directions of $E(\sigma , \theta)$ and $S_{ds, br} (\sigma , \theta)$, respectively). For the other negative (mildly nonlinear) source terms, i.e., whitecapping, bottom friction and negative triad wave-wave interactions a similar accuracy of estimating S^n can be achieved with the following simpler, and therefore more economical approximation in which $(\partial S / \partial E)^{n-1}$ of Eq. (14) has been replaced by $(S / E)^{n-1}$

$$S^n \_ \Phi^{n-1} E^{n-1} + \left(\frac{S}{E} \right)^{n-1} (E^n - E^{n-1}) \ . \qquad (C11)$$

With $S = \phi \ E$, this reduces to:

$$S^n \_ \Phi^{n-1} E^n \ . \qquad (C12)$$

These approximations for the source terms are added to the elements of the matrix for the propagation. To suppress the development of numerical instabilities, the maximum total change of action density per iteration at each discrete wave component is limited to a fraction of 10% of the Phillips (1957) equilibrium level (reformulated in terms of action density and wave number to be applicable in shallow water; as in the WAM model and in the WAVEWATCH III model; Tolman,

1992a): $| \Delta \ N (\sigma , \theta) |_{max} = \dfrac{0.1}{2 \pi \sigma} \dfrac{\alpha_{PM} \ \pi}{k^3 c}$ (C13)

where $\alpha_{PM} = 0.0081$ is the Phillips' "constant" of the Pierson-Moskowitz (1964) spectrum. To retain the very rapid but realistic decrease of wave energy near the shore due to depth-induced wave breaking, this limiter is not applied if the waves actually break (in SWAN: $H_{rms} / H_{max} < 0.2$ with $H_{rms} = \sqrt{8 \ E_{tot}}$ which implies a fraction of breakers $Q_b > 0.00001$).

The fraction of depth-induced breakers (Q_b) is determined in SWAN with

$$Q_b = 0 \qquad\qquad\qquad\qquad\qquad\qquad\qquad \text{for } \beta \_ 0.2$$

$$Q_b = Q_0 - \beta^2 \, \frac{Q_0 - \exp((Q_0 - 1)/\beta^2)}{\beta^2 - \exp((Q_0 - 1)/\beta^2)} \qquad \text{for } 0.2 \prec \beta \prec 1$$

one step Newton-Raphson iteration)   (C14)

$$Q_b = 1 \qquad\qquad\qquad\qquad\qquad\qquad\qquad \text{for } \beta \_ 1$$

where $\beta = H_{rms} / H_{max}$. For $\beta \_ 0.5$, $Q_0 = 1$ and for $0.5 \prec \beta \_ 1$, $Q_0 = (2\beta - 1)^2$.

Wave-induced set-up
In 1D cases the wave-induced set-up is calculated in SWAN with a simple trapezoidal rule.

In 2D cases the Poisson equation of the divergence-free force field is solved in SWAN with the same solver that is used for wave propagation with ambient currents. The boundary conditions for this elliptical partial differential equation are:

m)   not-nested computations: a1)   at open boundaries: equilibrium between wave force and hydrodynamic pressure gradient normal to the model boundary

a2)   at last grid points before shoreline: equilibrium between wave force and hydrodynamic pressure gradient normal to the model boundary

a3)   at deepest boundary point: set-up is zero

n)   nested computations: b1) at open boundaries: set-up at taken from larger computation

b2) at last grid points before shoreline: equilibrium between wave force and hydrodynamic pressure gradient normal to the model boundary

The shoreline in SWAN moves as dictated by the wave-induced set-up. The set-up computations are available on both the recti-linear and curvi-linear grids.

Curvi-linear grid
The propagation scheme in SWAN for geographic space is formulated on a curvi-linear geographic grid (irregular, quadrangular, not necessarily orthogonal) rather than the rectilinear grid of SWAN Cycle 1. This modification is based on approximating the geographic distribution of the energy (action) density between each three neighbouring grid points with a flat triangle. The gradient in each grid point at location (x_i, y_j) is then readily approximated from the up-wind grid points. For the x-direction this is for grid point i, j (the grid points are ordered in x, y-space with labels i and j respectively):

$$\frac{\partial C_x N}{\partial x} \quad - \left[\frac{[c_x N]_{i,j} - [c_x N]_{i-1,j}}{\Delta \tilde{x}_1} \right] + \left[\frac{[c_x N]_{i,j} - [c_x N]_{i,j-1}}{\Delta \tilde{x}_2} \right]$$

(C15)

where $\Delta \tilde{x}_1 = \Delta x_1 - (\Delta y_1 / \Delta y_2) \Delta x_2$,
$\Delta \tilde{x}_2 = \Delta x_2 - (\Delta y_2 / \Delta y_1) \Delta x_1$. The increments are
$\Delta x_1 = x_{i,j} - x_{i-1,j}$, $\Delta x_2 = x_{i,j} - x_{i,j-1}$, $\Delta y_1 = y_{i,j} - y_{i-1,j}$
and $\Delta y_2 = y_{i,j} - y_{i,j-1}$. The gradient in y-direction is similarly estimated.